RICE FIELD MAPPING AND PRODUCTION ESTIMATION USING REMOTE SENSING DATA IN BALI PROVINCE, INDONESIA

January 2012

I WAYAN NUARSA

GRADUATE SCHOOL OF SCIENCE

CHIBA UNIVERSITY

ABSTRACT

Forecasting rice yield before harvest time is important to supporting planners and decision makers to predict the amount of rice that should be imported or exported and to enable governments to put in place strategic contingency plans for the redistribution of food during times of famine. The main objectives of this study are to develop the algorithms for rice field mapping and production estimation using remote sensing data.

The results of research show that application of variance analysis algorithm using MODIS data for rice field mapping produced overall accuracy of 87.91% and Kappa value of 0.8371. Overall accuracy more than 80% and Kappa value greater than 0.8 show a good agreement between analysis result and reference data. Accuracy assessment between analysis result and reference data in form of chart showed a linear relationship with the R^2 of 0.92 and 0.97 for district and regency level comparison respectively.

Rice Growth Vegetation Index (RGVI) is the new vegetation index developed in this study. It has the highest correlation with rice age, and it was used to develop the algorithm for rice field distribution mapping using Landsat ETM data. The quantitative evaluation of the rice field mapping model compared with the statistical data showed a high correlation with the R^2 of 0.975.

Water availability for rice irrigation is one of the constrain factor in the study area. Therefore, study difference of rice plant characteristic in healthy and water deficiency condition are important to investigate. The result of the study shows that rice spectral under water deficiency had significant differences compared to those of healthy rice. When water deficiency happened, the reflectance of the visible bands increased significantly, while the reflectance of near- and middle-infrared bands decreased. The RVI is the best vegetation index for both early detection of water deficiency and distinguish the two rice conditions.

Total of the rice NDVI during its life ($\sum$NDVI) using MODIS data showed the best exponential relationship with the rice yield compared with the maximum value of NDVI during its lifetime and age of rice plant where the maximum NDVI is occurred. Estimation of rice yield can be performed using equation $y = 0.4745e^{0.0504x}$, where y is the rice yield and x is the $\sum$NDVI.

Application of Landsat ETM+ data and field observation for rice yield estimation show that rice yield can be estimated in rice age of 63 days using the equation $y = 0.3419e^{4.1587x}$, where y and x are rice yield and NDVI, respectively. An accuracy assessment with the reference data showed a linear relationship with the R^2 is 0.9262.

According to this study both Landsat ETM+ and MODIS data have a good potential for rice field mapping and rice production estimation.

TABLE OF CONTENS

CHAPTER 1

GENERAL INTRODUCTION

1.1 Rice characteristic in Bali, Indonesia

Rice is still considered the most important grains in Indonesia since this crop is the staple food for majority of the people. In addition millions of people engaged in rice production, rice processing and other post-harvest activities related to rice. Considering the importance of rice, Government of Indonesia has launched many programs to boast rice production in order to meet the demand, and trying not too much dependent on imported rice (Sidik. 2004).

Total of rice field in Indonesia in 2010 was 7.7 million ha with the rice production was 66,411,469 ton (9.4% of world rice production). In Bali, total of agriculture land was 355,271 ha (63.03%), consist of 81,908 ha (14.53%) rice field and 273,363 ha (48.50%) non rice field. Total rice production in Bali was 867,185 ton with the average of production rate was 5.74 ton/ha (BPS, 2010; FAO, 2009).

Agriculture rice fields in Bali consist of irrigated fields and non-irrigated fields. The water source for the irrigated rice fields are rivers, whereas the water for non-irrigated rice fields comes from rainfall. Annually, both irrigated and non-irrigated rice field lands are not only used for rice paddies but also for seasonal crops, such as corn, soybeans, and nuts. However, the type of seasonal plant grown from year to year is usually similar from one place to another. In humid tropic regions, such as in the study area, rice cultivation is only limited by the water availability for irrigation. Therefore, for irrigated land, rice planting alternates between regions, whereas in non-irrigated land, rice planting occurs in the rainy season. Farmers usually plant the rice two or three time per year, and use the remaining time for other seasonal crops. The crop growth duration is approximately three months (Food Crops Agriculture Department 2010).

1.2 Remote Sensing in Based-Agriculture

Basic understanding of rice physiology is essential to the success of remote sensing applications in rice-based agricultural systems. This knowledge can play a critical role in

the planning stages of a remote sensing project (e.g., identifying optimum acquisition dates for the purchase of imagery) as well as in the final stages of analysis (e.g., aiding in the delineation of rice paddies or the estimation of growth stages) (Ribbes and Toan, 1999, Le Toan *et. al.*, 1997). The growing cycle of rice can be separated into two stages with respect to most analyses of remotely sensed data: vegetative and reproductive (Casanova *et. al*, 1998, Ribbes and Toan, 1999).

The vegetative stage includes the part of the growth cycle where the plant develops and grows, starting after sowing and ending when the plants start to reproduce. This stage is characterised by a steady increase in plant height and biomass. The reproductive stage starts when the plant stops growing taller and ends after maturity and includes panicle and grain development (Ribbes and Toan, 1999). It may be beneficial at times to further split the reproductive stage into two categories: reproductive pre-heading and reproductive postheading. Reproductive pre-heading defines the period from panicle primordia initiation to heading and post-heading refers to the period from heading to maturity (Casanova *et. Al.*, 1998).

The length of the growth cycle of rice can vary from 3 to 6 months for different varieties (Casanova *et. Al.*, 1998), and can also be categorised into two main groups for many remote sensing applications: tropical and temperate. Growth cycles for tropical rice varieties last about 110- 120 days, while those of temperate varieties usually last around 140-150 days (Le Toan et al., 1997). However, this duration can vary based on cultivar. For example, short duration varieties have been bred with growth cycles less than 90 days. These differences in growth cycle length are due to differences in vegetative stage duration: the vegetative stage can be anywhere from 40 to 120 days in length (Senanayake et al., 1994).

Irrespective of cultivar, reproductive pre-heading duration is about 23-25 days, while reproductive post-heading duration lasts 30-35 days (Senanayake et al., 1994). During the reproductive stage, plant height and biomass typically remain stable at around 100 cm and 2000 gm^{-2}, respectively. The vertical characteristics of the rice plant also change as the plants grow, with stem inclination decreasing and the leaf angle increasing (Ribbes and Toan, 1999).

Remote sensing based applications, then, will not only take advantage of both the characteristics and timing of growth cycle, but will also consider the spectral reflectance of different crops. Since rice is the focus of this report, the basic spectral patterns of rice must be understood. The reflectance from rice, like all green vegetation, can be

summarized by a generalized vegetation response. It is the differences in this basic vegetation response that allow discrimination between vegetation types. However, these vegetative-type responses are harder to differentiate between each other than a non-vegetative-type response like soil or water. This is true since non vegetative-type features usually reveal drastically different response curves when compared to vegetation

As irrigated rice fields are flooded, the spectral characteristics of water can be used to distinguish potential rice paddocks and provide an early estimate of rice area (Barrs and Prathapar, 1996). Inaccuracies result, however, when this early estimate is not adjusted by a later image, which can aid in elimination of permanent water bodies and other irrigated crops from the classification (Barrs and Prathapar, 1996). The visible and near infrared wavelength response of rice, once the vegetation starts to cover the water in flooded paddocks, is much the same as other crops. However, rice was found to be more distinguishable from other crops due to its water absorption characteristics by including middle infrared (MIR) wavelengths in the crop discrimination (Martin and Heilman, 1986).

The spectral dimension is the basis of remote sensing based class discrimination, temporal and spatial resolution play very important role in classification accuracy. The spatial and temporal information included in single date and time series data usually play a secondary role but can aid in the classification procedure. Currently, high temporal remote sensing data now available from various platforms offers an opportunity to exploit the temporal dimension for crop classification. Use of high temporal vegetation indices data sets for crop studies call for new classification approaches. Moderate Resolution Imaging Spectroradiometer (MODIS) is one of the satellite image that has daily revisit time. The MODIS has a good capability to discriminate an agriculture crops (Tingting *et al* 2010, Boschetti *et al* 2009).

1.3 Crop Area Measurement

Crop area measurement is a very common practice in agriculture. Remote sensing is often used for this purpose because of its strengths in regard to spatial extent, temporal density, relative low costs, and potential for rapid assessment of spatial features. Many of the same issues concerning crop type identification also affect crop area measurement from remotely sensed data. This is because crop type identification is a necessary first step to area estimation. In many cases, though, crop type identification is more concerned

with classifying all crop types from each other, where area estimation often is concerned with only a few target crops. In either case, these two applications are frequently performed in sequence: first crop identification and then area estimation. There are a few issues that are not exclusively related, but tend to more specifically pertain to crop area estimation, including positional accuracy, mixed pixels and pixel size, and a mismatch between individual and overall accuracies of the results.

Positional accuracy, here, can be defined as the difference in the position of a feature on a map compared to the feature's real world or 'true' position. As such, the position of boundary lines on the map, for instance, are most likely not where they are in the real world, but are more accurately represented as a belt or swath around that boundary line on the map. This swath contains the 'true boundary line' and has a width that is inversely related to the scale of the source. For example, as the scale of the source gets smaller (area representation gets larger) the width of the swath around the line generally represents a larger distance, making the positional accuracy decrease (Niel and McVicar, 2000). In other words, as the swath gets wider, the relative certainty of the position of the 'real boundary' gets smaller and the error likely increases. Therefore, when attempting to estimate crop areas accurately, considerable thought should be given to achieving high positional accuracy of crop boundary lines if GIS data are used in conjunction with remote sensing. Ground validation points are extremely important, in this case, to quantify positional accuracy and thus spatial uncertainty. Knowledge of spatial uncertainty is essential in making appropriate managerial decisions on crop area measurements (Niel and McVicar, 2000). For example, if crop area estimation is performed in an attempt to monitor year-to-year land use, it is extremely important to know how much potential error is included in the estimate solely due to uncertainties. With this knowledge, the manager has a better idea if the year-to22 year difference in area is reliably measured from the remotely sensed data or if it is 'absorbed' by the inaccuracies of the dataset itself.

Pixel size of the remotely sensed data also affects positional accuracy of boundary lines in crop area estimates, and therefore should be considered for its appropriateness to a particular application. One prominent issue is the relation of the pixel size to the paddock size (or feature element) being measured (Pax-Lenney and Woodcock, 1997). Although for large areas AVHRR data is very attractive due to its spatial extent and high repeat cycle, the 1 km pixel size is often disproportionately larger than paddock sizes. This may not be an insurmountable problem when monitoring areas with many

contiguous smaller fields of the same crop type (Quarmby et al., 1993b), but at the same time, must be considered. In an attempt to either compensate for mismatched pixel-to-field sizes or to increase the accuracy of area estimations, the spectral characteristics of impure or 'mixed' pixels can be 'unmixed' by linear mixture modelling.

In linear mixture modelling, the analyst assumes that any mixed pixel's spectral signature is made up of a combination of pure spectral signatures of all the separate land cover types contained in that pixel in proportion to the area of which that cover type is found in the pixel (Maas, 2000). The spectral signatures resulting from a pixel containing only one cover type (pure pixel) are known as end members. Proper unmixing of mixed pixels relies upon the identification of good end member spectra (Quarmby et al., 1992). Different combinations and proportions of the end members are combined to best match the signature of the mixed pixel, supposedly allowing for a better estimate of crop areas. Problems can arise when end members are either not a good representation of a particular land cover class, or when a land cover class' end member is not collected. Even when numerous and representative end members are gathered, results can still be spurious due to confusion caused by mixed pixel spectra being explained by multiple possibilities of end member combinations. Also, green crops can produce very similar end members at certain times of the year, resulting in erroneous unmixing in agricultural systems.

As with identification of crop types, ground validation is also very important in area estimation. Traditional estimates of crop area have come from census data over rather large areas, and are usually rather gross and usually contain little specific spatial context. This means that there is often no explicit locational knowledge contained in the 'ground truth'. This leads to very ambiguous results where overall values may be closely related, but the analyst often has no idea what sort of spatial variation exists between the 'ground truth' and the estimates from the remotely sensed data, leaving the comparison less meaningful. It is important, then, to make sure that the 'ground truth' data is defensibly more reliable than the observation as well as spatially explicit, wherever possible (Niel and McVicar, 2001)

1.4 Rice yield estimation using remote sensing data

Forecasting crop yield well before harvest is crucial especially in region characterized by climatic uncertainties. This enables planner and decision maker to predict how much to import in case of shortfall or optionally, to export in case of surplus.

It also enables governments to put in place strategic contingency plans for redistribution of food during times of famine. Therefore, monitoring of crop development and of crop growth, and early yield prediction are generally important.

Crop yield estimation in many countries are based on conventional techniques of data collection for crop and yield estimation based on ground-based field visits and reports. Such reports are often subjective, costly, time consuming and are prone to large errors due to incomplete ground observation, leading to poor crop yield assessment and crop area estimation (Reynolds *et al*., 2000). In most countries the data become available too late for appropriate actions to be taken to avert food shortage.

In some countries weather data are also used and models based on weather parameters have been developed. This approach is associated with a number of problem including the spatial distribution of the weather station, incomplete and/or unavailable timely weather data, and weather observation that do not adequately represent the diversity of weather over the large areas where crops are grown (Liu and Kogan, 2002, Rugege, 2002). In Indonesia the number of weather stations is very limited, it was mostly found in Java (Notohadiprawiro, 2006). Objective, standardized and possibly cheaper/faster method that can be used for crop growth monitoring and early crop yield estimation are imperative.

Many empirical models have been developed to try and estimate yield before harvesting. However, most of the methods demand data that are not easily available. The models complexity, their data demand, and methods of analysis, render these models unpractical especially at field level (Sawasawa, 2003).

With the developed of satellites, remote sensing images provide access to spatial information at global scale; of features and phenomena on earth on an almost real-time basis. They have the potential not only in identifying crop classes but also of estimating crop yield (Mohd *et al.*, 1994). They can identify and provide information on spatial variability and permit more efficiency in field scouting (Schuler, 2002). Remote sensing could therefore be used for crop growth and yield estimation.

Positive correlations exist between measurements of LAI (Nemani and Running, 1989a, McVicar et al., 1996a), plant condition (Sellers, 1985), and VI's. Based on this relationship, and assuming that LAI (or biomass) is related to yield, there are 3 main approaches used to forecast yield. These are: 1) correlate yield with NDVI (Maselli et al., 1992, Smith et al., 1995); 2) correlate yield with integration under the NDVI curve,

denoted ∫NDVI (Benedetti and Rossini, 1993; Rasmussen, 1998, Honghui et al., 1999); or 3) simulate yield with crop models (sometimes using remotely sensed inputs) (Rosenthal et al., 1998, Inoue et al., 1998).

1.5 Formulation of the Problems

Information on the area and spatial distribution of rice fields is needed for estimating gas emission, management of water resources, and food security (Xiao et al, 2005). Methane is as an important greenhouse gas which can contribute to global warming. It has the second largest radiative forcing (0.48 Wm^{-2}) after CO2 (1.66 Wm^{-2}) and contributes some about 16% of the global warming resulting from the increasing concentrations of greenhouse gases in the atmosphere. The cultivation of irrigated rice may account for up to 12% of this flux (Khosa et al, 2011). Indonesia has 7.7 million ha rice field. It will give a significant impact to the global methane gas emission. Changes extents of rice fields will affect the amount of methane emissions into the atmosphere. Therefore, mapping of rice field periodically is important to perform.

Agricultural water use accounted for approximately 70% of global fresh water withdrawals and majority of Asian rice agriculture is irrigated (Xiao et al, 2005). In Indonesia, water for agriculture becomes an important issue because of the availability of water decreases while the need increases along with increasing population. Reduced forest area, degradation of watershed, and increasing of land use change from agricultural land into residential and industrial area causes of water availability is reduced (Boehm and Sieger, 2001; BPS, 2010). Competing use of water between agricultural and non-agricultural sectors are becoming increasingly stringent. Availability of updated information on agricultural land, especially rice fields is very important for appropriate water use planning.

Rice becomes important agriculture plant in Asia because 87 % of world rice consumption located in Asia. In Indonesia, rice problem lies in the rice import policy. Our government sometime import the rice when rice harvest season. It will hurt the farmers (Sidik, 2004). This is because the lack of data on the rice harvested area, either speed of availability, accuracy or continuity of the data. Therefore, estimation of rice yield before harvest time is very important for food security policy.

Mostly previous study of application remote sensing for rice crops focused on detecting the phenological stages of paddy rice (Sukamoto et al, 2005; Boschetti et al, 2009, Uchida, 2010) and limited study concern to developing of algorithm for rice field mapping and production estimation, especially in Indonesia. Investigations of rice plants under abnormal conditions are currently still very limited. Most of them concern on spectral characteristics of rice plants infested by pests and plant diseases (Qin and Zhang, 2005; Yang and Cheng, 2001; Yang et al., 2007), and only a few studies related to water deficiency (Yang and Su, 2000; Köksal et al., 2008).

The ultimate goal of this study is to estimate the rice yield. For this purpose a series of research should be conducted including rice field mapping, rice age mapping, spectral differences between normal and abnormal of rice field, relationships between rice spectral and rice yield, and finally prediction of rice yield. All of these studies using satellite imagery capabilities.

1.6 General Objective of this Study

The objectives of the study are:

1. Develop the algorithms for rice field distribution mapping using Landsat and Modis data.
2. Study differences of spectral characteristics between rice plant in healthy and water-deficiency conditions.
3. Find out the relationships between rice spectral and rice yield.
4. Develop the algorithms for estimate rice yield using remote sensing data and field observations.

CHAPTER 2

USING VARIANCE ANALYSIS OF MULTITEMPORAL MODIS IMAGES FOR RICE FIELD MAPPING IN BALI PROVINCE, INDONESIA

2.1 Introduction

Rice is one of the most important agriculture crops in many Asian countries, and it is a primary food source for more than three billion people worldwide (Khush, 2005; Yang *et al*., 2008). Mapping the distribution of rice fields is important not only for food security but also for the management of water resources and estimations of trace gas emissions (Xiao *et al*., 2005; Matthews *et al*., 2000). Therefore, more accurate data related to the total rice field area, its distribution, and its changes over time are essential.

Satellite remote sensing has been widely applied and is recognised as a powerful and effective tool for identifying agriculture crops (Toan *et al*., 1997; Liew *et al*., 1998; Bouvet *et al*., 2009; Pan *et al*., 2010; Bachelet, 1995; Okamoto and Kawashima 1999; Fang, 1998; Fang *et al*., 1998; Niel *et al*., 2003). This process primarily uses the spectral information provided in the remotely sensed data to discriminate between perceived groupings of vegetative cover on the ground (Niel and McVicar, 2001). Although spectral dimension is the basis of remote sensing based class discrimination, temporal and spatial resolution play very important role in classification accuracy. Discrimination of crops is usually performed with 'supervised' or 'unsupervised' classifiers. The basic difference between these types of classification is the process by which the spectral characteristics of the different groupings are defined (Atkinson and Lewis, 2000). Common classification algorithms include the maximum likelihood, minimum distance to mean, and parallelepiped (Jensen, 1986).

The high temporal remote sensing data now available from various platforms offer an opportunity to exploit the temporal dimension for crop classification. The use of data sets of high temporal vegetation indices for crop studies calls for new classification approaches. The Moderate Resolution Imaging Spectroradiometer (MODIS) is one of the satellite images that provide daily revisit time. The MODIS image has a good capability to discriminate agricultural crops (Tingting *et al.*, 2010, Boschetti *et al.*, 2009).

Agricultural rice fields have a large variety of land covers that can range from water bodies just before rice transplanting, to mixed water, vegetation, or bare soil just after harvesting time. The range of land covers and complex relationships between ecological factors and land cover distribution cannot accurately be expressed through deterministic decision rules (Hutchinson, 1982; Mas and Ramirez, 1996). Alternatively, the large variety of rice field land covers compared to other land uses can be advantageous in distinguishing it from the other land uses.

The objectives of the first study are to develop the new algorithm for rice field classification using the temporal variance analysis and quantitatively compare the classification result using the new method with the reference data.

2.2 Study area, data, and method

2.2.1 Background and study area

The study area is located in the Bali Province of Indonesia and centred at latitude 8°40’00” S and longitude 115°19’00” E (Figure 2.1). Agriculture rice fields in Bali consist of irrigated fields and non-irrigated fields. The water source for the irrigated rice fields are rivers, whereas the water for non-irrigated rice fields comes from rainfall. Annually, both irrigated and non-irrigated rice field lands are not only used for rice paddies but also for seasonal crops, such as corn, soybeans, and nuts. However, the type of seasonal plant grown from year to year is usually similar from one place to another. In humid tropic regions, such as in the study area, rice plants can be planted at any time. However, planting is influenced by water availability. Therefore, for irrigated land, rice planting alternates between regions, whereas in non-irrigated land, rice planting occurs in the rainy season. Farmers usually plant the rice two or three time per year, and use the remaining time for other seasonal crops (Food Crops Agriculture Department, 2006). The crop growth duration is approximately three months, with a production of around five tons per hectare. The total rice acreage of the study region as reported for the year is 107,437.50 ha (Table 2.1).

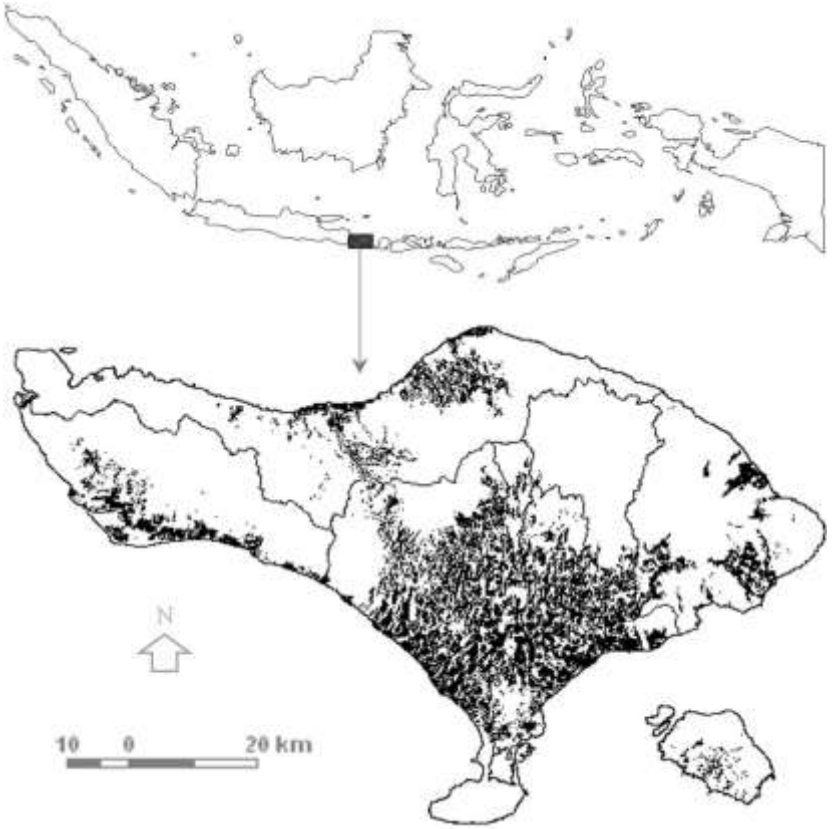

Figure 2.1 Map of the study area. Bali province consists of nine regencies. A black colour indicates the distribution of rice fields.

Table 2.1 Regency- wise reported total rice acreage in Bali (National Land Agency, 2008).

Regency	Total Area (ha)	Rice field area (ha)	Percentage
Badung	39450.00	12887.50	32.67
Bangli	52718.75	3537.50	6.71
Buleleng	131925.00	13606.25	10.31
Denpasar	12506.25	4181.25	33.43
Gianyar	36431.25	16800.00	46.11
Jembrana	85418.75	9462.50	11.08
Karangasem	83662.50	11418.75	13.65
Klungkung	31231.25	6462.50	20.69
Tabanan	84818.75	29081.25	34.29
Total	558162.50	107437.50	100.00

2.2.2 MODIS images

This study used daily MODIS 1b level images (calibrated radiances), with a spatial resolution of 250 m (MOD02QKM). The images can be downloaded free from the NASA website (www.ladsweb.nascom.nasa.gov/data/search.html). This data product offers the best available spatial resolution among all other MODIS products. A coarser spatial resolution will increase the possibility of mixed land coverage occurring in one pixel, decreasing the accuracy of the classification result (Strahler *et al*., 2006). In addition, at this level of MODIS imaging, there are several images for each acquisition date taken at different times. This level of imaging can increase the possibility of a clear image without clouds, which has become a big challenge in optical remote sensing.

Two spectral band data viz. red (620-670 nm) and near-infrared (841-875 nm) were used for this. We collected most of the MODIS images for different acquisition dates and times over a two-year period (2008 and 2009). Data of 2009 were used to develop the model, and that of 2008 were utilized to validate the model because the reference land use map was that of 2008. Cloud cover is not intense in the rice region of the study area, as clouds more frequently occur at higher elevations. However, to produce a cloud free image, cloud masks were generated using two band data for each acquisition date. The cloudy pixel was replaced with a clear pixel in a range of 14 days. Total 26 composite images were used in this study.

2.2.3 Calculation of vegetation index

Three vegetation indices were selected: the Normalised Difference Vegetation Index (NDVI), Ratio Vegetation Index (RVI), and Soil Adjusted Vegetation Index (SAVI). We used the radiance value of the MODIS images for each 14-day composite. The equations for these vegetation indices are as follows:

$$NDVI = \frac{nir-r}{nir+r} \tag{2.1}$$

$$RVI = \frac{nir}{r} \tag{2.2}$$

$$SAVI = \frac{(1+L)(nir-r)}{nir+r+L} \tag{2.3}$$

where *nir* is the near-infrared of the MODIS band (841-876 nm), *r* is the red band (620-670 nm), and *L* is a constant (related to the slope of the soil-line in a feature-space plot) that is usually set to 0.5.

Whereas NDVI is correlated to the leaf area index (LAI) of rice fields (Xiao *et al*., 2002), it has some limitations, including saturation under closed canopy and soil background (Huete *et al*., 2002; Xiao *et al*., 2003). The SAVI can minimise soil brightness influences from spectral vegetation indices involving red and near-infrared (NIR) wavelengths (Huete, 1988). On the other hand, the RVI is a good indicator of agriculture crop growth for the entire growth cycle (Gupta, 1993).

The advantages of using a vegetation index compared to a single band is the ability to reduce the spectral data to a single number that is related to physical characteristics of the vegetation (e.g., leaf area, biomass, productivity, photosynthetic activity, or percent cover) (Baret and Guyot, 1991; Huete, 1988). At the same time, we can minimise the effect of internal (e.g., canopy geometry, and leaf and soil properties) and external factors (e.g., sun-target-sensor angles, and atmospheric conditions at the time of image acquisition) on the spectral data (Baret and Guyot, 1991; Huete and Warrick, 1990; Huete and Escadafal, 1991).

2.2.4 Algorithm for Rice Field Mapping

The main difference in agriculture rice field characteristics compared with other land uses is the variation of land cover due to many types of vegetation planted in those areas. In irrigated rice fields, when the rice is planted, its land cover can vary from flooded at the beginning of transplanting, mixed between water and vegetation in the first month, almost full vegetation in the second and third month, to bare area just after harvesting time. The variation in land cover can be greater when the rice field area is planted with other seasonal crops. Similar cases also occur in non-irrigated rice fields, which have a significant difference in land cover between the rainy season (rice season) and dry season (other seasonal crops). On the other hand, other land uses, such as settlement, forest, and water, generally have similar land covers within a certain period. This situation will affect the reflectance value at certain times. Rice fields will have a fluctuating reflectance value, whereas other land uses will have relatively stable values. Based on these phenomena, temporal variance analysis is used to distinguish between rice

field areas and other land uses. The hypothesis proposed is that the radiance variance of the rice field will be much higher when compared to other land uses.

Temporal VI data was used to generate temporal variance map. A field survey was done to ensure the location of the training area on the Image, besides using the available land use/cover map. The training classes covered under field survey were: irrigated rice field, non-irrigated rice, mixed forest, settlement, lake water, mixed garden, shrub, dry land, mangrove, and bare land. These ten training classes were used to determine their variance in a year in each of the three VI image data sets. From the VI variance map, we calculated the mean and standard deviation of variance for the ten objects. The formula for the variance, mean of variance, and standard deviation of variance were calculated using the following equation:

$$Variance = \frac{1}{n-1}\sum_{i=1}^{n}(x_{i-}\bar{x})^2 \quad (2.4)$$

where x_i is the VI value of a pixel for image i, $\bar{x}$ is the mean of VI, and n is the number of images. In this study, n is equal to 26.

$$Mean = \frac{1}{n}\sum_{i=1}^{n} x_i \quad (2.5)$$

$$Standard\ Deviation = \sqrt{\frac{1}{n-1}\sum_{i=1}^{n}(x_{i-}\bar{x})^2} \quad (2.6)$$

Here, x_i is the variance values of a pixel for the training area i, $\bar{x}$ is the mean of variance, and n is the number of pixels in the training area.

The vegetation indices with the highest difference in the mean variance were selected as the best indices for distinguishing rice field and other land uses. Threshold values were required for rice field mapping. The pixel ranges within the threshold were mapped as rice fields with the following equation:

$$MeanVar - (n * Std) < x < MeanVar + (n * Std) \quad (2.7)$$

where *MeanVar*, *Std*, *n*, and *x* are the average of the rice field variance, the standard deviation of the rice field variance, the maximum distance from the standard deviation, and the variance average of the MODIS image that will be mapped as a rice field class, respectively.

2.2.5 Quantitative evaluation of classification result

The quantitative evaluation was performed by comparing the classification result with the existing land use maps released by the National Land Agency. To determine accuracy of the classification method developed in this study, we used two evaluation methods. First, we used a regression method using the area of analysis result and the reference data on the rice field as the dependent and independent variables, respectively. The coefficient of determination (R^2) and the root mean square error (RMSE) were the two statistical parameters evaluated in this study. The regression methods were applied at the regency and district level using 9 and 52 samples respectively, based on the number of regencies and districts in the study area. The R^2 and RMSE were calculated as follows:

$$R^2 = \frac{\sum(y-\hat{y})^2}{\sum(y-\bar{\hat{y}})^2} \tag{2.8}$$

where R^2, y, $\hat{y}$, $\bar{\hat{y}}$, and $\bar{\hat{y}}$ are the determination coefficient, a measured value, an estimated value, and an mean of the estimated values, respectively, and

$$RMSE = \sqrt{\frac{1}{n}\sum_{i=1}^{n}(\hat{y}_{i-}y_i)^2} \tag{2.9}$$

where *RMSE*, $\hat{y}_i$ y_i, and n are the root mean square error, an estimated value of i sample, a measured value of i sample, and the number of samples, respectively.

The second evaluation method used Kappa analysis (Congalton and Green, 1999). The Kappa analysis determined accuracy assessments and level of agreement between the remotely sensed classification and the reference data. The first step of Kappa analysis is to create an error matrix for all examined methods. In this study, only two classes were used, rice field and non-rice field. From the error matrix, we can calculate the commission error, omission error, and overall accuracy as follows:

$$Commission\ error = \frac{Total\ pixel\ of\ non\ rice\ field\ is\ classified\ as\ rice\ field}{Total\ pixel\ of\ rice\ field\ classification\ result} x\ 100 \tag{2.10}$$

$$Omission\ error = \frac{Total\ pixel\ of\ rice\ field\ is\ not\ classified\ as\ rice\ field}{Total\ pixel\ of\ actually\ rice\ field} x\ 100 \tag{2.11}$$

$$Overall\ accuracy = \frac{Total\ pixel\ of\ correctly\ classified}{Total\ sample} x\ 100 \tag{2.12}$$

The next step of the Kappa analysis is to calculate the estimated Kappa and Kappa variance as follows:

$$\hat{K} = \frac{n\sum_{i=1}^{k} n_{ii} - \sum_{i=1}^{k} n_{i.} n_{.i}}{n^2 - \sum_{i=1}^{k} n_{i.} n_{.i}} \tag{2.13}$$

where $\hat{K}$ is the estimated Kappa, n is number of sample tests, n_i is the sample row i, n_j is sample column j, and k is 'row x column'. The formula of Kappa variance is

$$\hat{\text{var}}(\hat{K}) = \frac{1}{n}\left(\frac{\theta_1(1-\theta_1)}{(1-\theta_2)^2} + \frac{2(1-\theta_1)(2\theta_1\theta_2 - \theta_3)}{(1-\theta_2)^3} + \frac{(1-\theta_1)^2(\theta_4 - 4\theta_2^2)}{(1-\theta_2)^4} \right) \tag{2.14}$$

where $\hat{\text{var}}(\hat{K})$ = Kappa variance,

$$\theta_1 = \frac{1}{n}\sum_{i=1}^{k} n_{ii},$$

$$\theta_2 = \frac{1}{n^2}\sum_{i=1}^{k} n_{i.} n_{.i},$$

$$\theta_3 = \frac{1}{n^2}\sum_{i=1}^{k} n_{ii}(n_{i.} + n_{.i}),$$

$$\theta_4 = \frac{1}{n^3}\sum_{i=1}^{k}\sum_{j=1}^{k} n_{ij}(n_{i.} + n_{.j})$$

Estimated Kappa values range from 0 to 1, though they can be negative and range from -1 to 1. However, because there should be a positive correlation between the remotely sensed classification and the reference data, positive Kappa values are expected. A perfect classification would produce a Kappa value of one and Kappa variance of zero. Typically, values greater than 0.80 (i.e, 80%) represent strong agreement between the remotely sensed classification and the reference data, whereas values between 0.4 and 0.8 represent moderate agreement. Anything below 0.4 is indicative of poor agreement (Congalton *et al*., 1983). Schematically, the research procedure is shown in Figure 2.2.

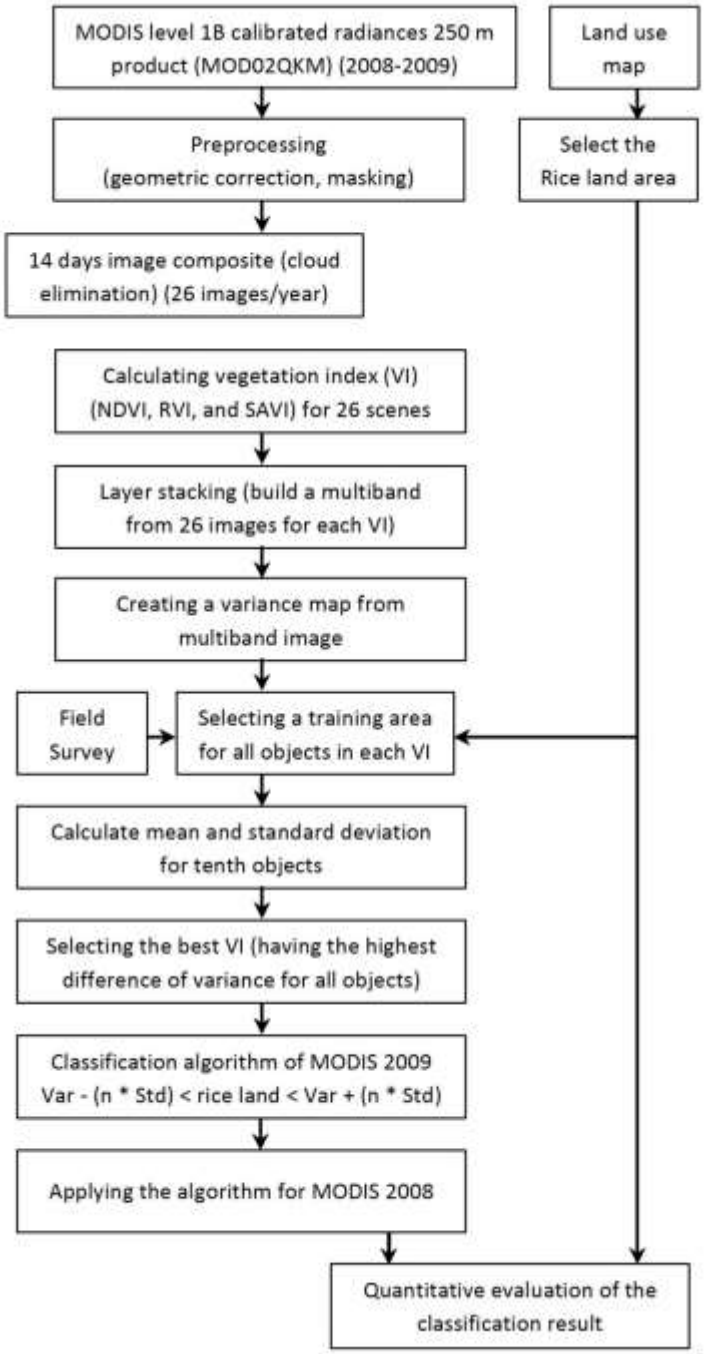

Figure 2.2 Flowchart of the research procedure.

2.3 Results and discussion

2.3.1 Temporal variability of the land uses vegetation index

The vegetation index of land uses varied in the study area during 2009. The highest variability appeared in the irrigated rice fields, followed by the non-irrigated rice fields. The other land uses, such as settlement, mixed garden, mixed forest, lake water, dry land, shrub, mangrove, and bare land had a relatively stable vegetation index for a year. The NDVI of the irrigated rice field was high at certain times and overlapped with mixed forest, mixed garden, dry land, and mangrove. However, the value was low at other times and was similar to the values for settlement and shrub (Figure 2.3). The non-irrigated rice field also had a similar tendency, although NDVI values were not as high as compared to the irrigated rice field. The high fluctuations in the vegetation index of irrigated and non-irrigated rice fields were due to the high variation in their land covers. When the areas were being planted with rice plants or other seasonal crops, the vegetation index was similar to that of mixed forest, mixed garden, mangrove or shrubs. However, if no crops were planted, the land cover resembled settlement or bare land.

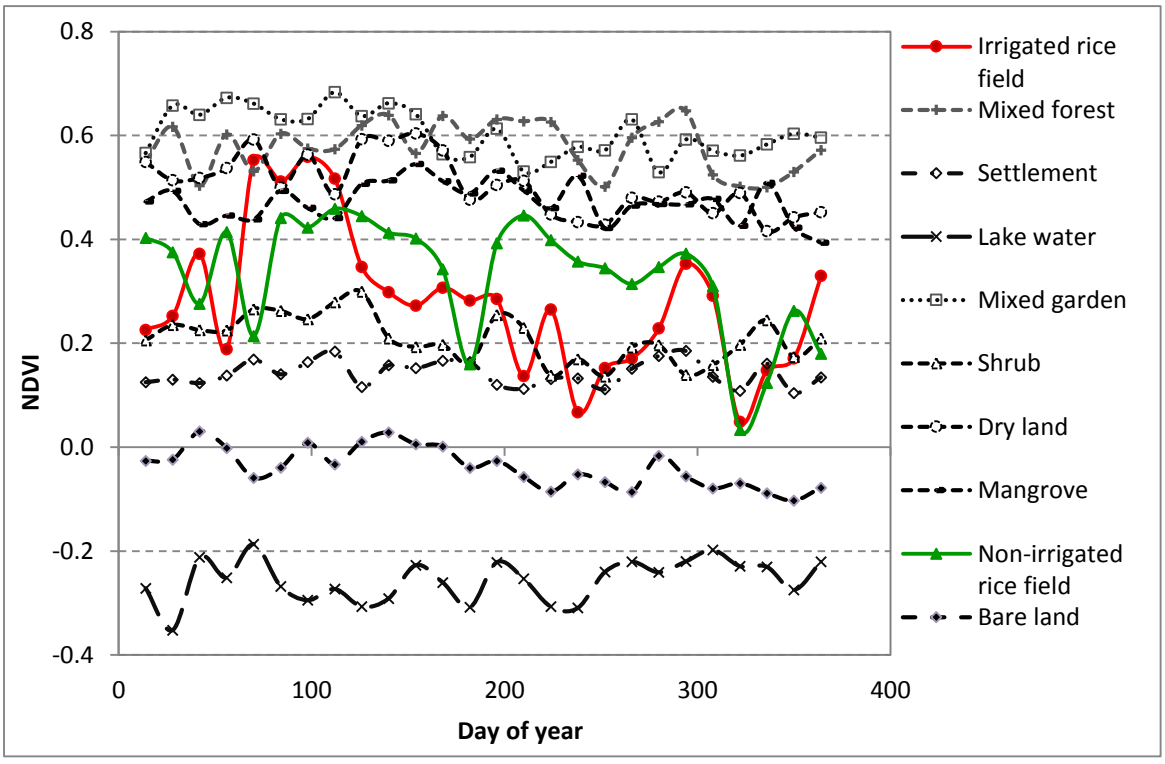

Figure 3 The NDVI temporal variability of irrigated rice fields, non-irrigated rice fields, and almost all of the land cover in study area from January 1 to December 31, 2009.

The irrigated rice field had the highest average variance of 0.0174, 0.4721, and 0.1892, for the NDVI, RVI, and SAVI, respectively. The non-irrigated rice field was next, with index values of 0.0166, 0.0989, and 0.1023 for the NDVI, RVI, and SAVI, respectively. The lowest average variance occurred for settlement, with the values of 0.0006 and 0.0040 for the NDVI and RVI, respectively. The bare land had a lowest average variance for the RVI with the value of 0.0033. Compared with other land uses, the average variance of the irrigated rice fields was higher, ranging from 5.6129 to 29.0000 times higher for the NDVI, 1.6432 to 118.0250 times higher for the RVI, and 2.4862 to 56.8828 times higher for the SAVI. Whereas for the non-irrigated rice fields, the average variances were 5.3548 to 27.6667 higher for the NDVI, 1.4817 to 106.4250 higher for the RVI, and 1.3443 to 30.7564 higher for the SAVI (Table 2.2).

To distinguish both irrigated and non-irrigated rice fields from other the land uses, the RVI can easily be used to differentiate between them from settlement, lake water, shrub, and bare land. However, it would be difficult to use the RVI to distinguish irrigated and non-irrigated rice fields from mixed forest and dry land because the differences in their variances are small. A similar case occurred for the SAVI. The SAVI can easily separate irrigated and non-irrigated rice fields from mixed garden, shrub, dry land, mangrove, and bare land. However, it was very difficult to differentiate mixed forest and lake water from non-irrigated rice fields. On the other hand, the NDVI can distinguish both irrigated and non-irrigated rice fields from other the land uses easily due to the minimum value of their difference variances, which were 5.6129 and 5.3548 for irrigated and non-irrigated rice fields, respectively. Therefore, the NDVI was selected for the rice field mapping.

Table 2.2 Mean of irrigated and non-irrigated rice field variance compared with other land uses.

Land Uses	NDVI	RVI	SAVI
Irrigated rice field variance	0.0174	0.4721	0.1892
Non-irrigated rice field variance	0.0166	0.4257	0.1023
Mixed forest variance	0.0025	0.2873	0.0761
Ratio from irrigated rice field	6.9600	1.6432	2.4862
Ratio from non-irrigated rice field	6.6400	1.4817	1.3443
Settlement variance	0.0006	0.0040	0.0352
Ratio from irrigated rice field	29.0000	118.0250	5.3750
Ratio from non-irrigated rice field	27.6667	106.4250	2.9063
Lake variance	0.0019	0.0041	0.0723
Ratio from irrigated rice field	9.1579	115.1463	2.6169
Ratio from non-irrigated rice field	8.7368	103.8293	1.4149
Mixed garden variance	0.0021	0.1255	0.0054
Ratio from irrigated rice field	8.2857	3.7625	35.2449
Ratio from non-irrigated rice field	7.9048	3.3927	19.0569
Shrub variance	0.0020	0.0207	0.0044
Ratio from irrigated rice field	8.7000	22.7800	43.1384
Ratio from non-irrigated rice field	8.3000	20.5411	23.3248
Dry land variance	0.0031	0.2364	0.0070
Ratio from irrigated rice field	5.6129	1.9969	27.0309
Ratio from non-irrigated rice field	5.3548	1.8006	14.6155
Mangrove variance	0.0015	0.0785	0.0035
Ratio from irrigated rice field	11.6000	6.0125	54.3151
Ratio from non-irrigated rice field	11.0667	5.4216	29.3680
Bare land variance	0.0014	0.0052	0.0033
Ratio from irrigated rice field	12.4286	90.5390	56.8828
Ratio from non-irrigated rice field	11.8571	81.6404	30.7564

2.3.2 Classification of rice fields

To apply the NDVI variance for rice field mapping, a threshold value was determined. According to Equation 2.7, the mean and standard deviation of the rice field NDVI variance will be used as the threshold value. The mean and standard deviation were 0.0174 and 0.0028 for irrigated rice fields and 0.0166 and 0.0023 for non-irrigated rice fields, respectively (Table 2.3).

Table 2.3. Mean and standard deviation of irrigated and non-irrigated rice fields variance.

Rice Field	Mean	Std. deviation
Irrigated rice field variance	0.0174	0.0028
Non-irrigated rice field variance	0.0166	0.0023

The differences in the mean and standard deviations of the irrigated and non-irrigated rice fields variance were not large. Therefore, using irrigated and non-irrigated rice fields as separate classes proved difficult because of some overlapping values. Therefore, both types of rice field were mapped as one class. Based on the analysis results, using an n value of 1.2 in Equation 2.7 provided the best result. Therefore, the threshold value of both types of rice field is as follows:

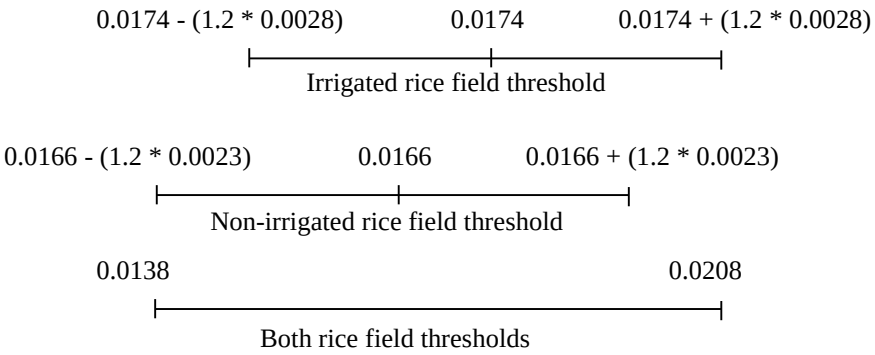

The pixels having a temporal variance between 0.0138 and 0.0208 were classified as a rice field. Although irrigated and non-irrigated rice fields had the highest mean temporal variance, we did not use a threshold value ≥ 0.0138 because of the cloud effect in the MODIS images. Although a 14-day composite was created to replace cloudy images with clearer images, to remove all of the clouds from MODIS images is very difficult, especially in tropical areas. Thin clouds greatly affect the reflectance and the vegetation indices and increase the temporal variance of the pixel. Therefore, to avoid classifying a cloudy pixel as a rice field, we used the maximum threshold. In this study, we did not classify all of the land uses found in study area because only rice fields had a high variability in the temporal variance. Other land uses, such as mixed garden, shrub, and mixed forest had similar variances and would become a single class if the algorithm were applied. The same is true for lake water, mangrove and bare land (Table 2.2).

The change in land cover of the rice fields from the initial flooding of the fields to harvesting takes place over a short time period. This change will produce large differences in spectral values and in the rice field indices over that time. The high degree

of variation in the land cover of the rice field could be used to obtain more effective separation of rice fields from other land uses, using the variance analysis presented here.

The results of the rice field classification using the algorithm developed in this study are shown in Figure 2.5. Compared with the reference data (National Land Agency, 2008) (Figure 2.5b), the rice field map produced from our analysis (Figure 2.5a) was visually similar to the reference. Differences of pixel location between analysis result and reference data shows at Figure 1.5c.

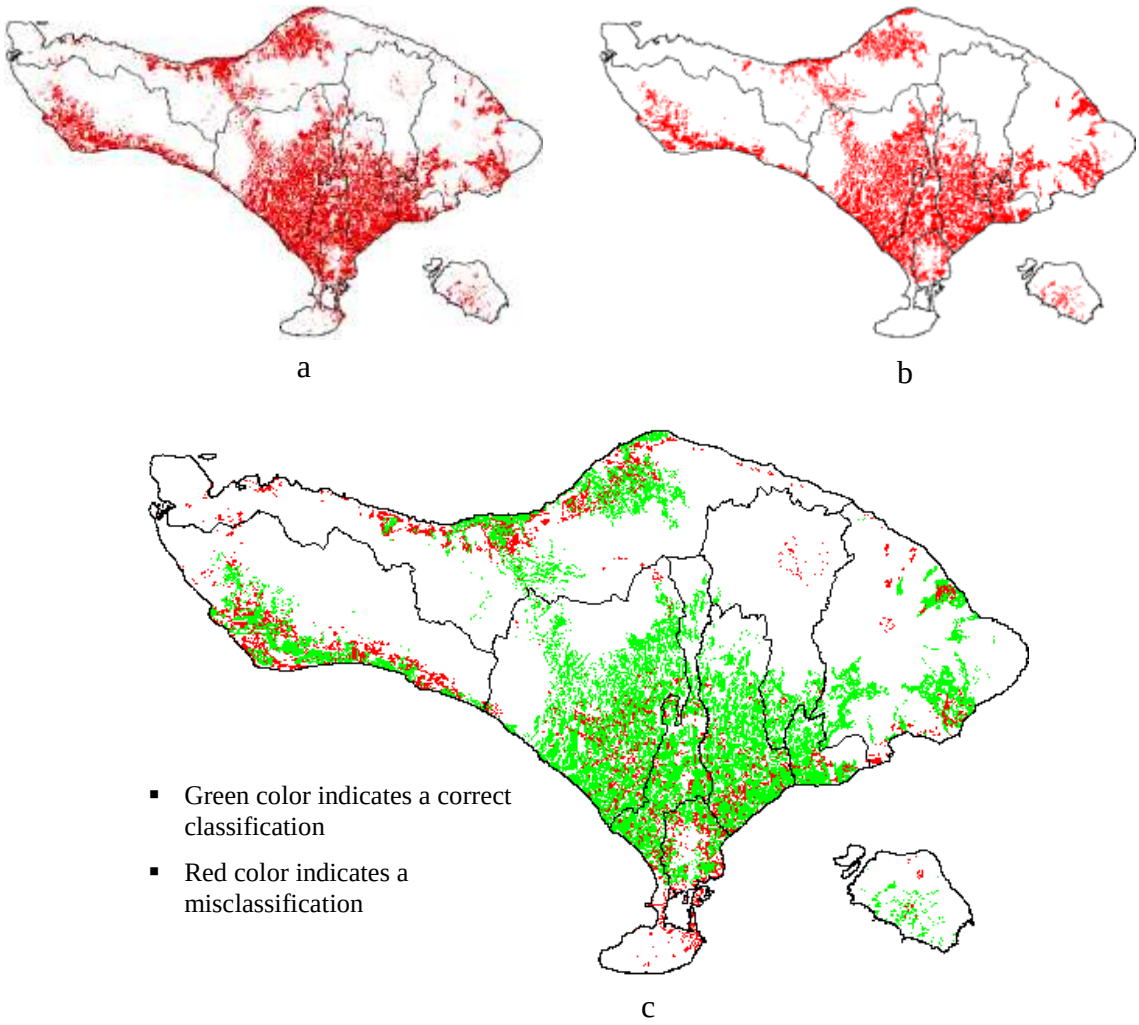

Figure 2.5 Rice field maps derived from this analysis (a) compared with reference data (b), and pixel locatioan difference of analysis and reference data (c)

If we look at the misclassification pixel at Figure 3.5c, mostly it found in northern and western part of the study area. This is caused by at this locations, total of rice field area was narrow compared to at the middle of study area. The narrow rice field will give greater possibilities to find a mixed pixel. Mixed pixel is one pixel of satellite data (6.25

ha in Modis image) can contain more than one land cover. Presence of mixed pixel will decrease the accuracy of land cover classification (Strahler *et al*., 2006).

Table 2.4 shows a quantitative comparison between the algorithm used in this study and the reference data. The analysis showed 19.92% deviation compared to the reference data.

Table 2.4 Comparison of rice area derived from this analysis with the reference data at the regency level.

Regency	Reference data		Analysis Result	
	Area (ha)	%	Area (ha)	%
Badung	12 887.50	12.00	15 106.25	11.73
Bangli	3 537.50	3.29	4 481.25	3.48
Buleleng	13 606.25	12.66	18 900.00	14.67
Denpasar	4 181.25	3.89	4 643.75	3.60
Gianyar	16 800.00	15.64	18 987.50	14.74
Jembrana	9 462.50	8.81	13 706.25	10.64
Karangasem	11 418.75	10.63	12 506.25	9.71
Klungkung	6 462.50	6.02	6 475.00	5.03
Tabanan	29 081.25	27.07	34 031.25	26.41
Total	107 437.50	100.00	128 837.50	100.00
Ratio from reference data %	0.00	-	19.92	-

2.3.3 Accuracy assessment of classification result

The first accuracy assessment was performed using regression analysis. The classifications produced from this study were compared with the reference data at the regency and district level using a linear relationship. The values of the coefficient of determination (R^2) were 0.9749 and 0.9229 for the regency and district level comparisons, respectively. The root mean square error (RMSE) was used to assess the accuracy of the classification results. The RMSE values for the analyses in this study were 1570.70 ha and 551.36 ha for the regency and district level comparisons, respectively (Figure 2.6). A high R^2 and low RMSE imply good agreement between the analysis results and the reference data. The good agreement between analysis of the MODIS data and the reference data for the rice field study is consistent with results reported by Tingting *et al.* (2010) at the provincial level and by Boschetti *et al.* (2009), with a R^2 of 0.92 (n = 24).

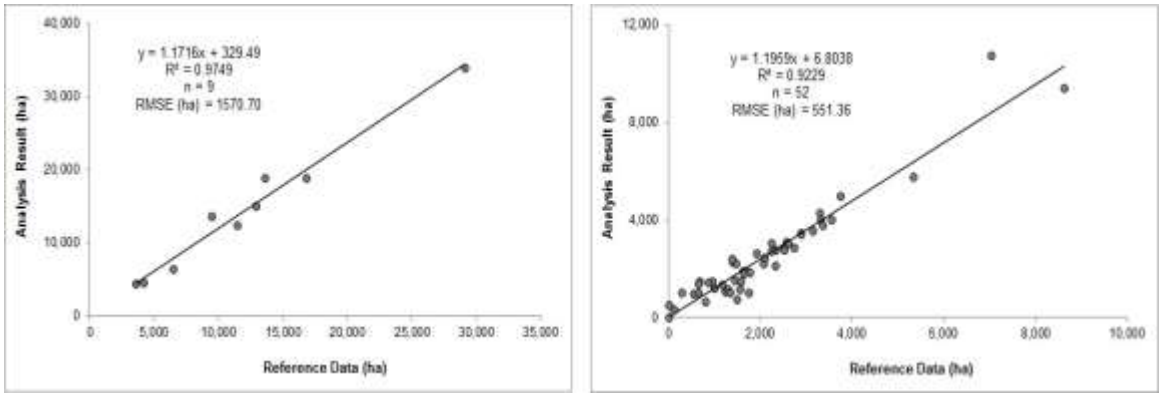

(a) (b)

Figure 2.6 Relationship between rice area from the reference data and produced from this analysis at the regency (a) and district (b) level.

Kappa analysis is one of the most popular methods for determining accuracy, error, and agreement between the remotely sensed classification and the reference data (Congalton and Green, 1999). To apply the Kappa analysis, an error matrix for the classification result was created. After the images were classified, we took 1795 points (2% of the total MODIS pixels) from a stratified random sample of rice field and non-rice field classes. The error matrices are shown in Table 2.5.

Table 2.5 Error matrices of the rice field classification results.

		Reference data		
		Rice Field	Non-rice field	Total
Classification Result	Rice field	263	146	409
	Non-rice field	82	1304	1396
	Total	345	1450	1795

From the error matrices, the commission, omission, and overall accuracy were calculated using equations 3.10 - 3.12. The algorithm developed in this study had commission error, omission error, and overall accuracy of 35.45%, 17.68%, and 87.91% respectively. Furthermore, estimated Kappa and Kappa variance were calculated using equations 3.13 – 3.14. Value of 0.8371 and 0.000109, respectively, were obtained (Table 2.6). The overall accuracy of more than 80% and the estimated Kappa of more than 0.8

demonstrate strong agreement between the remotely sensed classification and the reference data (Lillesand and Kiefer, 2000; Congalton *et al*., 1983).

Table 2.6. Kappa parameters of rice field classification results.

Kappa parameters	Value
Commission error (%)	35.45
Omission error (%)	17.68
Overall accuracy (%)	87.91
Estimated Kappa	0.8371
Kappa variance	0.000109

Compared to other previous study, Gumma et al., 2011 reported rice classification in South Asia using spectral matching techniques and decision trees method of multi-temporal Modis produced overall accuracy of 80%. Xiao et al., 2005 mapped agriculture rice field in southern China used three vegetation indices (LSWI, EVI, and NDVI) derived from Modis images to identify that initial period of flooding and transplanting in paddy rice fields. The accuracy in flat and hilly province was 79.4% and 55%, respectively. Ekahitanonda *et al* (2004) applied fuzzy logic and genetic algorithms of multi-temporal Landsat TM for rice classification. The accuracy of classification rice was 63.28%. On the other hand, Chen *et al* (2007) used supervised wishart classifier for rice mapping using multi-temporal Envisat Asar Aps data. They found the overall accuracy was 79.4%. In Indonesia, Uchida (2010) mapped the rice field in West Java using Landsat data and five vegetation indices with own method resulted similar accuracy with this study of 87.9%, and Sari *et al* (2010) used Modis data with phenology approach to map the rice field in Northern part of West Java produced R^2 of 0.6, 0.7 and 0.6 for monthly, quarterly, and yearly, respectively compared with the statistical data.

2.4. Conclusions

The temporal variability of the vegetation index for irrigated and non-irrigated rice fields was higher compared to other land uses. From the three vegetation indices evaluated in this study, NDVI emerged as the best choice for rice field mapping because of large variance differences of rice classes compared to other land use/cover classes. Using variance threshold values from 0.0138 to 0.0208 provided the best rice field classification results. The regression analysis showed that the method in this study

produced high R^2 values of 0.9749 and 0.9229 for the regency and district level comparison, respectively. The method in this study also produced low RSME values of 1,570.70 ha and 551.36 ha for the regency and district level comparisons, respectively. The overall accuracy of the method in this study was at 87.91%. The commission and omission errors were 35.45 and 17.68, respectively. The Kappa analysis demonstrated strong agreement between the analysis of the MODIS data using the method developed in this study and the reference data, with a Kappa value of 0.8371. This study shows that temporal variance analysis is one of best suited method to map the rice areas compared to previous method.

CHAPTER 3

SPECTRAL CHARACTERISTICS AND MAPPING OF RICE PLANTS USING MULTI-TEMPORAL LANDSAT DATA

3.1 Introduction

Rice is one of the world's major staple foods, and paddy rice fields account for approximately 15% of the world's arable land (IRRI, 1993). In Indonesia, rice is one of the most important agricultural plants because rice is the main food consumed by Indonesians. Food security has long been an important political goal in Indonesia, and this goal is most commonly associated with rice self-sufficiency. In the mid-1980s, Indonesia briefly achieved 100% self-sufficiency for rice; however, growth of rice production slowed in the 1990s, leading to an increase in imports and a lower self-sufficiency ratio. The rice self-sufficiency ratio has remained around 95% over the last two years, but it dropped below 90% during the El Niño drought of 1998 (Bappenas, 2002).

To determine the potential for rice self-sufficiency, rice production must be estimated. Conventionally, calculation of rice production is usually performed after harvest by collecting information from farmers. Another way rice production can be determined involves taking a rice grain from a sample area and then converting it to total of the harvest area. Both methods of rice production estimation are conducted during rice harvesting periods. These methods frequently takes a long time; therefore, it would be beneficial to gain information about rice production more quickly prior to harvest to make better judgments related to rice self-sufficiency and rice import. In addition, mapping of rice fields is important for management of water resources and estimation of gas emissions (Xiao *et al*., 2005)

Rice plants have specific land cover properties. Rice land coverage changes during the rice life circle. In irrigated rice fields, almost all land coverage is dominated by water during the plantation period. As the rice ages, rice vegetation coverage grows and reaches a maximum (rice age = 2 months) and then gradually decreases until harvest time (Shao *et al*. 2001, Nuarsa *et al*., 2005).

Satellite remote sensing has been widely applied and has been recognised as a powerful and effective tool in detecting land use and land cover changes (Ehlers *et al*.,

1990; Meaille and Wald, 1990; Treitz *et al*., 1992, Westmoreland and Stow, 1992; Harris and Ventura, 1995; Yeh and Li, 1999; Patil *et al*., 2003). Satellite remote sensing provides both cost-effective multi-spectral and multitemporal data (Paine, 1981). Satellite imagery has been used to monitor discrete land cover types by spectral classification. Additionally, it has been utilised to estimate biophysical characteristics of land surfaces via linear relationships with spectral reflectance or indices (Steininger 1996, Nuarsa *et al*., 2007).

Studies using satellite imaging to monitor rice growth have been reported (Shao *et al.*, 1997; Kuroso *et al*., 1997; Le Toan *at al*., 1997; Panigrahy and Sharma, 1997; Oette *et al*., 2000; Shao *et al*., 2001; David *et al*., 2004). Some of this research has been used globally as along with moderate image resolution, such as National Oceanic and Atmospheric Administration Advanced Very High Resolution Radiometer (NOAA AVHRR) and Moderate Resolution Imaging Spectroradiometer (MODIS), to monitor rice fields (Panigrahy *et al*., 1992; Fang *et al*., 1998; Wataru *et al*., 2006; Xiao *et al*., 2005). However, the use of moderate and global spatial resolution of satellite imaging has been restricted, particularly in small rice areas because many types of land cover appear in one pixel, which reduces the accuracy of the assessment (Strahler *et al*., 2006). In contrast, utilisation of fine or medium spatial resolution of satellite images, especially in session plants, has been limited because fewer images are available during the 120-day rice growth period (Currey *et al*., 1987).

In capture 2, the algorithms for rice field classification have developed using Modis image because Modis data has a good temporal resolution. The algorithm is suitable to be applied to broad rice field. On a narrow rice field, a better spatial resolution of satellite image is required. Landsat ETM+ has a good temporal, spatial, and spectral resolution for rice monitoring. The revisit time of Landsat ETM+ is 16 days with a spatial resolution of 30 m. Landsat ETM+ has six bands with the same pixel size, and it has become beneficial in the development of the algorithms for rice modelling (Christopher, 2004).

The objectives of this study included the following: (1) to find out relationship between rice spectral and rice age; (2) to develop a rice growth vegetation index (RGVI); (3) to map rice distribution and its age; and (4) to quantitatively compare the rice plant area between the analysis result and reference data.

3.2 Methodology

3.2.1 Description of the study area

The study was conducted in the Tabanan Regency of the Province of Bali, Indonesia, centred at latitude 8°29'46" S and longitude 115°29'48" E (Figure 3.1). The Tabanan Regency was selected for the study area because Tabanan is the central production area of rice in Bali. The irrigated paddy rice area in Bali was not only planted by the rice but also with other session agriculture plants, such as corn and soybeans. Rice planting in Bali is coordinated by the social farmer organisation, namely *Subak*, and it is related to the management of water resources. Each Subak usually consist of around 150 - 300 ha of paddy rice. In each *Subak*, farmers plant rice at the same time; thus, identification of the agriculture rice area from space using remote sensing data, such as Lantsat ETM+, may be easier. This study involved the use of three Subaks in three different districts, including Bengkel Subak (Kediri district), Sungi Subak (Marga District), and Risaja Subak (Penebel District). Field observation was done at 9 station points (Table 3.1).

The elevation of the study area ranged from 30 – 290 m asl. All rice plants observed were of the Ciherang rice variety, with a life cycle of around 115 days and yields reaching 5.0 tons/ha.

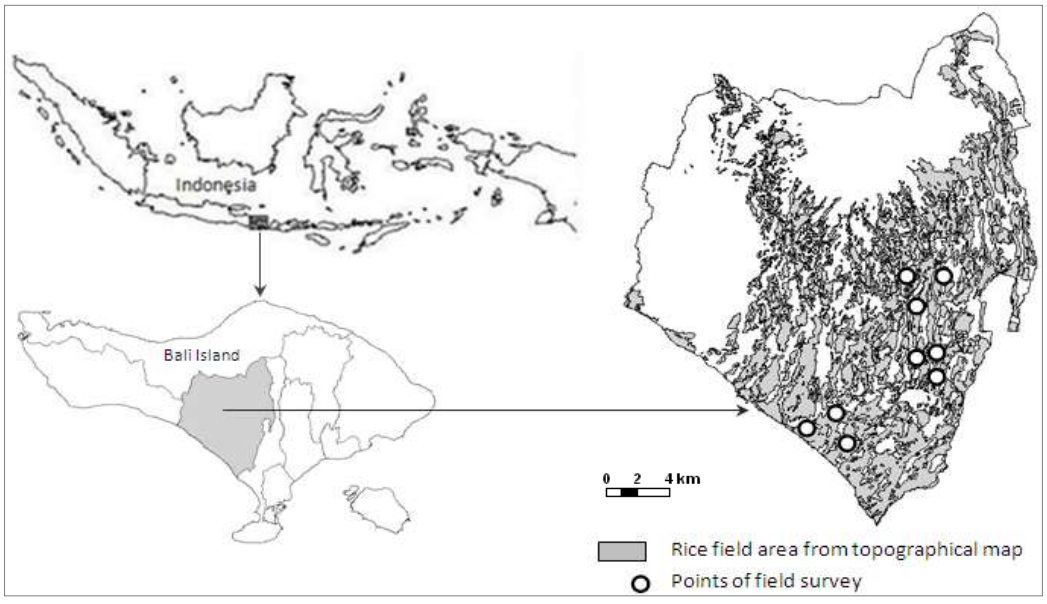

Figure. 3.1. Location map of the study area.

Table 3.1. Description of the field observation location

Site Code	Site Name	Coordinate		Elevation (m asl)	Plantation Date	Rice Variety
		X	Y			
K1	Kediri-1	289310	9048966	46	12-Jun-2005	Ciherang
K2	Kediri-2	288746	9049668	38	23-May-2005	Ciherang
K3	Kediri-2	289833	9050236	52	8-Jun-2005	Ciherang
M1	Marga-1	297438	9056641	168	15-Jul-2005	Ciherang
M2	Marga-2	297777	9056203	163	13-Jul-2005	Ciherang
M3	Marga-3	298158	9057479	171	7-Jul-2005	Ciherang
P1	Penebel-1	292220	9064219	287	20-Jul-2005	Ciherang
P2	Penebel-2	291817	9063737	266	24-Jul-2005	Ciherang
P3	Penebel-3	292487	9063358	272	27-Jul-2005	Ciherang

3.2.2 Landsat image data

Landsat satellite images have 8 bands, including a thermal and a panchromatic band. In visible, near infrared and middle infrared regions, Landsat ETM+ has 30-m spatial resolution. However, in thermal and panchromatic regions, spatial resolutions are 60 m and 15 m, respectively. This study used both visible and reflectance infrareds (Band-1 - 5 and band-7) of Landsat ETM+ (Table 3.2). Although the Landsat ETM+ used in this study had the SLC off, considerations of better spatial, spectral, and temporal resolution of these images made it relevant to use. With 16 days of temporal resolution, Landsat ETM+ was the good satellite image for rice monitoring because rice has a growth circle length around 90 days.

Table 3.2. Spectral ranges and spatial resolutions of Landsat 7 ETM+ bands.

Band number	Band divisions	Spectral range (μm)	Spatial resolution (m)
1	Blue	0.45–0.515	30
2	Green	0.525–0.605	30
3	Red	0.63–0.690	30
4	Near-infrared	0.75–0.90	30
5	Mid-infrared	1.55–1.75	30
7	Mid-infrared	2.09–2.35	30

The total of amount of time series images that could be collected in one rice growth circle was approximately six images at different acquisition dates. Some of the images could not be used due to cloud conditions or the appearance of SLC-off on station points, which caused a reduced availability of images. Fortunately, our study area was covered by two scenes of Landsat images in different paths. The Landsat images from two different years (2002 and 2005) used in this study are shown in Table 3.3. Landsat Images from 2005 were used for rice modelling, and in 2002, they were utilised to apply the model for rice plant distribution mapping.

Table 3.3. Value of τ_0[(1)], S_0[(2)], and a[(3)] for every spectral Landsat Band

Band	τ_0	S_0 ($Wm^{-2}\mu m^{-1}$)	a
ETM1	0.5	1997	0.7757
ETM2	0.3	1812	0.7957
ETM3	0.25	1533	0.6192
ETM4	0.20	1039	0.9655
ETM5	0.125	230.8	0.1257
ETM7	0.075	84.9	0.0437

Sources: (1) Dozier (1989); (2) Chander *et al.* (2009); (3) our image with calculation

3.2.3 Data analysis

a. Radiometric corrections

In temporal analysis of the remote sensing data, radiometric corrections are the important part of the image analysis. The digital number (DN) of the Landsat ETM+ at different acquisition dates was converted to the corrected digital number (cDN) to eliminate the effect of the radiometric and atmospheric of images, so they had comparable values. In this study, we used a simple radiometric correction model introduced by Pons and Solé-Sugrañes (1994). The form of the model is shown in the following equation:

$$cDN = 1000a(DN - K_l)d^2/[\mu_s S_0 e^{(-\tau_0/\mu_0)} e^{(-\tau_0/\mu_v)}] \quad (3.1)$$

(i) (if 250 < cDN ≤ 318.3; cDN = 254),
(ii) (if cDN > 318.3; *cDN* = 255),
(iii) (if $\mu_s \leq 0$; Vc = 255),

where cDN is the corrected digital number, cDN is the conversion of the effective reflectance to the common 8-bit format of most image processors, and the output range of values was limited to between 0 and 255. Note that a, K_l, S_0, and τ_0 depend on the wavelength and have different values for each spectral band; K_l depends on each image because it is related to atmospheric conditions; μ_0 and μ_s depend on latitude, date, and time of the satellite pass; μ_s depends on the slope and aspect of each pixel; d depends on the date of the satellite pass; and μ_v depends on the sensor viewing angle. The parameter μv is 1 in most cases of Landsat-ETM images because V is 0 at the nadir and has small values on the rest of the image (Pons and Solé-Sugrañes, 1994)

Practically, to apply the algorithm above we only needed a DEM with good quality (altimetrically and planimetrically) because the other parameters were known (e.g., S_0) or could be inferred from images (e.g., K_l). To avoid overcorrections and undercorrections on the ridges and channels and to account for local phenomena, it was important to use a DEM with a planimetric resolution comparable to the geometric resolution of the image. Naugle and Lashlee (1992) showed that a DEM of 95 m can be insufficient for a Landsat TM image over rugged terrain. In this study, we derived a DEM from a topographical map with a spatial resolution of 30 m. The values of parameters used in Equation 3.1 are shown in Table 3.3-3.4.

Table 3.4. Value of $d^{(1)}$, μ_0 [(2)], and $K_l^{(3)}$ for every acquisition date of Landsat ETM+

Acquisition date	Path	Row	DOY	d	μ_0	K_l					
						ETM1	ETM2	ETM3	ETM4	ETM5	ETM7
26 April 2002	116	66	116	1.00626	0.79414	51	31	23	20	17	11
12 May 2002	116	66	141	1.01210	0.75100	53	32	22	23	19	14
7 July 2005	117	66	188	1.01669	0.71514	52	34	22	25	21	11
1 August 2005	116	66	213	1.01497	0.74624	50	31	23	19	16	12
17 August 2005	116	66	229	1.01244	0.78085	53	33	23	22	18	13
24 August 2005	117	66	236	1.01103	0.80312	55	35	24	23	15	10
4 October 2005	116	66	277	1.00033	0.88006	54	34	24	21	17	12
5 November 2005	116	66	309	0.99152	0.89145	53	32	23	20	16	10
12 November 2005	117	66	316	0.98983	0.90081	52	31	22	24	21	11

Sources: (1) Chander *et al* (2009); (2) our image with calculation; (3) DN of our image. DOY is day of year

b. Calculating the relationship between rice spectral and rice age

Gathering cDN values from the Landsat pixels for the ninth site observation in of the entire rice growth period was the next step of our data analysis. In each acquisition

date of the Landsat images, pixel samples were taken randomly in the ninth field observation site (Figure 3.1). The average value of the sample was used as a representative cDN value in that acquisition date. The relationship between rice age and rice spectral was done for both band spectral of Landsat ETM+ and vegetation index with the following equation:

$$y = f(x) \tag{3.2}$$

where y is the rice age, and x is the rice spectral. Several vegetation indexes that were evaluated in the study are shown in Table 3.5.

Table 3.5. Several existing vegetation indices used in the study

No	Vegetation Index	Formula
1	Normalized Difference Vegetation Index (NDVI)	$NDVI = \frac{nir - r}{nir + r}$
2	Ratio Vegetation Index (RVI)	$RVI = \frac{nir}{r}$
3	Infrared Percentage Vegetation Index (IPVI)	$IPVI = \frac{nir}{nir + r}$
4	Difference Vegetation Index (DVI)	$DVI = nir - r$
5	Transformed Vegetation Index (TVI)	$TVI = \frac{100}{\sqrt{\frac{nir - r}{nir + r} + 0.5}}$
6	Soil Adjusted Vegetation Index (SAVI)	$SAVI = \frac{(1 + L)(nir - r)}{nir + r + L}$

Where nir, r, and L are near infrared band, red band, and canopy background brightness correction factor, respectively.

The relationship between rice age and both the cDN and vegetation index was evaluated using statistical parameters, including determination coefficient (R^2), level of significant value of analysis of variance (ANOVA), and standard error of estimation. The highest R^2, lowest significant value of ANOVA, and lowest standard error of estimation of the relationship between rice age and Landsat spectral of rice was selected and used for rice plant mapping model. The R^2 and standard error of estimation (SE) was calculated using the following equation:

$$R^2 = 1 - \frac{\sum y - \bar{y}')^2}{\sum y - y')^2} \tag{3.3}$$

$$SE = \sqrt{\frac{\sum(y - y')^2}{n}} \tag{3.4}$$

c. Development of a rice growth vegetation index (RGVI)

Theoretically, rice plants in normal conditions are the same, like vegetation in general. Chlorophyll pigments that are present in leaves absorb red light. In the NIR portion, radiation is scattered by the internal spongy mesophyll leaf structure, which leads to higher values in NIR channels. This interaction between leaves and the light that strikes them is often determined by their different responses in the red and NIR portions of reflective light (Niel and McVicar, 2001). In contrast, absorption properties of the middle infrared band cause a low reflectance of rice plants in this channel (Lilliesand and Kiefer, 1994). In irrigated rice fields, especially in early transplanting periods, water environment plays an important role in rice spectral. The blue band of Landsat ETM+ has good sensitivity to the existence of water; therefore, development of a rice growth vegetation index (RGVI) in this study used the B1, B3, B4, B5, and B7 of Landsat ETM+ with the following equation:

$$RGVI = \frac{(B4 + B5 + B7) - (B1 + B3)}{(B4 + B5 + B7)} \tag{3.5}$$

The equation above is then simplified as follow:

$$RGVI = 1 - \frac{(B1 + B3)}{(B4 + B5 + B7)} \tag{3.6}$$

where RGVI is the rice growth vegetation index, and B1, B3, B4, B5, and B7 refer to the band of Landsat ETM+.

d. Mapping rice plant and age

Mapping distribution of rice plants used at least two Landsat images from sequential acquisition dates, with the following steps:

1. Converting the VI of the Landsat image to rice age using the best relationship equation between VI and rice age for both Landsat images from sequential acquisition dates. This procedure produces two rice plant maps, age_t and age_{t+n}.
2. Calculating the difference of rice plant age (Δage) with the equation below:

$$\Delta age = age_{t+n} - age_t \tag{3.7}$$

where Δage, age_t and age_{t+n} are maps of different rice plant ages from two sequential acquisition dates of Landsat imaging, rice age map in t acquisition date, rice age map in t + n day acquisition date, respectively.

3. Calculating different days of sequential acquisition dates of Landsat image (Δt).
4. Comparing Δage and Δt. The pixels that satisfy with the following equation are classified as rice plants, which include the standard error of calculation (SE).

$$\Delta age - SE \leq \Delta t \leq \Delta age + SE \quad (3.8)$$

Schematically, the research procedure used in this study is illustrated in the following flowchart.

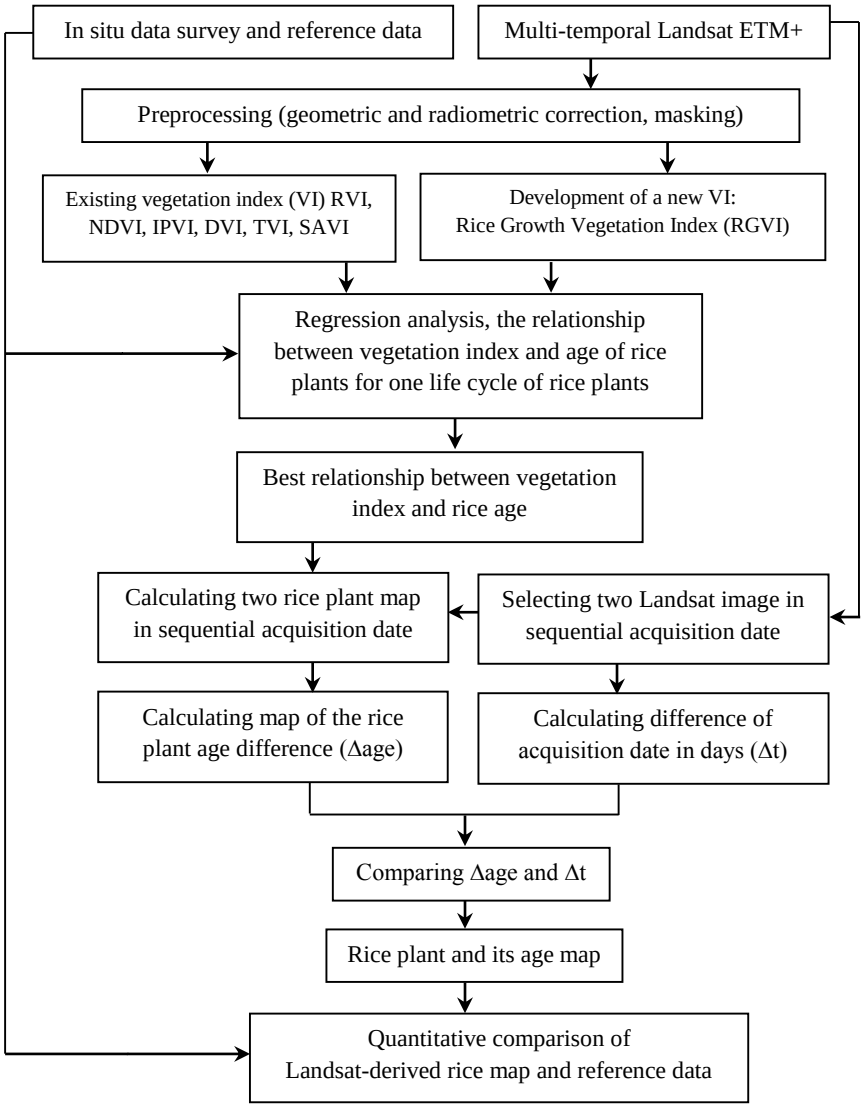

Figure 3.2. Data analysis procedure used in this study

e. Quantitative evaluation of rice plant area

Quantitative evaluation of rice plant area was performed by comparison of rice plant areas derived from analysis of Landsat to rice plant areas from the reference data in district level comparison. The reference data was obtained from the Statistic Center Agency of Tabanan Regency (BPS, 2002). Rice plant area data were then plotted in a chart to determine their relationship, R^2, and standard error of the estimation.

3.3 Results and Discussion

3.3.1 Relationship between rice spectral and rice age

In normal condition, rice vegetation indices form a quadratic relationship with the age of rice. Low vegetation index values were found in the beginning of transplanting time. Along with increasing the rice age, the vegetation index is rising as well until the peak of rice growth approximately 2 months and decreasing again until the harvest time (Nuarsa and Nishio, 2007). In this case, the rice vegetation indices could be estimated in each rice age.

In other case, if we would like to predict the rice age from the rice spectral, we not only need to flip the X and Y axis, but also reversed the X or Y value to obtain the proper relationship. Because of the possibility of vegetation index is negative, in this study, the age of the rice plant was inverted first before find out their relationship with the vegetation index.

Based on statistical analysis, reversal of rice age into 1/rice age$^{0.5}$ showed a good relationship between rice plant spectral and rice age. Figure 3.3 shows a linear relationship between rice age and rice cDN, whereas Figure 3.4 illustrates an linear relationship between rice age and vegetation index. The best relationship between rice age and rice cDN was provided by Band 5, followed by Band 4 and Band 7 of Landsat ETM+, with the determination coefficients (R^2) of 0.8735, 0.8143, and 0.7633, respectively. Visible bands (Band 1, Band 2, and Band 3) showed weak relationships to rice plant age, with R^2 values of 0.2721, 0.0854, and 0.3761, respectively. However, using multiple bands of Landsat ETM+ as a vegetation index gave a better relationship between rice plant age and rice spectral than was obtained utilising a single band. All vegetation indexes evaluated in this study showed a strong relationship with rice age. The

Rice Growth Vegetation Index (RGVI) that was developed in this study gives the best relationship, with R^2 = 0.9646, followed by TVI, NDVI, IPVI, SAVI, and DVI, with R^2 values of 0.8719, 0.8138, 0.8137, 0.8134, and 0.7841, respectively.

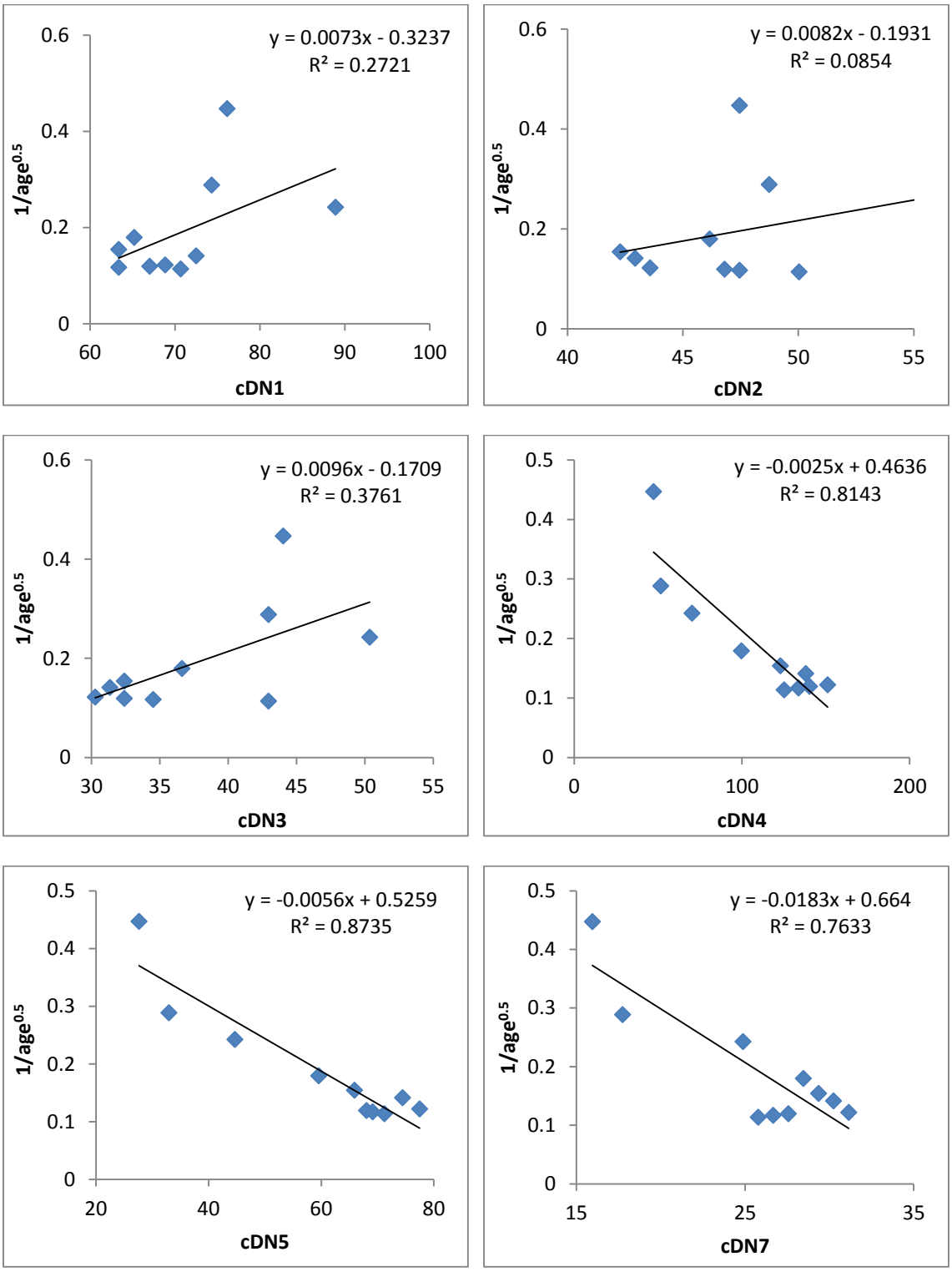

Figure 3.3. Relationship between rice cDN (cDN1-cDN7) of Landsat ETM+ and rice age in $1/age^{0.5}$

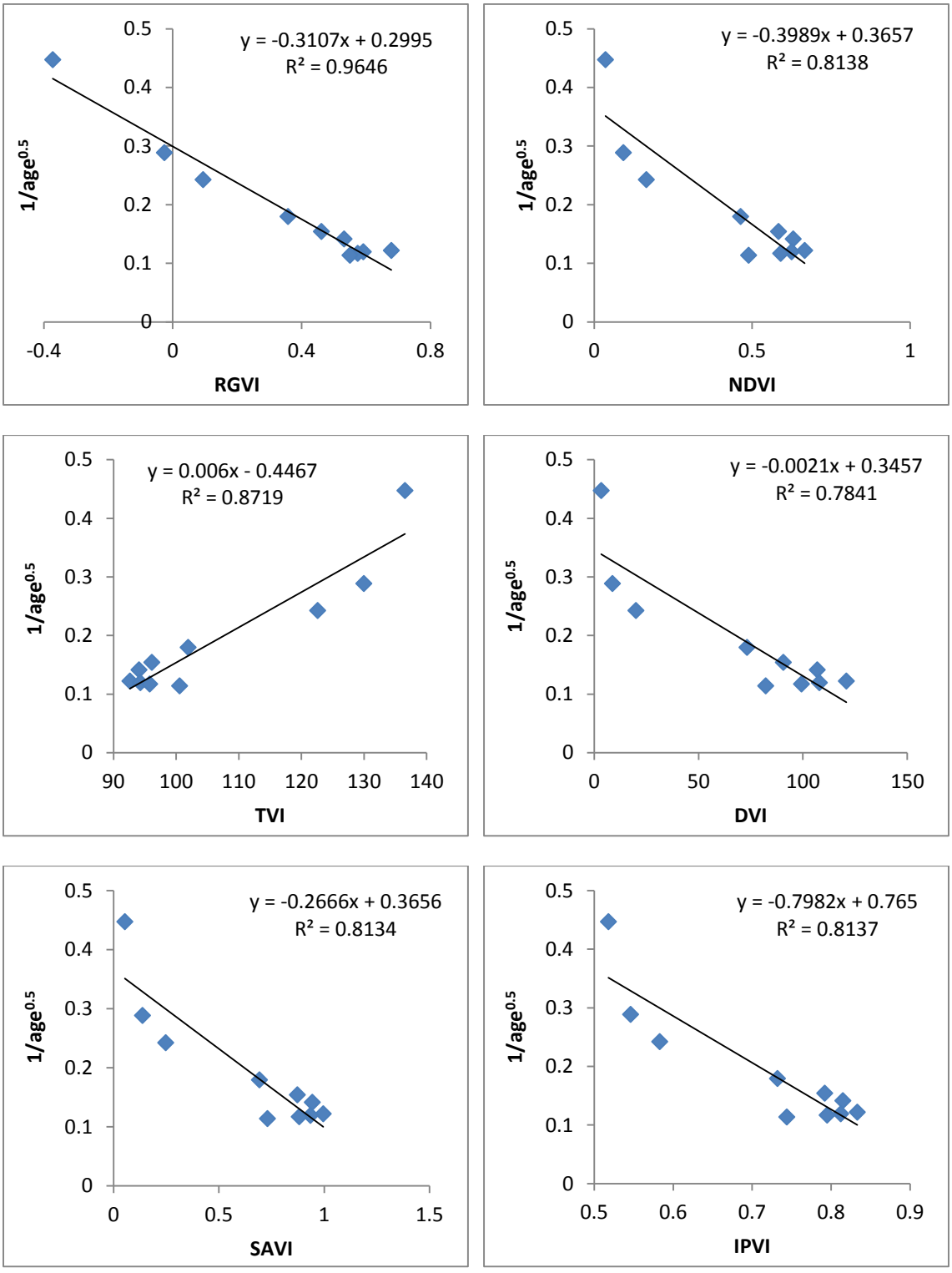

Figure 3.4. Relationship between rice vegetation index of Landsat ETM+ and rice age in $1/age^{0.5}$

The advantage of using a vegetation index compared to use of a single band was to reduce the spectral data to a single number that is related to physical characteristics of vegetation (e.g., leaf area, biomass, productivity, photosynthetic activity, or percent cover) (Baret and Guyot, 1991; Huete, 1988) while minimising the effect of internal (e.g., canopy geometry, and leaf and soil properties) and external factors (e.g., sun-target-sensor angles, and atmospheric conditions at the time of image acquisition) on the spectral data (Baret and Guyot, 1991; Huete and Warrick, 1990; Huete and Escadafal, 1991).

3.3.2 Rice plant mapping

According to the statistical analysis of the relationship between rice spectral and rice age, RGVI was the best vegetation index to explain rice age due to the fact that it had the highest value of R^2 as well as the lowest value of analysis of variance (Sig) and standard error of estimation (SE) (Table 3.6). Therefore, the linear equation form of RGVI was used for rice plant mapping with the following equation:

$$y = -0.3107x + 0.2995 \quad (3.9)$$

where y is the rice age in $\frac{1}{\sqrt{age}}$ and x is the RGVI, respectively. After y value is found from the equation 3.9, the original value of rice age should be restored using the following equation:

$$y = \frac{1}{x^2} \quad (3.10)$$

Where y is the original rice age value and x is $\frac{1}{\sqrt{age}}$

Table 3.6. Value of determination coefficient, significant and standard error of relationship between rice spectral and rice age.

Rice Spectral	Rice age < 55 days		
	R2	SE	Sig
cD1	0.2721	0.097	0.122
cD2	0.0854	0.109	0.412
cD3	0.3761	0.090	0.059
cD4	0.8143	0.049	0.000
cD5	0.8735	0.040	0.000
cD7	0.7633	0.055	0.001
RGVI	0.9646	0.021	0.000
TVI	0.8719	0.041	0.000
NDVI	0.8138	0.049	0.000
IPVI	0.8137	0.049	0.000
SAVI	0.8134	0.049	0.000
DVI	0.7841	0.053	0.001

Rice plant age was estimated using Equation 3.9 and 3.10 in two sequential acquisition dates of Landsat ETM+. The pixels that had the same difference values between predicted rice age in two sequential acquisitions dates, and the day distinction of two sequential acquisitions dates, were classified as a rice plant area after standard error of estimation was included (Equation 3.8).

Figure 3.5 and Table 3.7 show the distribution of the rice area resulting from classification process using Equation 3.8. The map on Figure 3.5 not only describes the distribution of rice plants but also their age. This information is important to estimate the total amount of rice plants that can be harvested.

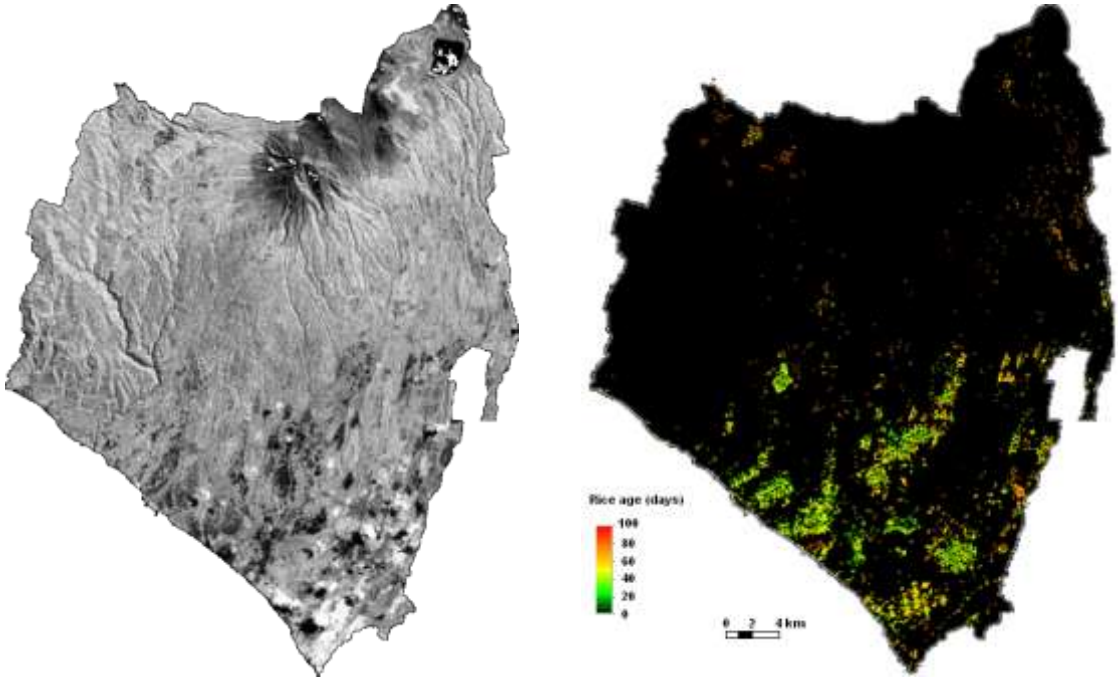

(a) (b)

Figure 3.5. Rice plant distribution map of the study area from the analysis of Landsat ETM+ data (b) and false colour composite of Landsat ETM+ (a)

Table 3.7. Rice plant area of analysis results in each district

District	nPixel	Area (ha)
Kerambitan	6682	601.38
Selemadeg	7917	712.53
Pupuan	855	76.95
Tabanan	2023	182.07
Kediri	5727	515.43
Marga	2999	269.91
Penebel	1547	139.23
Baturiti	2193	197.37

Rice fields in our study area had a narrow area mixed with other land uses, such as settlement, which is different from most characteristics of rice fields in other countries. The small area of rice plant is one of the challenges of mapping rice plants using remote sensing data. Therefore, use of Landsat ETM+ data with a 30-m spatial resolution is more comfortable and appropriate in our study area than the use of a coarser spatial resolution of remote sensing data, such as MODIS and NOAA AVHRR data.

3.3.3 Quantitative evaluation of Landsat-derived rice map

Evaluation of Landsat ETM+ accuracy quantitatively for rice plant distribution mapping was performed by comparing the total area derived from Landsat ETM+ to the data released by the Statistic Center Agency. The agriculture department of the local government did not publish the spatial data for land that was being planted with rice; therefore, the study results were carried out using a district-level comparison. Table 3.8 shows the comparison of total rice area between analysis results of Landsat ETM+ and reference data.

Table 3.8. Comparison in district levels of rice area between analysis result of Landsat ETM+ and reference data

District	Analysis Result (ha)	Reference data (ha)	Difference (%)
Kerambitan	601.38	560	7.39
Selemadeg	712.53	809	-11.92
Pupuan	76.95	95	-19.00
Tabanan	182.07	203	-10.31
Kediri	515.43	591	-12.79
Marga	269.91	314	-14.04
Penebel	139.23	165	-15.62
Baturiti	197.37	242	-18.44

Based on Table 3.8, estimation results of total rice plants that were being planted in our study area is an under-estimation for all districts, except for the Kerambitan district. For the districts of Selemadeg, Pupuan, Tabanan, Kediri, Marga, Penebel, and Baturoti, total of estimation area from the Landsat data was lower, in the amounts of 11.92%, 19.00%, 10.31%, 12.79%, 14.04%, 15.62% and 18.44%, respectively, compared to the Statistic Center Agency data. However, in the Kerambitan district, estimation results from Landsat images were greater than the reference data (around 7.39%). The under-estimation for almost all of the rice area obtained from Landsat image compared to the data from the local government caused by some of the Landsat rice pixel contained several objects besides rice plant. The mixed pixel can decrease the accuracy of the calculation (Strahler *et al*., 2006). Xiao *et al.* (2005) has carried out the same phenomena

using MODIS data. They found that the estimation result of the rice field area in the Southern China using MODIS imaging was lower than the references data.

The estimated rice area of Landsat ETM+ and reference data shows a strong relationship. The determination coefficient (R^2) was 0.9745 with the equation of y = 0.9354x - 11.475, where y is estimation area from the Landsat ETM+, and x is the reference data (Figure 3.6). The standard error of the estimation was 41.135 ha.

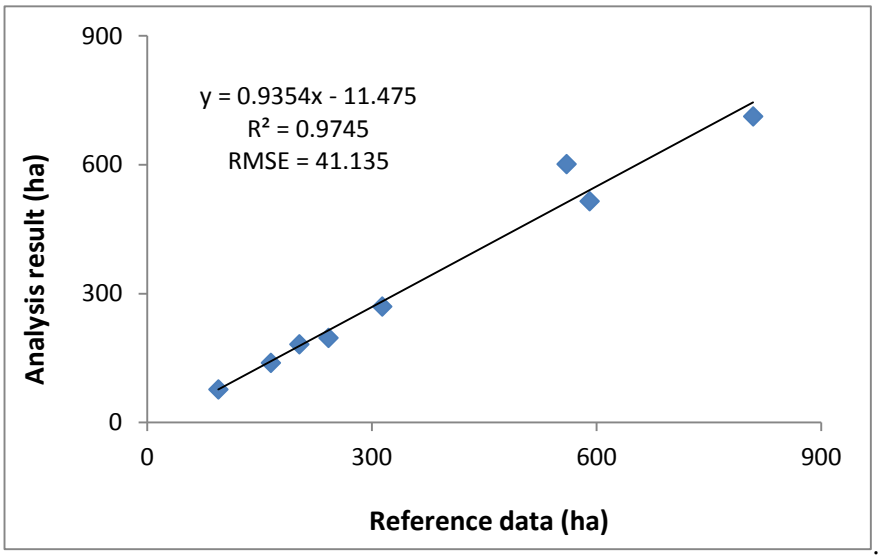

Figure 3.6. District-level comparison of the rice area from the Landsat ETM+ and the data from the local government

3.4 Conclusions

The visible band of Landsat ETM+ (Band 1, Band 2, and Band 3) showed a weak relationship to rice age; however, the reflective infrared band of Landsat ETM+ (Band 4 and B5) and the entire vegetation index showed a strong relationship to rice age. Use of vegetation indexes to monitor and map rice plants gives better results than use of a single band of Landsat ETM+. A Rice Growth Vegetation Index (RGVI) was a new vegetation index developed in this study. RGVI is a better vegetation index to describe rice age than existing vegetation indexes. The relationship between rice age and RGVI has shown the highest determination coefficient (R^2) of 0.9646 with the equation y = -0.3107x + 0.2995, where y and x are the 1/√rice age and RGVI, respectively. Quantitative comparison of rice plants between analysis results and reference data showed a linear relationship with the equation y = 0.9354x - 11.475 and R^2 = 0.9745, where y is the rice plant area of

analysis results of the Landsat ETM+, and x is the rice plant area of the reference data. The standard error of this estimation is 41.135 ha. Landsat ETM+ has good capabilities to monitor and map rice plants.

CHAPTER 4

SPECTRAL CHARACTERISTIC COMPARISON OF RICE PLANTS UNDER HEALTHY AND WATER-DEFICIENT CONDITIONS USING LANDSAT ETM+ DATA

4.1 Introduction

Rice is the primary food source for more than three billion people and is one of the world's major staple foods. Paddy rice fields account for approximately 15% of the world's arable land (Khush, 2005; IRRI, 1993). The growth and yield of rice crops are not only determined by their genetic compositions but are also affected by the environmental factors of their habitats. The progress of a crop is conventionally evaluated by periodical plant samplings, and management practices are guided by the performance in the field (Yang *et al*., 2008). Nowadays, remote sensing is the preferred technology adopted worldwide for large-scale field monitoring of plant populations, and, through its use, timely and precise site-specific actions may be taken (Bouman, 1995; Pierce *et al*., 1999). If rice crops can be attended to using accurate knowledge of their status in the growth stages, it is possible to respond positively to the supply and demand of varietal growth and production rates.

Vegetation reflectance is a function of optical properties, canopy biophysical attributes, viewing geometry, illumination conditions, and background effects (Asner, 1998; Barrett and Curtis, 1992; Jacquemoud *et al*., 1992; Myneni *et al*., 1989). The biophysical attributes of a vegetation crop drive variation in the canopy reflectance characteristics due to the three-dimensional orientation, which provides a better structure and opportunities for photons to interact with multiple surfaces of different plant parts (e.g., leaves, stems), thus favouring radiometric reception (Yang and Cheng, 2001; Baret *et al*., 1994; Jacquemoud, 1993; Kupiec and Curran, 1995; Yang and Su, 2000).

The reflectance of agricultural crops in the visible and infrared regions is currently being used to assess different crop parameters and plant growth status (Carter and Knapp, 2001; Lee *et al*., 2008; Yang and Chen, 2004). Most green plants exhibit a spectral reflectance profile of a higher reflectance in the near-infrared and a lower reflectance in visible light when grown under normal conditions (Hall *et al*., 2002). In 'water stress' environments, a reverse fashion is observed due to a decrease in plant vigour and canopy

coverage and an increase in the reflectance of chlorophyll absorption (Knipling, 1970; Yang *et al*., 2007). Crop foliage density and changes in geometry play a key role in the reception of incident radiation and the following biomass formation and accumulation. Variations in crop vegetation, in regular conditions or under stresses, differ greatly in reflectance behaviour, and this may be assessed from the canopy spectral characteristics (Carter and Knapp, 2001; Yang and Chen, 2004).

The monitoring of rice plants using remote sensing data has been widely done. However, the studies have been focused on estimations of rice field areas and production estimations using either optical remote sensing (Bailey *et al*., 2001; Okamoto and Kawashima, 1999; Fang *et al*., 1998; Nuarsa *et al*., 2005; Nuarsa and Nishio, 2007) or radar systems (Shao *et al*., 2001; Kurosu *et al*., 1997; Chakraborty *et al*., 2000; Ribbes and Le Toan, 1999).

In chapter 2 chapter 3, two algorithms for rice field mapping were developed. In chapter 3, the algorithms to distinguish the age of rice plants were also found. To predict the rice yield accurately, we need to study about the difference characteristic of rice plant under normal and abnormal condition since the rice production is affected by the rice condition. In case of our study area, water for irrigation was a limiting factor for rice cultivation. This can cause abnormal growth of rice plants.

Investigations of rice plants under abnormal conditions are currently still very limited. Most of them concern the spectral characteristics of rice plants infested by pests and plant diseases (Qin and Zhang, 2005; Yang and Cheng, 2001; Yang *et al*., 2007), and only a few studies relate to water deficiency (Yang and Su, 2000; Köksal *et al*., 2008). Studies of the rice plants under abnormal conditions have been done mostly using ground sensing spectroradiometers to acquire the reflectance of rice plants (Yang *et al*., 2007; Tong *et al*., 2001). The use of actual remote sensing data of rice plants under abnormal conditions has been limited by difficulties in finding sufficient areas under such conditions (Currey *et al*., 1987). This study used the actual remote sensing data (Landsat ETM+ images) to monitor the spectral properties of rice plants under water stress. The ground data were obtained from the harvest failure of farms caused by drought (low rainfall) in a broad area of about 421 ha. The objectives of the studies was to analyse differences in the spectral characteristics of rice plants under water stress compared to those under normal conditions using Landsat ETM+ data.

4.2 Study Area, Data, and Methods

4.2.1 Background and Study Area

The study area was located in Tabanan Regency, Bali Province, Indonesia, centred at latitude of 8°31’50” S and a longitude of 115°02’30” E (Figure 4.1). The Tabanan Regency was selected for the study area due to Tabanan being the central production area of rice in Bali. In the study area, the rice planting is organised by a *subak*. The *subak* is the farmer’s social organisation that manages the irrigation water. Each subak controls around 150 – 300 ha of rice fields (Food Crops Agriculture Department, 2006). They usually plant rice at the same times. An advantage for the remote sensing study with this farming system is that the monitoring is made easier due to the availability of a wide rice area.

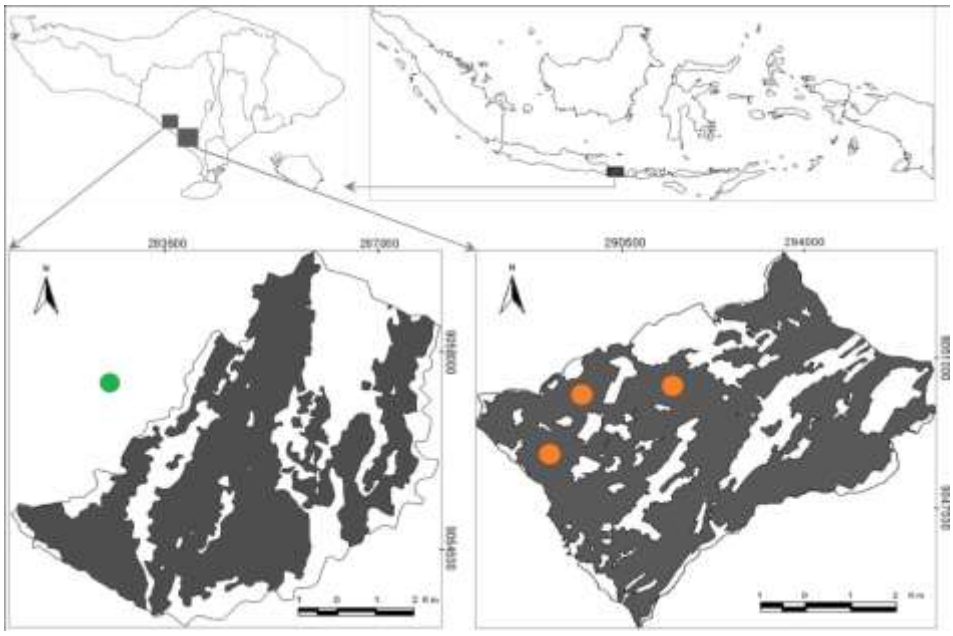

a b

Figure 4.1 Location map of the study area. The black colour indicates rice field areas, and the white colour indicates other land use areas. Left below (a) is the study area for the rice under water deficiency. The green point next to the study area is the nearest rainfall station used to obtain a rainfall data. Right below (b) is the study area for the rice under healthy conditions. The three orange points in that image are the ground sites where the field measurement was done.

Because irrigation water is a constraining factor in the study area, rice planting is done in turns between the *Subaks*. Alternative plants to rice plants include session

agriculture crops such as corn, soybeans, etc. The length of the growth cycle of rice can vary from three to six months for different varieties (Casanova *el. Al.*, 1998). In the study area, the average length of the growth cycle of rice is 115 days, with production reaching 5.0 tons/ha (Food Crops Agriculture Department, 2006). In one year, the farmer usually plants rice twice in two planting sessions.

This study was carried out on two different sites and during two planting sessions. One experimental session was conducted under healthy rice conditions, and the other session was conducted under water deficiency. For the healthy rice conditions, field surveys were done in three different site stations every 16 days when the Landsat Satellite passed the study area. Some rice growth parameters, such as the rice height, the total number of stem, the percentage of rice coverage, and the rice age, were measured. For the water deficiency conditions, field surveys were not performed, as in this case the condition was not anticipated. This event became known after the Agriculture Department of the local government released relevant reports. However, the locations and planting dates of these areas were precisely recognised. Hence, the investigation of rice under healthy and water deficiency conditions could evidently be done successfully.

According to the Agriculture Department of the local government, the cause of the occurrence of drought was that the planting of rice was done outside the normal planting season. The farmers had speculated on rain coming soon after planting. Unfortunately, the rainfall had not begun from the rice age of 15 days after planting until one month after (Table 4.1). This situation caused around 421 ha of rice plants in the study area to experience a drought. The rice production under these circumstances was approximately 0.35 ton/ha of grain dry weight (less than 6% of normal condition) (Food Crops Agriculture Department, 2006).

Table 4.1 Monthly rainfall of the nearest rainfall station from the study area (BMG, 2006)

Month	Rainfall (mm)
January	322
February	183
March	295
April	138
May	0
June	27
July	106
August	14
September	76
October	214
November	53
December	391

The zero value of rainfall in May indicated that the rainfall in that month was less than 1 mm. Planting was done on 15 April 2005. Beginning from May, the rice plants did not get water, and in June the rainfall was very low. This condition caused the rice to experience drought.

The site characteristics of the rice under healthy and water-deficient conditions during the rice growing circle were the same for the soil type and rice variety and were similar for the land slope, elevation, average temperature, average duration of solar radiation as well as fertiliser and pesticide treatment. However, the water resources for the rice field irrigation were different (Table 4.2). According to field observation and data from the Food Crops Agriculture Department (2006), in the healthy rice area, water was mainly derived from the permanent irrigation water. On the other hand, for rice in water-deficient sites, water comes solely from rainfall. The permanent irrigation water guarantees the availability of water and the sustainability of healthy rice crops more than rainfall can. The peak of transplanting was done on 12 June 2005 at healthy rice and 12 April 2005 at Water-deficient rice.

Table 4.2 Site characteristics of rice under healthy and water-deficient conditions

Parameters	Healthy rice	Water-deficient rice
Soil type	Latosol/Vertisol	Latosol/Vertisol
Land slope (%)	0 - 15	0 - 8
Elevation (m above sea level)	38 - 52	5 -15
(Fertiliser and pesticide used)	Agriculture Department recommendation	Agriculture Department recommendation
Water source	Permanent irrigation	Rainfall
Rice variety	Ciherang	Ciherang
Peak of Transplanting	12 June 2005	15 April 2005
Average temperature in planting session (^oC)	25.7	26.1
Average duration of solar radiation in planting session (%)	75	79

4.2.2 Landsat Image Data

Landsat satellite images had eight bands including thermal and panchromatic bands. In the visible, near-infrared, and middle-infrared regions, Landsat ETM+ had a 30-m spatial resolution. However, in the thermal and panchromatic regions, the spatial resolutions were 60 m and 15 m, respectively. This study used visible and reflectance infrared bands (Bands 1 - 5 and Band 7) of Landsat ETM+. Although the Landsat ETM+ used in this study has a scan-line corrector (SLC) off, the better spatial, spectral, and temporal resolution of its images caused it to still be relevant for use. With the 16 days of temporal resolution, Landsat ETM+ is the ideal satellite image for rice monitoring seeing as rice has only a 115-day cycle from planting to harvest. These images can be downloaded at USGS Global Visualization Viewer (http://glovis.usgs.gov).

Because the length of the rice growth cycle is around 115 days and the temporal resolution of Landsat ETM+ images is 16 days, the total of the time series images that can be collected in one rice growth cycle is around six images for different acquisition dates.

Some of the images cannot be used, due to cloud conditions or the appearance of gap values in the SLC-off mode of the station points. This caused a reduced availability of images. Fortunately, this study area was covered by two scenes of Landsat images in different paths. The total of the Landsat images used in this study is shown in Tables 3 and 4 for rice in sites with healthy and water-deficient conditions, respectively.

4.2.3 Data analysis

a. Radiometric corrections

In the temporal analysis of remote sensing data, radiometric corrections are an important part of the image analysis. The digital number (DN) of the Landsat ETM+ at different acquisition dates should be converted to the corrected digital number (cDN) to eliminate the radiometric and atmospheric effects, so that they have comparable values. In this study, we used the simple radiometric correction model introduced by Pons and Solé-Sugrañes (1994). The formula of this model is shown in the following equation:

$$cDN = 1000a(DN - K_l)d^2/[\mu_s S_0 e^{(-\tau_0/\mu_0)} e^{(-\tau_0/\mu_v)}], \quad (4.1)$$

(i) (if 250 < cDN ≤ 318.3; cDN = 254),

(ii) (if cDN > 318.3; *cDN* = 255),

(iii) (if $\mu_s \leq 0$; Vc = 255),

where cDN = corrected digital number
a = gain value of each Landsat band
DN = digital number
Kl = radiances value of zone totally in shade
d = actual Sun-Earth distance
μs = cosine of the incident angle
S0 = exoatmospheric solar irradiance
τ0 = optical depth of the atmosphere
μ0 = cosine of the solar zenith angle
μv = cosine of sensor view angle

cDN is the corrected digital number and the conversion of the effective reflectance to the common 8-bit format of most image processors. The range of the output values has

been limited to between 0 and 255. Note that a, K_l, S_0, and τ_0 depend on the wavelength and have different values for each spectral band; K_l varies for each image because it is related to and depends on atmospheric conditions; μ_0 and μ_s depend on the latitude, date, and time of the satellite pass; besides that, μ_s also depends on the slope and aspect of each pixel; d depends on the date of the satellite pass, and μ_v depends on the sensor viewing angle. The parameter μ_v is 1 in most Landsat images because v is 0 at the nadir and has small values on the rest of the images (Pons and Solé-Sugrañes, 1994). The parameters needed in the study to calculate cDN are shown in Tables 4.3-4.5.

Practically, to apply the algorithm above we only need a DEM of enough quality (altimetrically and planimetrically) because all of the other parameters are known (e.g., S_0) or can be inferred from images (e.g., K_l). To avoid overcorrections and undercorrections on the ridges and channels and to account for local phenomena, it is important to use a DEM with a planimetric resolution comparable to the geometric resolution of the image. Naugle and Lashlee (1992) showed that a DEM of 95 m can be insufficient for a Landsat TM image over rugged terrain. In this study, we derived a DEM from the topographical map with a spatial resolution of 30 m.

Table 4.3 Values of d(1), μ_0 (2), and K_l(3) for every acquisition date of Landsat ETM+ in healthy rice

Acquisition date	Path	Row	DOY	d	μ_0	K_l					
						ETM1	ETM2	ETM3	ETM4	ETM5	ETM7
26 April 2002	116	66	116	1.00626	0.79414	51	31	23	20	17	11
12 May 2002	116	66	141	1.01210	0.75100	53	32	22	23	19	14
7 July 2005	117	66	188	1.01669	0.71514	52	34	22	25	21	11
1 August 2005	116	66	213	1.01497	0.74624	50	31	23	19	16	12
17 August 2005	116	66	229	1.01244	0.78085	53	33	23	22	18	13
24 August 2005	117	66	236	1.01103	0.80312	55	35	24	23	15	10
4 October 2005	116	66	277	1.00033	0.88006	54	34	24	21	17	12
12 November 2005	117	66	316	0.98983	0.90081	52	31	22	24	21	11

Sources: (1) Chander *et al.* (2009); (2) our image with calculations; (3) the DN of our image. DOY is the day of year.

Table 4.4 Values of d (1), μ_0 (2), and K_l (3) for every acquisition date of Landsat ETM+ in water-deficient rice

Acquisition date	Path	Row	DOY	d	μ_0	K_l					
						ETM1	ETM2	ETM3	ETM4	ETM5	ETM7
18 April 2005	117	66	108	1.00409	0.80647	52	33	23	18	15	11
27 April 2005	116	66	117	1.00653	0.79287	52	31	23	23	18	15
13 May 2005	116	66	133	1.01043	0.76522	56	34	23	22	17	12
20 May 2005	117	66	140	1.01191	0.75302	48	30	22	18	15	12
29 May 2005	116	66	149	1.01355	0.73857	54	34	23	22	18	12
21 June 2005	117	66	172	1.01625	0.71480	62	41	25	23	13	9
30 June 2005	116	66	181	1.01665	0.71309	57	36	27	21	18	12
23 July 2005	117	66	204	1.01592	0.72621	51	33	23	24	22	12

Sources: (1) Chander *et al.* (2009); (2) our image with calculations; (3) the DN of our image. DOY is the day of year.

Table 4.5 Values of τ_0(1), S_0(2), and a(3) for every spectral Landsat Band for both healthy and water-deficient rice

Band	τ_0	S_0 ($Wm^{-2}\mu m^{-1}$)	a
ETM1	0.5	1997	0.7757
ETM2	0.3	1812	0.7957
ETM3	0.25	1533	0.6192
ETM4	0.20	1039	0.9655
ETM5	0.125	230.8	0.1257
ETM7	0.075	84.9	0.0437

Sources: (1) Dozier (1989); (2) Chander *et al.* (2009); (3) our image with calculations.

b. Spectral Characteristic Analysis of Rice Plants

Gathering reflectance values from the Landsat pixels for both rice conditions over the entire time period of rice growth was the next step of the data analysis. In each image of an acquisition date, a 200-pixel sample was taken randomly in the field observation site at both healthy and water-deficient sites (Fig. 1). The average value of the sample was used as a representative of the spectral value of that acquisition date. Based on the spectral value, the vegetation index was calculated. Several vegetation indexes that were evaluated in the study are shown in Table 4.6.

Table 4.6 Several vegetation indexes used in the study for identifying the spectral characteristics of rice in healthy and water-deficient conditions

No	Vegetation Index	Formula
1	Normalised Difference Vegetation Index (NDVI)	$NDVI = \frac{nir - r}{nir + r}$
2	Ratio Vegetation Index (RVI)	$RVI = \frac{nir}{r}$
3	Infrared Percentage Vegetation Index (IPVI)	$IPVI = \frac{nir}{nir + r}$
4	Difference Vegetation Index (DVI)	$DVI = nir - r$
5	Transformed Vegetation Index (TVI)	$TVI = \frac{100}{\sqrt{\frac{nir - r}{nir + r} + 0.5}}$
6	Soil-Adjusted Vegetation Index (SAVI)	$SAVI = \frac{(1 + L)(nir - r)}{nir + r + L}$
7	Normalised Difference Water Index (NDWI-1)	$NDWI1 = \frac{nir - swir1}{nir + swir1}$
8	Normalised Difference Water Index (NDWI-2)	$NDWI2 = \frac{nir - swir2}{nir + swir2}$

Here, nir, r, swr1, swr2, and L are the near-infrared band, red band, middle-infrared (Band-5 of Landsat ETM+), middle-infrared (Band-7 of Landsat ETM+), and canopy background brightness correction factor, respectively.

Based on the spectral and vegetation index values, spectral analysis was performed by means of comparing the values for rice under healthy and water-deficient conditions, using statistical analysis (paired-samples T test).

4.3 Results and Discussion

4.3.1 Rice growth parameters under healthy condition

Based on field survey data and statistical analysis of rice under healthy condition, there was a quadratic relationship between some of rice growth parameters (rice height and stem total) and rice age. However, percentage of rice coverage was better expressed by a linear relationship with rice age. Rice coverage height showed the best relationship with the rice age, followed by rice height and stem total with the R^2 value were 0.9617, 0.9544, and 0.9294 respectively (Figure 4.2a, Figure 4.2b, and Figure 4.2c).

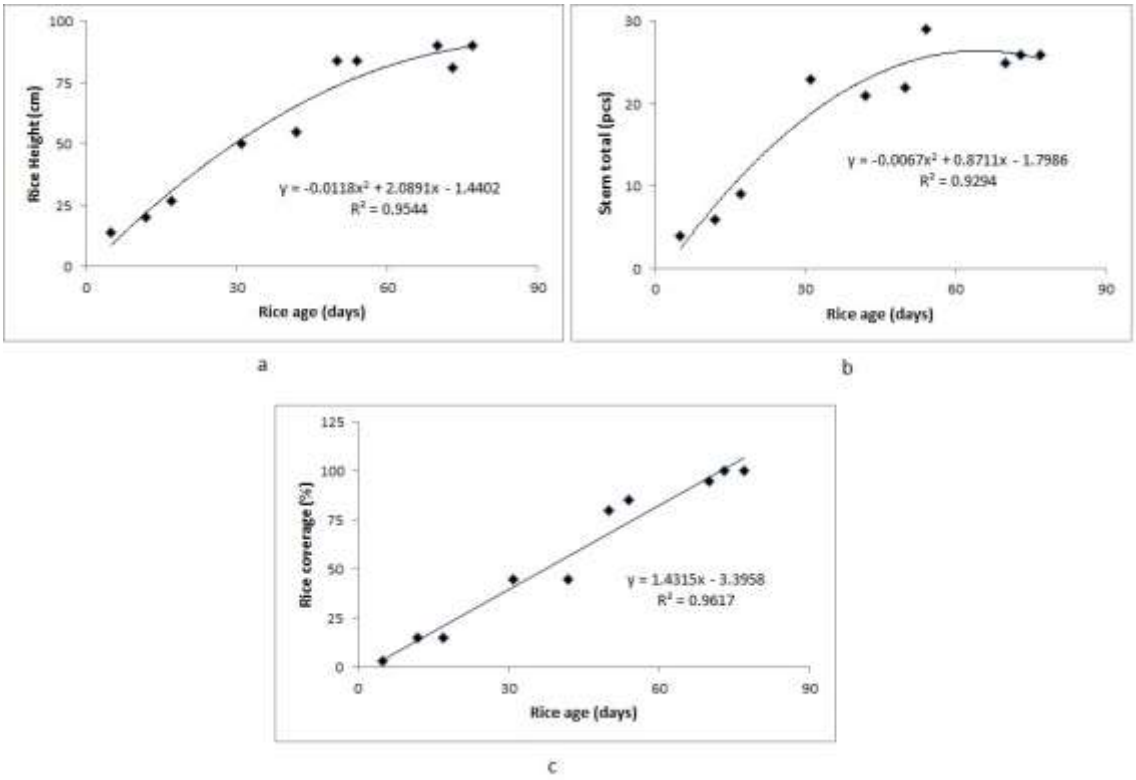

Figure 4.2 Relationship between rice height (a), stem total (b) and rice coverage (c) with rice age.

4.3.2 Spectral characteristics of rice under healthy and water-deficient conditions

The trends of rice spectra under both conditions for rice aged 30 days after planting are similar. The tendency towards differences in reflectance values is only seen when the rice enters its second month (Figure 4.3). In the first month, when rice from both conditions are in a healthy state, the reflectance of rice under water deficiency appears higher than that in healthy condition sites for most Landsat ETM+ bands (Figure 4.4). This result is caused by the effect of water coverage. In healthy rice sites, the availability of water for irrigation is sufficient. However, in water-deficient rice sites, the availability of water is limited. Therefore, the reflectance of the rice area for healthy rice sites is controlled by the water, whereas in water-deficient sites, the reflectance is influenced by the moist soil surface. Moist soil has a higher reflectance than water in the visible, near-infrared and middle-infrared regions of the electromagnetic spectrum (Harrison and Jupp, 1989).

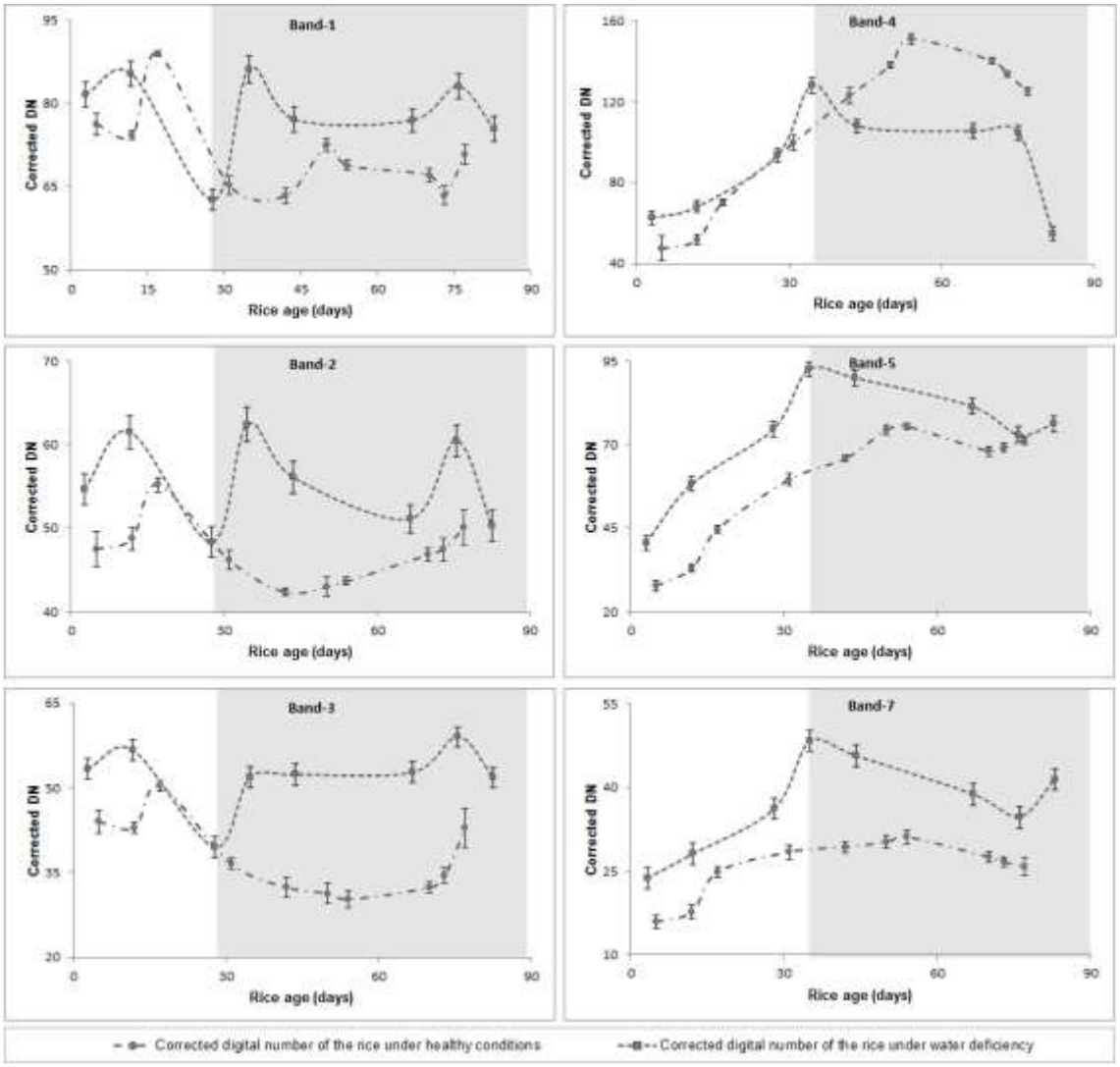

Figure 4.3 Spectral characteristic of rice under healthy and water-deficient conditions for all reflective bands of Landsat ETM+. The white areas in the chart indicate that both reflectances of the rice have similar forms, while the dark areas show different forms of rice reflectance.

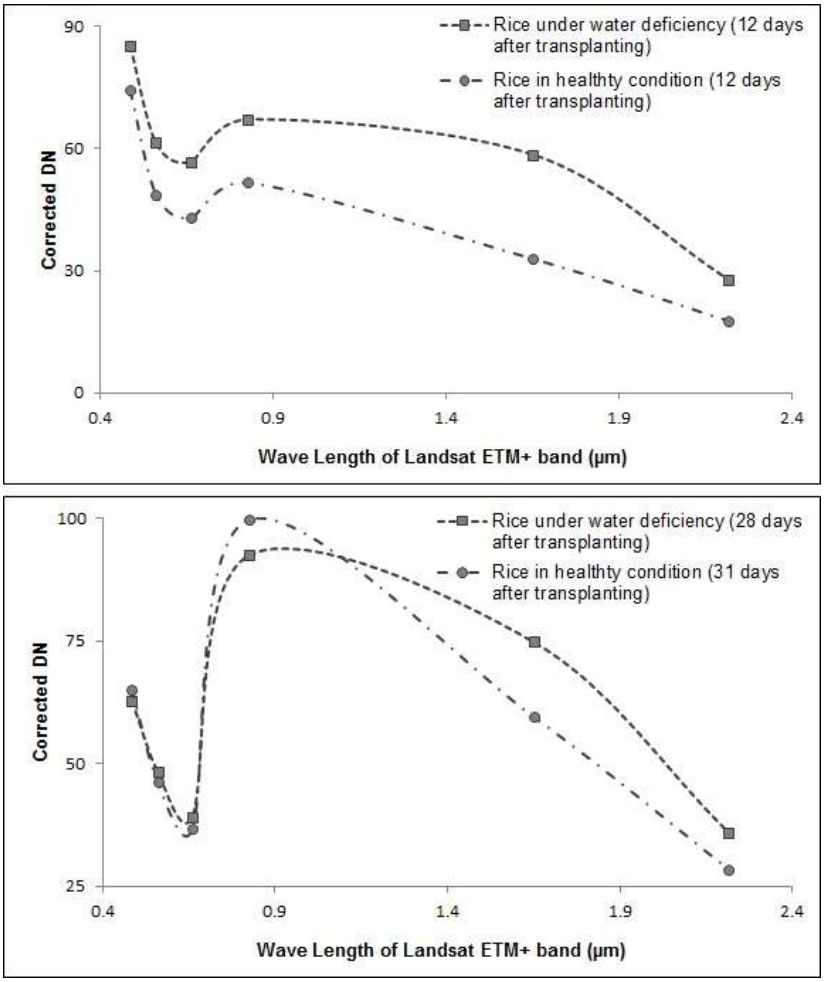

Figure 4.4 Differences of the spectral characteristics of rice at similar ages at times when the rice plants under water deficiency did not yet show signs of water stress.

In the second month, the trend of spectral changes for the rice became inverted. Under normal conditions, when the rice enters the second month, the reflectance values of Band-1, Band-2, and Band-3 should decrease, while in Band-4, Band-5, and Band-7 they should increase. However, at the water-deficient site, the reverse occurs (see Fig. 3 in the dark area). This result shows that there has been water stress. The appearance of water stress in the second month in the water-deficient site is supported by the rainfall data obtained from the nearest rainfall station from the study area (Table 4.1). Although the rain did not come until the third week after rice planting, signs of water deficiency are only seen in the second month because rice plant can still use the water stored in the soil. When the water reserves run out in the soil, the rice plants begin to show signs of wilting. The NDVI of rice under water deficiency decreased significantly in the beginning of the second month compared with the rice under normal conditions (Figure 4.5).

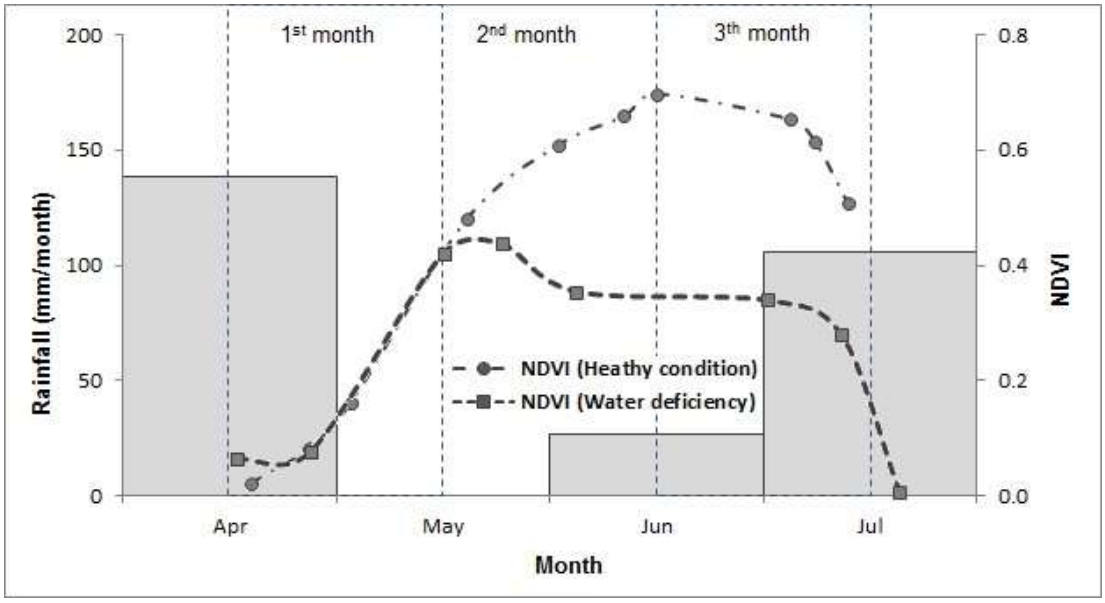

Figure 4.5 The total monthly rainfall in water-deficient sites beginning from the plantation time through the next three months. Rice was transplanted in the middle of April. Starting from a rice age of two weeks, there was no rain at all until the next month. Rainfall in small amounts occurred at a rice age of seven weeks. The chart also illustrates the relationship between monthly rainfall and periods of water stress (see the dashed line). The connected line just shows a comparison of the rice under normal conditions in the same rice age (it does not the actual of rice planting).

Beginning from the second month after transplantation, when the rice in the water-deficient site shows signs of water stress, the spectral values at all Landsat bands are higher than those from the healthy rice, except for Band-4 (Figure 4.3). The maximum difference was seen for rice that was around two months (67 – 70 days after plantation time) old (Figure 4.6). This is caused by differences in the chlorophyll and water contents of the rice plants. On rice aged two months, most of the rice area coverage is attributed to rice plants. The reflectance properties of the rice will be similar to vegetation in general (Martin and Heilman, 1986). An increase in leaf reflectivity in the visible light portion as a response to water stress is caused by the metabolic sensitivity of chlorophyll, resulting in a less efficient absorption of light (increased reflection) (Knipling, 1970). The water absorption properties of the middle-infrared (Thenkabail *et al.*, 1994b) cause the reflectance values of rice under water deficiency in Band-5 and Band-7 of Landsat ETM+ to be higher than those of healthy rice. However, in Band-4, the chlorophyll pigments that are present in leaves have higher levels in healthy rice. In the near-infrared portion, the radiation is scattered by the internal spongy mesophyll leaf structure, which leads to

higher values on the NIR channels (Baret and Guyot, 1991). Therefore, the reflectance of Band-4 in healthy rice is higher than that of water-deficient rice (Figure 4.3).

In addition, when moisture is limited, the stomata close to slow transpiration and conserve water. When stomata are closed, photosynthesis cannot occur, and growth stops. Water stress significantly decease leaf chlorophyll (Pirzad et al., 2010). Total chlorophyll content in high water stress was reduced by 55% compared to normal condition (Kirnak et al., 2001). Water stress can destroy the chlorophyll and prevent making it (Mensha et al., 2006). Water stress decreased both mesophyll and bundle sheath cell areas. The leaf-elongation rate was reduced by one-half and the mitotic activity of mesophyll cells was reduced to 42% of well-watered controls (Schupper *et al*., 1998).

Chlorophyll pigments that are present in leaves absorb red light. In the NIR portion, radiation is scattered by the internal spongy mesophyll leaf structure, which leads to higher values in the NIR channels. This interaction between leaves and the light that strikes them, often determined by their different responses in the red and NIR portions of reflective light (Niel and McVicar, 2001).

Decrease in chlorophyll content and mesophyll due to water stress, will reduce both absorption of red light and scattering of NIR light. As a result, the reflection of red light will increase while the NIR light decrease. Because the value is directly proportional to NIR vegetation indices except for TVI, the decrease in NIR reflectance will decrease the value of vegetation index.

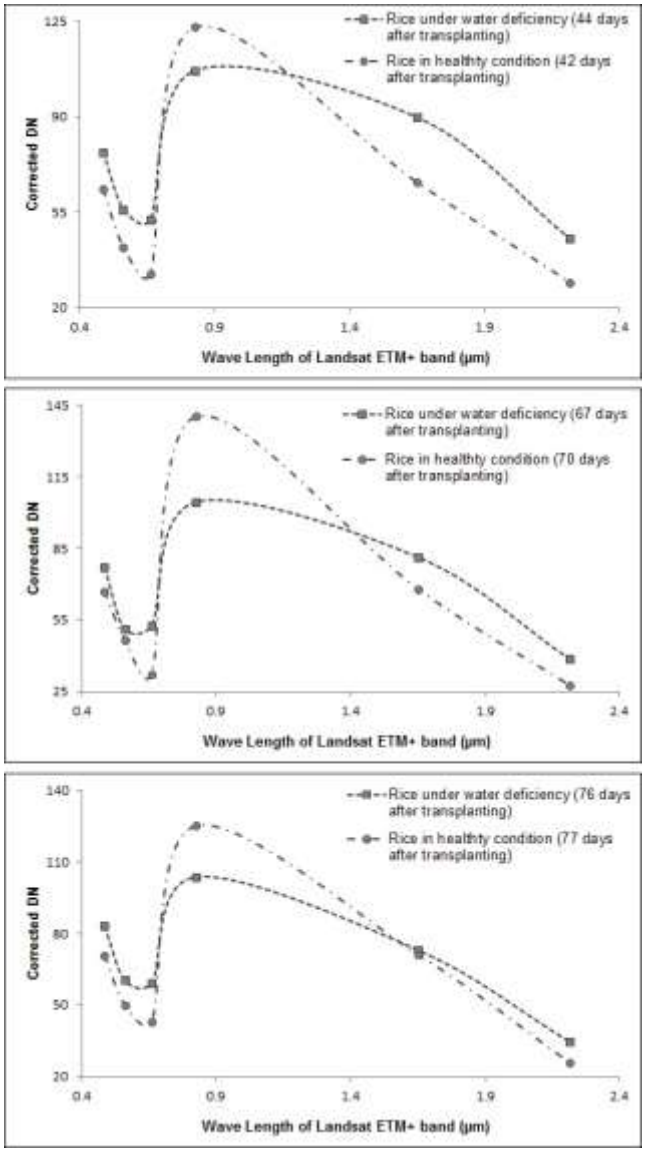

Figure 4.6 Differences of the spectral characteristics of rice at similar ages at times when the rice plants in water deficiency did show signs of water stress. The third comparisons were done for rice ages greater than one month.

For the early detection of water deficiency, the visible band (Bands 1 - 3) is more sensitive than near- and middle-infrared bands of Landsat ETM+. In the visible band, the changing trend of reflectance values was detected at the beginning of the third observation (before rice is one month old); in near- and middle-infrared, however, it was just detected at the fourth observation (rice aged more than one month) (Figure 4.3). This means that the visible band is more sensitive for early water deficiency detection than the near- and middle-infrared bands of Landsat ETM+. The highest percentage difference of values of Landsat ETM+ bands between healthy rice and water-deficient rice at similar rice ages was shown by Band-3 (Table 4.7).

The comparison by means of statistical tests (t-test) showed that the entire Landsat ETM+ bands evaluated in this study (B1-B5 and B7) for similar rice ages provided a significant distinction of spectra between rice under water deficiency and healthy conditions (Sig. < 0.05) in a two-tailed t-test (Table 4.7). It means that rice field spectral in water deficiency and healthy was different statistically.

Table 4.7 Average differences of spectral values and t-tests between rice under water deficiency and healthy conditions for similar rice ages.

Rice Condition	Rice age (days)	cDN Value					
		Band-1	Band-2	Band-3	Band-4	Band-5	Band-7
Healthy conditions (Avg/Std)	42	63.38/1.91	42.28/1.67	32.39/1.63	122.99/3.60	65.91/2.27	29.35/1.93
Water deficiency (Avg/Std)	44	77.11/2.15	56.03/1.90	52.38/1.93	106.99/3.48	89.79/2.27	45.37/1.93
Difference of value		21.65%	32.52%	61.74%	-13.01%	36.23%	54.56%
Sig. (2-tailed) t-test		< 0.01	< 0.01	< 0.01	0.034	< 0.01	< 0.01
Healthy conditions (Avg/Std)	70	67.03/1.96	46.80/1.73	32.39/1.63	140.28/3.71	68.04/2.27	27.57/1.93
Water deficiency (Avg/Std)	67	77.01/2.02	51.08/1.70	52.79/1.92	104.51/3.55	81.36/2.31	38.50/1.95
Difference of value		14.90%	9.14%	62.99%	-25.50%	19.58%	39.67%
Sig. (2-tailed) t-test		< 0.01	< 0.01	< 0.01	< 0.01	< 0.01	< 0.01
Healthy conditions (Avg/Std)	77	70.67/1.96	50.03/1.73	42.95/1.63	125.15/3.71	71.23/2.27	25.78/1.93
Water deficiency (Avg/Std)	76	83.01/2.19	60.38/1.92	59.29/1.92	103.71/3.60	73.04/2.29	34.46/1.95
Difference of value		17.46%	20.69%	38.04%	-17.13%	2.55%	33.67%
Sig. (2-tailed) t-test		< 0.01	< 0.01	< 0.01	0.038	< 0.01	< 0.01

T-tests of paired samples used 200 pixel samples. A value less than 0.05 in the T-tests of paired samples indicates that there is a significant different between the rice under water deficiency and healthy conditions for two-sample paired tests (two-tailed).

4.3.2 Vegetation index of healthy and water-deficient rice

Using multiple bands of Landsat ETM+ in the form of a vegetation index delivers a clearer distinction between rice under healthy and water-deficient conditions than when using a single band. Figure 4.7 shows that in the first month after plant time, the vegetation index has a similar pattern due to both rice still being under normal conditions. However, when the rice plants under water deficiency enter the second month of growth, when there is a period of water stress, the difference in the vegetation index for the two rice conditions is high for all vegetation indexes evaluated in this study. All vegetation index values for the water-deficient rice are significantly lower than those for the healthy rice, except for the TVI. The distinction of TVI trends compared with other vegetation

indexes is because the TVI equation is in a reverse form from other vegetation index equations (Table 4.6).

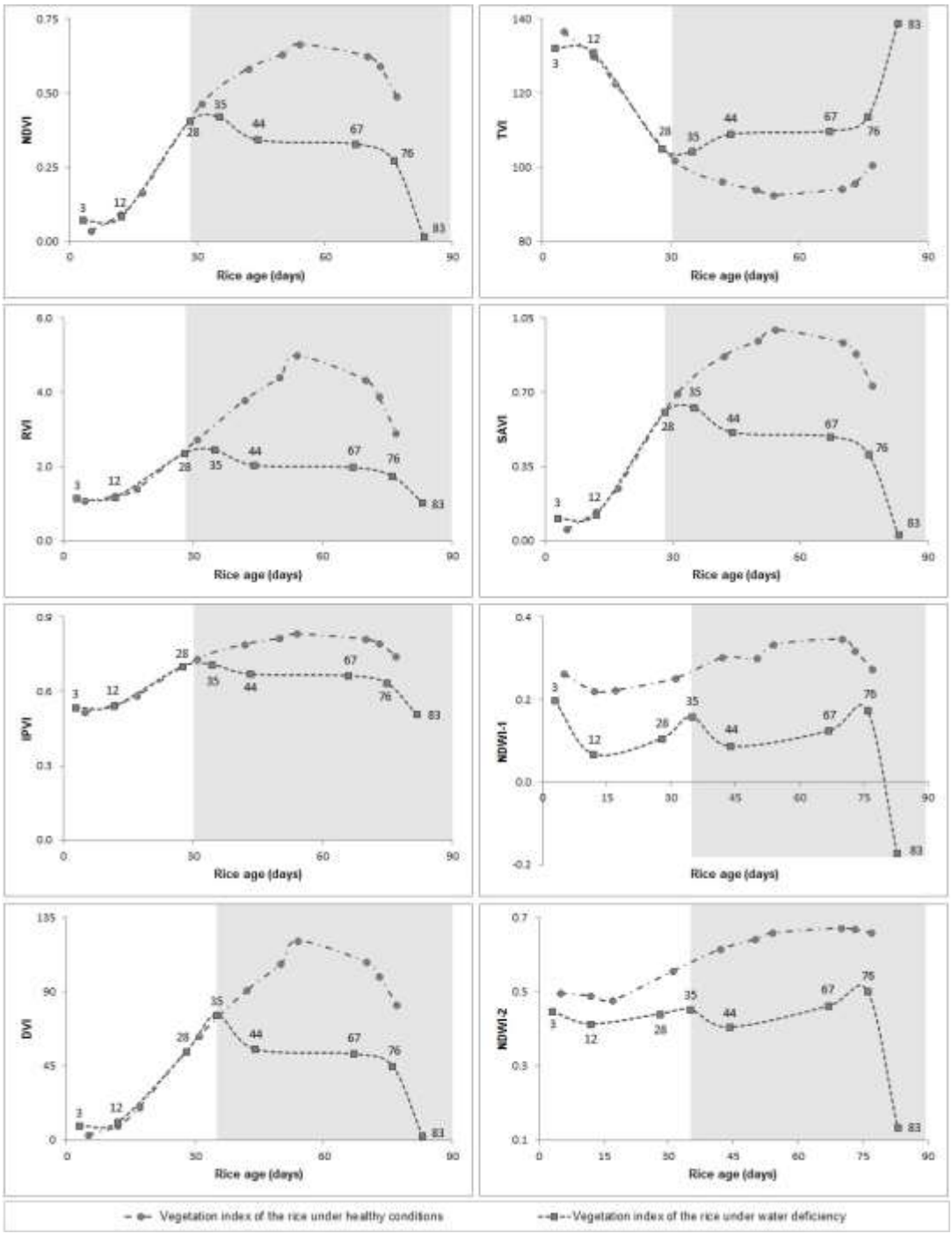

Figure 4.7 Vegetation index comparison of rice under healthy and water-deficient conditions. Eight vegetation indexes were evaluated, including NDVI, TVI, RVI, DVI, SAVI, IPVI, NDWI-1, and NDWI-2. The white areas in the chart indicate that both rice are still under normal conditions, while the dark areas show rice plants experiencing water deficiency.

For three observations of the vegetation index for similar rice ages, NDWI-1 provides the highest distinction between two rice conditions at rice ages of 42-44 days and 67-70 days, at -71.19% and -63.98%, while for rice ages of 76-77 days the highest difference of a vegetation index value is given by DVI with the value of -45.96% (Table 4.8). The highest difference average is provided by NDWI-1 with the value of -57.36% followed by RVI, SAVI and NDVI. However, for the early detection of water deficiency, the NDVI, RVI, and SAVI provided better responses. They could detect rice under water stress after the third observation (after rice age of 28 days). Other vegetation indices provided response after the fourth observation (after rice age of 35 days). A high distinction of vegetation index between rice under healthy conditions and in water stress was also shown by the statistical test (t-test). The entire vegetation index provided a significant difference between two rice conditions, with significant values in two-tailed t-tests lower than 0.05 (Table 4.8). Although NDWI-1 provided the highest difference average between two rice conditions compared with other vegetation index, the differences of NDWI-1 value between healthy and water deficiency rice is actually still smaller than the RVI. This is caused by differences of NDWI-1 values was already high when both rice plants are still in good health (Figure 4.7). Therefore, the RVI is the best vegetation index for both early detection of water deficiency and distinguish the two rice conditions.

The advantages of using a vegetation index compared with a single band is to reduce the spectral data to a single number that is related to the physical characteristics of vegetation (e.g., leaf area, biomass, productivity, photosynthetic activity, or percent cover) (Baret and Guyot, 1991; Huete, 1988) while minimising the effects of internal (e.g., canopy geometry and leaf and soil properties) and external (e.g., sun-target-sensor angles and atmospheric conditions at the time of image acquisition) factors on the spectral data (Baret and Guyot, 1991; Huete and Warrick 1990; Huete and Escadafal, 1991).

Table 4.8 Average differences of vegetation index values and t-tests between rice under healthy and water-deficient conditions in rice of similar ages. Negative values indicate that the vegetation value of water-deficient rice is lower than that in healthy rice and vice versa.

Rice Condition	Age	NDVI	RVI	IPVI	DVI	TVI	SAVI	NDWI-1	NDWI-2
Healthy conditions	42	0.583	3.797	0.792	90.602	96.087	0.872	0.302	0.615
Water deficiency	44	0.343	2.042	0.671	54.608	108.938	0.512	0.087	0.404
Difference of value		-41.17%	-46.22%	-15.28%	-39.73%	13.37%	-41.28%	-71.19%	-34.31%
Sig. (2-tailed) t-test		< 0.01	< 0.01	< 0.01	< 0.01	< 0.01	< 0.01	< 0.01	< 0.01
Healthy conditions	70	0.625	4.331	0.812	107.896	94.287	0.935	0.347	0.672
Water deficiency	67	0.329	1.98	0.664	51.724	109.842	0.492	0.125	0.462
Difference of value		-47.36%	-54.28%	-18.23%	-52.06%	16.50%	-47.38%	-63.98%	-31.25%
Sig. (2-tailed) t-test		< 0.01	< 0.01	< 0.01	< 0.01	< 0.01	< 0.01	< 0.01	< 0.01
Healthy conditions	77	0.489	2.914	0.744	82.201	100.555	0.731	0.275	0.658
Water deficiency	76	0.273	1.749	0.636	44.42	113.775	0.408	0.174	0.501
Difference of value		-44.17%	-39.98%	-14.52%	-45.96%	13.15%	-44.19%	-36.90%	-23.86%
Sig. (2 tailed) t-test		< 0.01	< 0.01	< 0.01	< 0.01	< 0.01	< 0.01	< 0.01	< 0.01
Average difference values		-44.23%	-46.83%	-16.01%	-45.92%	14.34%	-44.28%	-56.78%	-29.81%

T-tests of paired samples used 200-pixel samples. A value less than 0.05 in the t-test of paired samples indicates that there is a significant different between the rice under water deficiency and healthy conditions for a two-sample paired test (two-tailed).

4.4 Conclusions

Corrected digital number and vegetation indices of rice under water deficiency had significant differences compared to those of healthy rice. Rice plants under water deficiency in the study area were detected when the rice entered the second month after planting. When water deficiency happened, the reflectance of the visible bands increased significantly, while the reflectance of near- and middle-infrared bands decreased. For the early detection of water stress, the visible band was more sensitive than the near- and middle-infrared bands. The red band (B3) of Landsat ETM+ was the best band to distinguish rice plants under water stress and healthy conditions because it provided the highest difference in the reflectance percentage between rice under healthy and water-deficient conditions. The utilisation of the vegetation index to discriminate between rice under healthy and water-deficient conditions provided better results than when using a single band. The RVI is the best vegetation index for both early detection of water deficiency and distinguish the two rice conditions. Although Landsat ETM+ had SLC-off, it can still be used for rice monitoring because it has good spatial, spectral, and temporal resolutions, especially for session plants.

CHAPTER 5

RELATIONSHIP BETWEEN RICE SPECTRAL AND RICE YIELD USING MODIS DATA

5.1 Introduction

Rice is one of the important agricultural crops in Indonesia and Asia. Rice is the primary food source for more than three billion people and is one of the world's most important primary staple foods. Paddy rice fields account for approximately 15% of the world's arable land (IRRI, 1993; Khush, 2005). Information on the area and distribution of paddy rice fields is essential for food security management and water resource management (Xiao *et al*., 2005).

Satellite remote sensing has been used extensively and is recognised as a powerful and effective tool for detecting changes in land use and land cover (Treitz *et al*., 1992, Westmoreland and Stow, 1992; Harris and Ventura, 1995). Studies based on satellite imagery have been conducted to monitor rice growth and rice production (Shao *et al*., 1997; Panigrahy and Sharma, 1997; Oette *et al*., 2000; Shao *et al*., 2001; David *et al*., 2003). The estimation of rice yield from remote sensing data has been achieved with Landsat and NOAA AVHRR images (Rasmussen, 1992; Rasmussen, 1997; Honghui *et al*., 1999). However, the use of Landsat data is restricted by the availability of data for temporal analysis because the temporal resolution of Landsat is equal to 16 days (Quarmby *et al*., 1993). Alternatively, the utilisation of NOAA images is limited by the spatial resolution. In NOAA images, one pixel may correspond to 1000 m; thus, the probability is high that several types of land cover will be observed in one pixel, especially in small study areas. Moreover, the presence of multiple land uses in one pixel decreases the accuracy of the assessment (Strahler *et al*., 2006). The MODIS images provide better temporal resolution than Landsat imagery and offer better spatial resolution than NOAA images.

In chapter 1 until chapter 3, the algorithms for rice field mapping including its age and spectral differences of rice under normal and water stress have been developed. Before we perform rice production estimation, is necessary to study the rice plant growth parameters that most influence on rice production, and what kind of remote sensing parameter can be used to detect. In the present study, MODIS images at a spatial

resolution of 250 m were used to find out relationship between rice spectral and rice growth parameters. Thus, the objective of the present study was to assess the potential of MODIS images for the estimation of rice yield and to evaluate the relationship between MODIS rice spectral data and rice yield. The MODIS spectral data evaluated in this study were NDVI.

5.2 Study Area, Data and Method

5.2.1 Background and Study Area

The study area was located in Tabanan Regency, Bali Province, Indonesia, at 8°31’50” S latitude and 115°02’30” E longitude (Figure 5.1). The Tabanan Regency was selected as the study area because Tabanan is the central area for rice production in Bali. In the study area, rice plantings are organised by a *subak*, which is a social organisation centred around farming. The subak manages the irrigation water for approximately 150 – 300 ha of rice fields (Food Crops Agriculture Department, 2006). Moreover, rice fields managed by the subak are often planted at the same time. Due to the wide rice area, this type of farming system can be easily monitored by remote sensing.

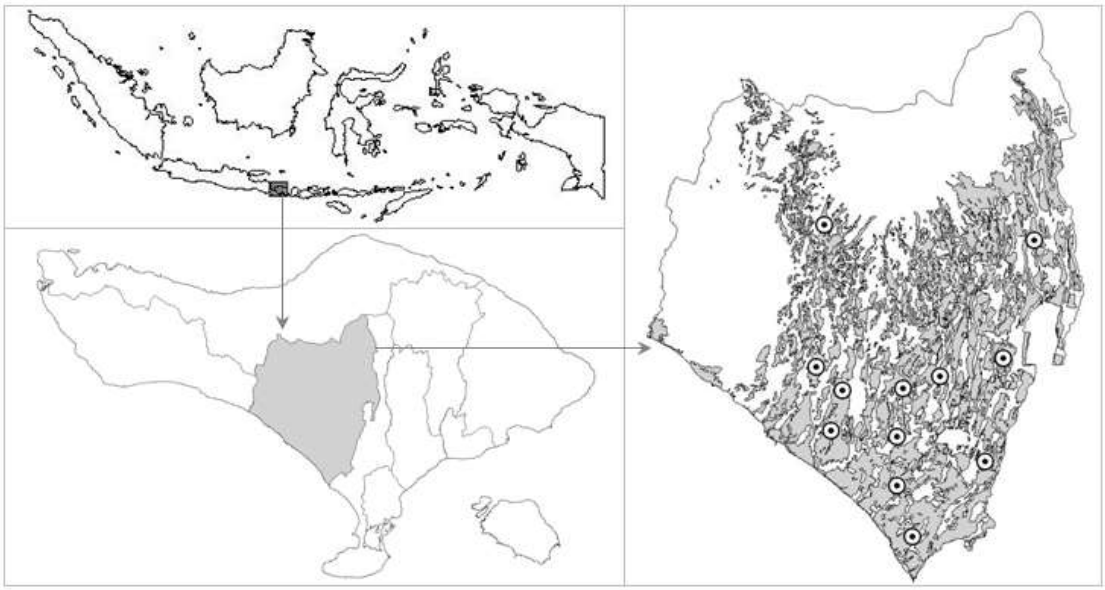

Figure 5.1. Location of the study area. In the image on the right, dark colours represent rice fields and regions in white represent other land uses. Rice harvest sampling sites are represented by points

5.2.2 Rice grain sample collection

The following considerations were used to select rice grain sampling sites: (1) the planted area should be wide and easily identifiable in MODIS images; and (2) the planted area should have the same rice variety. Therefore, based on the aforementioned considerations, a total of 12 samples were collected in the present study (Table 5.1). At each sampling site, rice grain was collected from a 2.5 m x 25 m area. The weight of the rice grain was measured in units of kg, and the yield was obtained in ton/ha.

Table 5.1. Sample location of harvested rice grain

Sample	Village Name	Geographic Coordinate		Rice age observation (day)	
		X	Y	Start	Finish
1	Beraban	290750.33	9048134.60	6	94
2	Pupuansawah	284957.98	9064585.63	5	93
3	Kukuh	289591.81	9055780.85	7	95
4	Gubug	290750.33	9053695.51	6	94
5	Kuwum	297701.47	9061805.17	7	95
6	RiangGede	292835.67	9060414.95	5	93
7	Abian Tuwung	296311.24	9053927.22	5	93
8	Tua	300018.52	9070841.65	6	94
9	Belimbing	284030.90	9072000.18	3	91
10	Sudimara	289591.81	9052073.85	5	93
11	Pangkungkarung	290055.22	9054390.63	4	92
12	Sembunggede	290055.22	9059488.13	4	92

Rice age is the age of the rice plant at the time the spectral data were obtained from the MODIS images.

5.2.3 MODIS Images

Among a suite of standard MODIS products available to users, we used the 8-day composite MODIS Surface Reflectance Band 1-2 Product (MYD09Q1). The spatial resolution of this MODIS product is 250 m, and two bands are provided, including the red band (620–670 nm) and the infrared band (841–876 nm). In the production of MOD09A1, atmospheric corrections for gases, thin cirrus clouds and aerosols are implemented (Vermote and Vermeulen, 1999). For each sample point, we collected 12

images from different MODIS composite dates. In total, 23 scene images were used in the present study. The MODIS images were obtained from the MODIS website (http://mrtweb.cr.usgs.gov/) as a free download using USGS MODIS Reprojection Tool Web Interface (MRTWeb).

5.2.4 Data Analysis

During the data analysis, the images were pre-processed, rice spectral information was collected from the MODIS images, and statistical analyses were conducted. To pre-process the data, MODIS images were obtained from the website, cloud-free images were selected and cropped, and the geographic coordinates were transformed. Last, the rice spectral information obtained from the MODIS images was transformed into the NDVI, according to the following expression:

$$NDVI = \frac{Infrared\ band - Red\ band}{Infrared\ band + Red\ band} \quad (5.1)$$

The red and infrared band of the NDVI equation were obtained from the MODIS images, which were collected from 12 different locations, and the relationship between rice age and the NDVI was determined. According to the results of our previous research (Nuarsa and Nishio, 2007), the quadratic equation best describes the relationship between rice age and the NDVI. From the quadratic equation, the maximum NDVI ($NDVI_{max}$), the age of the rice plant at the $NDVI_{max}$ ($Age_{NDVImax}$), and the total NDVI (∑ NDVI) was calculated, as shown in Figure 5.2.

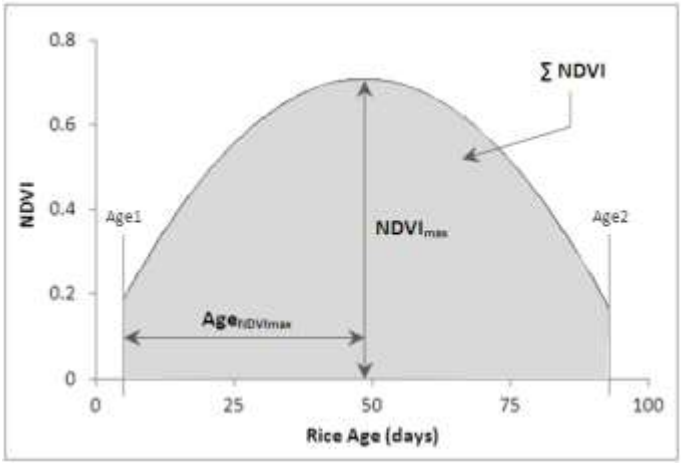

Figure 5.2 An illustration of the method used to calculate $Age_{NDVImax}$, $NDVI_{max}$, and ∑NDVI

If the relationship between rice age and the NDVI can be written as $y = ax^2 + bx + c$ (where y is the NDVI and x is the rice age), then the value of $Age_{NDVImax}$ can be determined when $\Delta y/\Delta x$ is equal to 0. In addition, the value of x can be calculated according to the following equation:

$$y = ax^2 + bx + c\,; \tag{5.2}$$

$$\frac{\Delta y}{\Delta x} = 2ax + b\,;$$

$$0 = 2ax + b\,;$$

$$x = \frac{-b}{2a};$$

where y is the NDVI, x is the rice age, a and b are the coefficients of x^2 and x, respectively, and c is a constant. In the aforementioned equation, x is equal to $Age_{NDVImax}$. By substituting the value of x into $y = ax^2 + bx + c$, the value of y at the $NDVI_{max}$ can be obtained. Alternatively, ∑NDVI can be computed from the following equation:

$$\sum NDVI = \int_{Age1}^{Age2} (ax^2 + bx + c)\, dx \tag{5.3}$$

where Age1 and Age 2 are the beginning and end of rice plant observation, respectively. The next step of the data analysis process was to determine the relationship between $Age_{NDVImax}$, $NDVI_{max}$, ∑NDVI and the yield of rice. In addition, the equation that provided the best fit to the experimental data was used to estimate the rice yield. To this end, the determination coefficient (R^2) and the standard error of the estimation (SE) were calculated to determine the optimal equation (Lane *et al.*, 2008). High values of R^2 and low values of SE indicate that the equation provides a superior fit to the experimental data.

$$R^2 = 1 - \frac{\sum y - \bar{y}')^2}{\sum y - y')^2} \tag{5.4}$$

$$SE = \sqrt{\frac{\sum (y - y')^2}{n}} \tag{5.5}$$

where R^2, SE, y, y', $\bar{y}$', and n are determination coefficient, standard error of estimation, actual value, predicted, value, average predicted value, and number of samples respectively.

5.3. Result and Discussion

For all 12 samples in the study area, the quadratic relationship between rice age and the NDVI is shown in Table 5.2. The R^2 values of the equations were high and varied from 0.916 to 0.973. The highest R^2 and the lowest standard error (SE) of estimation were observed in sample 6, which was obtained from Riang Gede Village (Figure 5.3). Alternatively, the lowest R^2 and highest SE were observed in sample 2, which was obtained from Pupuan Sawah village. The R^2 and SE of sample 2 were 0.916 and 0.067, respectively.

Table 5.2. Quadratic equation coefficients, correlation coefficient (R^2) and standard error of estimation (SE) of the relationship between rice age and the NDVI

Site no.	Equation Coefficient			R^2	SE of Estimation
	a	b	c		
1	-0.000317	0.032054	-0.002647	0.966	0.046
2	-0.000272	0.028490	-0.032086	0.916	0.067
3	-0.000279	0.030654	-0.034772	0.935	0.060
4	-0.000287	0.029929	0.038867	0.946	0.054
5	-0.000236	0.022010	0.099268	0.946	0.047
6	-0.000275	0.026677	0.060132	0.973	0.036
7	-0.000285	0.029746	-0.015355	0.943	0.056
8	-0.000279	0.028580	0.033137	0.921	0.064
9	-0.000323	0.029540	0.074942	0.942	0.063
10	-0.000284	0.029380	0.023629	0.941	0.057
11	-0.000266	0.029845	-0.009157	0.956	0.054
12	-0.000273	0.026384	0.053179	0.924	0.061

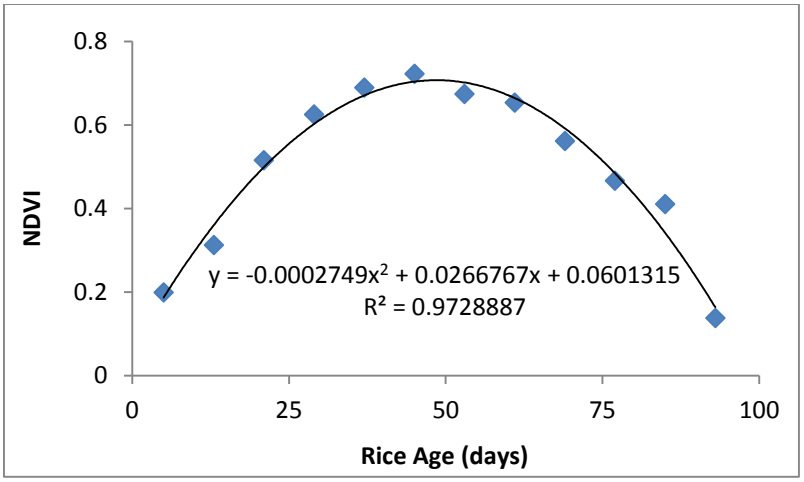

Figure 5.3 Relationship between rice age and the NDVI. Compared to other samples in the study area, this sample (sample 6) presented a quadratic equation with the highest R^2

The value of R^2 was high, indicating that the relationship between rice age and the NDVI was consistent. Moreover, the value of SE was low, which suggests that the difference between the estimated result and the actual value was small. An important factor that affects the R^2 and the SE of the NDVI is the appearance of clouds in the MODIS images. Thin cloud coverage can lead to inconsistencies in the reflectance values, which will affect the NDVI of the rice field. Therefore, the selection of cloud-free images is one of the most important steps in the data analysis. Moreover, the presence of mixed pixels reduces the rice spectral information and can affect the R^2 and the SE of the NDVI. In a mixed pixel, the rice plant and another object are present in the same pixel and can reduce the accuracy of the analysis (Strahler *et al*., 2006).

By applying Equation 5.2 and Equation 5.3, the $Age_{NDVImax}$, $NDVI_{max}$, and ∑NDVI can be calculated. The $Age_{NDVImax}$ values varied from 45.671 to 56.079; thus, from the beginning of the transplanting period, the NDVI of rice increased until the plant reached 1.5 months to 2 months of age, and then decreased until the end of the plant's life. The $NDVI_{max}$ values ranged from 0.631 to 0.828, and the value of the ∑NDVI fluctuated between 40.123 and 56.195 (Table 5.3).

Table 5.3. $Age_{NDVImax}$, $NDVI_{Max}$, ∑ NDVI,and rice yield in all 12 sampling points

Site no.	$Age_{NDVImax}$	$NDVI_{Max}$	∑ NDVI	Yield (ton/ha)
1	50.559	0.808	53.062	7.280
2	52.294	0.713	47.000	5.141
3	55.034	0.809	54.955	7.638
4	52.232	0.820	55.806	8.114
5	46.650	0.613	40.123	3.840
6	48.521	0.707	46.627	5.136
7	52.112	0.760	50.402	5.330
8	51.310	0.766	51.581	5.474
9	45.671	0.749	47.539	5.216
10	51.707	0.783	52.605	7.130
11	56.079	0.828	56.195	8.578
12	48.268	0.670	45.191	4.422

The following exponential equations best described the relationship between $Age_{NDVImax}$, $NDVI_{max}$, ∑NDVI and the yield of rice: $y = 0.2497e^{0.0623x}$, $y = 0.3376e^{3.8012x}$, and $y = 0.4745e^{0.0504x}$, respectively (Figure 5.4, Figure 5.5, and Figure 5.6). The strongest relationship was observed between the ∑NDVI and the rice yield. The highest value of R^2 (0.9230) and the lowest value of the SE (0.076) was obtained from the ∑NDVI and the rice yield (Table 5.4). Alternatively, $Age_{NDVImax}$ and $NDVI_{max}$ presented an R^2 and SE of 0.5776 and 0.175 and 0.8919 and 0.089, respectively. Similarly, a positive correlation between leaf area index (LAI), ∫NDVI and the rice yield was observed by Harrison *et al*. (1984), who used Landsat MSS data, and Rasmussen (1992), who utilised NOAA AVHRR data.

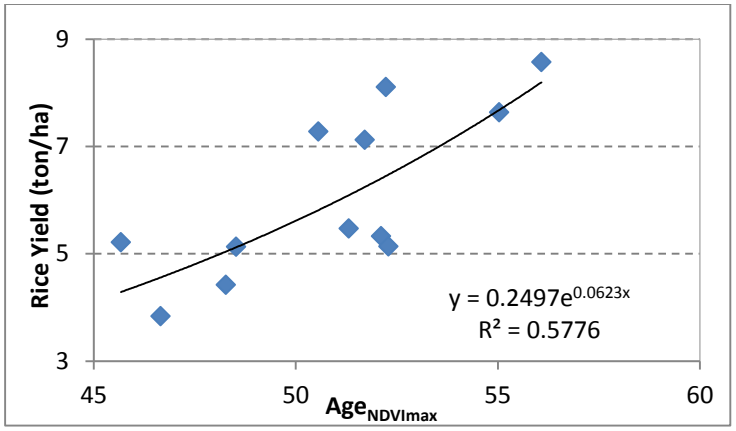

Figure 5.4. Relationship between rice age at the $NDVI_{max}$ and rice yield

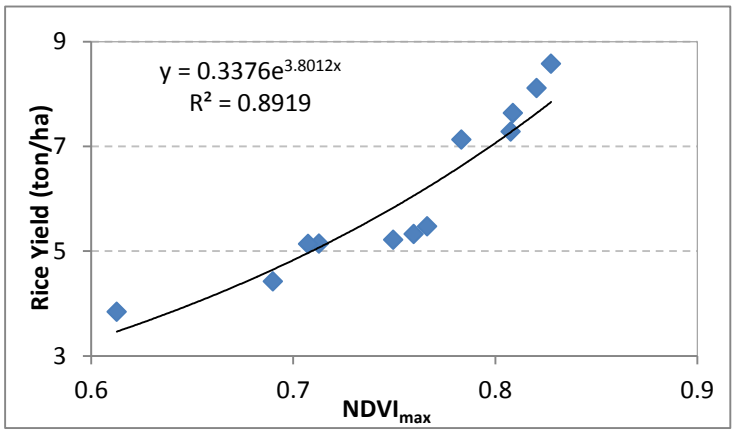

Figure 5.5. Relationship between the $NDVI_{max}$ and rice yield

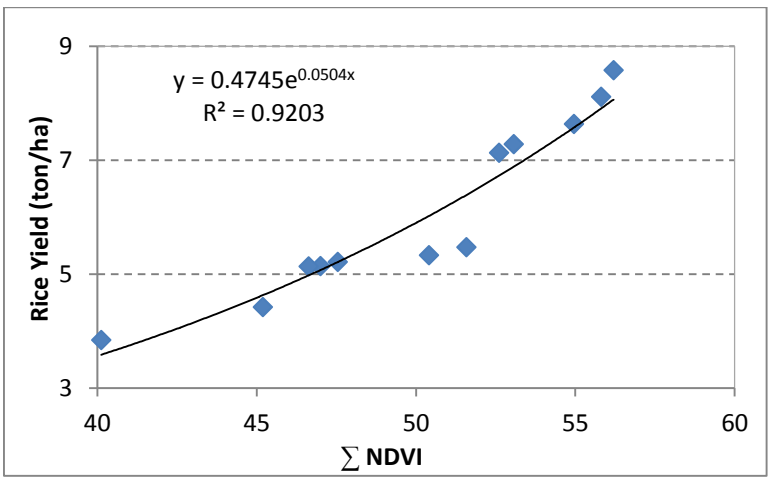

Figure 5.6. Relationship between the ∑NDVI and rice yield

Table 5.4. The R^2 and SE of $Age_{NDVImax}$, $NDVI_{max}$, and ∑NDVI

Variable	R^2	SE	Sig.
$Age_{NDVImax}$	0.5776	0.175	0.04
$NDVI_{max}$	0.8919	0.089	0.00
∑NDVI	0.9203	0.076	0.00

A strong positive correlation between the ∑NDVI and the yield of rice indicates that an increase in the total NDVI during the lifetime of the plant will improve the rice yield. Furthermore, high NDVI values indicated that the infrared (NIR) band of the rice plant was high (Equation 5.1). NIR reflectance of rice is directly related to green biomass (Niel and McVicar, 2001), and NIR light is highly scattered by water in spongy mesophyll cells (Harrison and Jupp, 1989). Thus, high NDVI values are indicative of high chlorophyll content. Chlorophyll is the most important part of the rice plant for photosynthetic activity, which produces carbohydrates to form rice plant tissue and rice grain, and has a significant effect on the yield at harvest.

5.4 Conclusions

A quadratic equation best described the relationship between the NDVI and rice age, and R^2 values ranging from 0.916 to 0.973 were observed. Among the three growth variables evaluated in this study, the total NDVI during the lifetime of the rice plant (∑NDVI) displayed the strongest exponential relationship to the rice yield (R^2 = 0.9203) and the lowest standard error of estimation (SE = 0.076). Compared to the ∑NDVI, the $NDVI_{max}$ and $Age_{NDVImax}$ presented lower R^2 (0.8919 and 0.5776, respectively) and higher SE values (0.089 and 0.175, respectively). Moreover, the results indicated that rice yield can be estimated from the following equation: $y = 0.4745e^{0.0504x}$, where y is the rice yield and x is the ∑NDVI. Based on the results of the present research, MODIS images can be used to estimate the yield of rice.

CHAPTER 6

RICE YIELD ESTIMATION USING LANDSAT ETM+ DATA AND FIELD OBSERVATION

6.1 Introduction

Rice is one of the most important agriculture crops in many countries, and it is a primary food source for more than three billion people worldwide (Khush, 2005; Yang *et al*., 2008). Forecasting crop yield well before harvest is crucial, especially in regions characterised by climatic uncertainties. Forecasting enables planners and decision makers to predict how much to import in the case of a shortfall or, optionally, to export in the case of a surplus. Forecasting also enables governments to put in place strategic contingency plans for the redistribution of food during times of famine. Therefore, the monitoring of crop development and crop growth and early yield prediction are generally of great importance (Sawasawa, 2003; Huang *et al*., 2002).

Crop yield estimation in many countries is based on conventional techniques of data collection for crop and yield estimation based on ground-based field visits and reports. Such reports are often subjective, costly, time-consuming and prone to large errors due to incomplete ground observation, leading to poor crop yield assessment and crop area estimations (Reynolds *et al*., 2000). In most countries, the data become available too late for the appropriate actions to be taken to avert food shortage (Sawasawa, 2003; Nuarsa *et al*., 2005).

Satellite remote sensing has been widely applied and is recognised as a powerful and effective tool for identifying agriculture crops (Bouvet *et al*., 2009; Pan *et al*., 2010; Niel *et al*., 2003; Nuarsa *et al*., 2011). An important goal of agricultural remote sensing research is to spectrally estimate crop variables related to crop conditions, which can subsequently be entered into crop simulation and yield models (Ahlrichs and Bauer, 1983). To utilise the full potential of remote sensing for the assessment of crop conditions and yield prediction, it is essential to quantify the relationships between the agronomic parameters and spectral properties of the crop (Patel *et al*., 1985; Nuarsa and Nishio, 2007). Use of satellite spectral data for the estimation of crop yields is an attractive prospect because yield is related to crop vigour, which is related to the spectral response of the crop vigour, which in turn is related to the spectral response of the crop measured

by satellite sensors (Barnett and Thompson, 1982). There are reports of various studies on the suitability of satellite data for estimating crop yields. The correlation between the spectral reflectance of crops and agronomic variables has encouraged the application of these data in crop yield models (Tucker *et al*., 1980; Richardson *et al*., 1982).

Some of the research regarding the use of remote sensing in rice yield estimation uses global resolution images, such as those from the National Oceanic and Atmospheric Administration Advanced Very High Resolution Radiometer (NOAA AVHRR), to monitor rice fields (Quarmby *et al*., 1993; Rasmussen, 1997; Huang *et al*., 2002). However, the use of the global spatial resolution of satellite imaging has been restricted, particularly in small rice areas, because many types of land cover can appear in one pixel, which reduces the accuracy of the assessment (Strahler *et al*., 2006). In contrast, the utilisation of fine or medium spatial resolution satellite images, especially in session plants, has been limited because fewer images are available during the 120-day rice growth period (Currey *et al*., 1987). Landsat ETM+ has a good temporal, spatial, and spectral resolution for rice monitoring. The revisit time of Landsat ETM+ is 16 days, with a spatial resolution of 30 m. Landsat ETM+ has six bands with the same pixel size, and it has become beneficial in the development of algorithms for rice yield modelling (Christopher, 2004).

In chapter 5, we have found that the ∑NDVI is the most influential factor on rice production. To find out at what rice age NDVI showed the best relationship, field observation needs to be done. It's important to do so that rice yield prediction can be performed at the age of rice. Thus, the research will become more efficient without the need to make observations on the entire lifetime of rice plant.

The objectives of this study include the following: (1) to determine the best rice age for the relationship between rice growth parameters and rice yield; (2) to develop a model for rice yield estimation based on Landsat spectral images (NDVI); and (3) to assess the accuracy of the rice yield estimation model.

6.2 Study Area, Data and Method

6.2.1 Background and Study Area

The study area was located in Tabanan Regency, Bali Province, Indonesia, at 8°31’50” S latitude and 115°02’30” E longitude (Figure 6.1). The Tabanan Regency was

selected as the study area because Tabanan is the central area for rice production in Bali. Within the study area, rice plantings are organised by a *Subak*, which is a social organisation centred around farming. The Subak manages irrigation water for approximately 150 – 300 ha of rice fields (Food Crops Agriculture Department, 2006). Moreover, rice fields managed by the Subak are often planted at the same time. Due to the wide rice area, this type of farming system can be easily monitored by remote sensing.

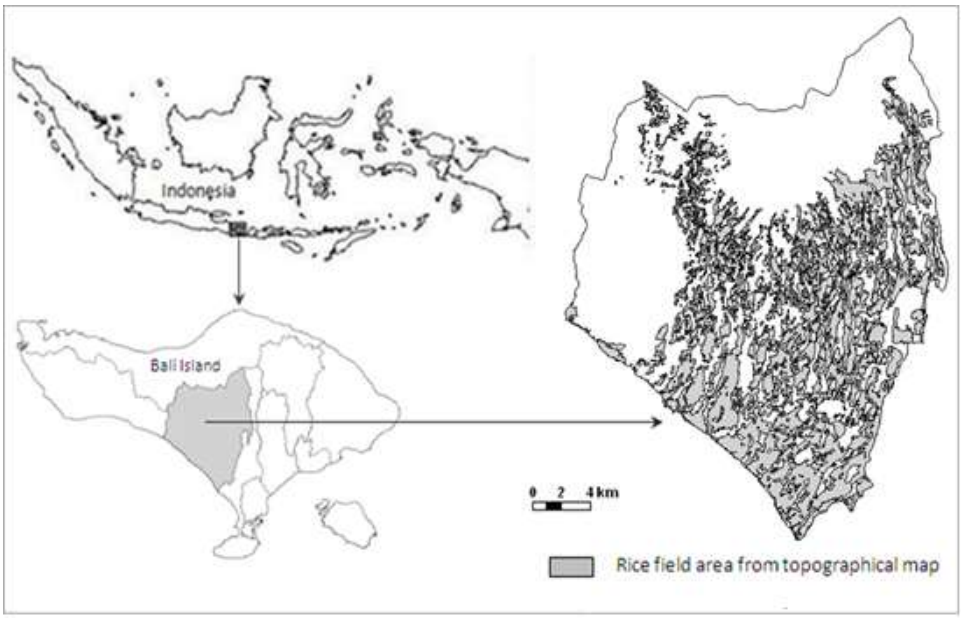

Figure 6.1 Location map of the study area

6.2.2 Field Observation

The field observation was conducted at eight stations from the middle of January 2011 to the middle of April 2011. The geographic coordinates of the field observations are shown in Table 6.1. The parameters measured in the field observation consist of transplanting date, rice variety, inter-row space, inter-plant distance, fertilisers and pesticides used, rice height, level of rice leaf greenness, and rice yield. The rice height and rice leaf greenness were measured using a ruler and the Minolta SPAD-502 leaf chlorophyll meter, respectively. The rice yield sample was performed in area of 2.5 m by 2.5 m in units of kg. The rice production was then converted into units of ton/ha. The measurement of rice height and the level of rice leaf greenness was performed from rice transplanting until harvest.

Table 6.1. Location coordinates, transplanting date, and harvesting date of the field observations

No	Subak Name	Geographic coordinate		Transplanting date	Harvesting date
		X	Y		
1	Gadon	291319	9048755	29-Nov-2010	27-Feb-2011
2	Gadon	291331	9048755	1-Dec-2010	7-Mar-2011
3	Medah 4	290738	9049284	3-Jan-2011	10-Apr-2011
4	Medah 4	290762	9049318	10-Dec-2010	21-Mar-2011
5	Medah 4	290200	9049257	14-Dec-2010	27-Mar-2011
6	Bengkel	290032	9049858	2-Dec-2010	7-Mar-2011
7	Bengkel	290113	9050166	25-Nov-2010	27-Feb-2011
8	Bengkel	289729	9050388	4-Dec-2010	27-Feb-2011

6.2.3 Collection of secondary data for rice grain sample

In addition to collecting rice yield from our field observation, we also collected rice yield from the secondary data (BPS, 2009; BPS, 2010). These data were used to develop an algorithm for rice yield estimation with satellite images (Landsat images). The following considerations were used to select the rice grain sampling sites: (1) the planted area should be wide and easily identifiable in Landsat images; (2) the planted area should have the same rice variety; (3) the age of the rice plant exhibits the best relationship between rice growth and rice yield according to the field observation survey. A total of 26 rice yield samples were collected in this study in 2008 and 2009 (Table 6.2).

Table 6.2. Location coordinates, transplanting date, harvesting date, and rice yield of the secondary data

No	Village Name	Geographic coordinate		Transplanting Date	Harvesting Date	Yield Ton/ha
		X	Y			
1	Nyambu	296565	9051325	17-Aug-2009	19-Nov-2009	5.696
2	Mengeste	294765	9070165	22-Aug-2009	21-Nov-2009	6.512
3	Wangaya Gede	291555	9071665	16-Aug-2009	20-Nov-2009	5.136
4	Kuwum	297705	9061855	18-Aug-2009	19-Nov-2009	6.368
5	Mekar Sari	300735	9074155	18-Aug-2009	24-Nov-2009	3.584
6	Belalang	289245	9047545	4-Aug-2009	6-Nov-2009	6.912
7	Wanagiri	286035	9070975	11-Mar-2009	9-Jun-2009	5.152
8	Tunjuk	296775	9061225	12-Mar-2009	16-Jun-2009	5.504
9	Perean Kangin	303015	9067285	14-Mar-2009	15-Jun-2009	6.128
10	Tengkudak	293805	9068935	10-Mar-2009	8-Jun-2009	7.648
11	Wangaya Gede	290835	9070015	12-Mar-2009	13-Jun-2009	5.920
12	Tajem	295815	9064945	6-Feb-2009	10-May-2009	7.488
13	Kuwum	297705	9061555	22-Jan-2009	25-Apr-2009	5.152
14	Denbantas	295245	9058825	24-Jan-2009	26-Apr-2009	6.160
15	Denbantas	294495	9058435	24-Jan-2008	23-Apr-2008	6.448
16	KukuhMarga	297255	9057745	18-Jan-2008	25-Apr-2008	6.896
17	Perean Kangin	302685	9069085	21-Jan-2008	23-Apr-2008	6.704
18	Biaung	297615	9069685	21-Jan-2008	20-Apr-2008	5.968
19	Pupuan Sawah	284985	9064735	28-Mar-2008	26-Jun-2008	5.344
20	Angseri	298185	9075355	27-Mar-2008	3-Jul-2008	5.456
21	Apuan	299175	9075445	22-Mar-2008	24-Jun-2008	7.024
22	Bangli	299205	9077215	24-Mar-2008	20-Jun-2008	6.064
23	Buruan	294555	9064495	25-Mar-2008	24-Jun-2008	6.736
24	Tengkudak	292455	9070405	22-Mar-2008	26-Jun-2008	7.328
25	Biaung	298035	9069415	25-Mar-2008	25-Jun-2008	6.928
26	Senganan	295605	9073825	23-Mar-2008	26-Jun-2008	7.731

6.2.4 Landsat images

Landsat ETM+ acquired in 2008 and 2009 were used in this study. This satellite image can be freely downloaded from the NASA website (http://glovis.usgs.gov). The Landsat in 2009 was used to develop the model for rice yield estimation, and the Landsat in 2008 was utilised to assess the accuracy of the model. The total of the Landsat images used in this study are 8 scenes for both 2008 and 2009 (Table 6.3).

Table 6.3 Values of d(1), μ_0 (2), and K_l(3) for every acquisition date of Landsat ETM+ in healthy rice

Acquisition date	Path	Row	DOY	d	μ_0	K_l					
						ETM1	ETM2	ETM3	ETM4	ETM5	ETM7
18-Mar-2008	116	66	96	1.00069	0.822732	45.77	27.02	14.81	25.80	2.02	0.31
21-May-2008	116	66	128	1.00928	0.776037	45.00	26.22	14.81	23.86	1.89	0.35
6-Apr-2009	116	66	288	0.99718	0.892566	54.30	36.57	21.01	34.49	3.27	0.57
8-May-2009	116	66	80	0.99612	0.833491	42.67	24.63	11.72	20.00	1.39	0.22
15-Oct-2009	116	66	112	1.00519	0.802622	47.32	28.61	14.81	23.86	1.89	0.31
21-Mar-2009	116	66	272	1.00177	0.876194	55.85	35.77	20.39	31.59	2.77	0.48
22-Apr-2009	116	66	78	0.99556	0.833224	45.77	26.22	12.34	21.93	1.77	0.22
29-Sep-2009	116	66	142	1.01230	0.75088	37.24	21.45	10.48	17.11	1.39	0.17

Sources: (1) Chander *et al.* (2009); (2) our image with calculations; (3) the DN of our image. DOY is the day of year.

6 2.5 Data analysis

There are three steps to the data analysis in this study: analysis of the field observations, digital image processing of Landsat ETM+, and an accuracy assessment of the analysis results.

a. Data analysis of the field observation

A data analysis of the field observations was performed to determine the relationship between the rice growth parameters and rice yield. The rice height, rice leaf greenness, and their combinations are the main aspects of rice growth evaluated in this study. These parameters can be monitored from the satellite images using a vegetation index. A question arises when the best relationship occurs between rice parameters and rice yield. To address this question, we calculated the relationship between rice height, rice leaf greenness, and rice height times leaf greenness with rice yield at every 7 days of rice age. The highest coefficient of determination (R^2) and the lowest standard error of estimation (SE) were judged as the best relationship. The R^2 and SE were calculated using the following equation.

$$R^2 = 1 - \frac{\sum y - \bar{y}')^2}{\sum y - y')^2} \quad (6.1)$$

$$SE = \sqrt{\frac{\sum (y - y')^2}{n}} \quad (6.2)$$

where R^2, SE, y, y', $\bar{y}\bar{y}$', and n are the determination coefficient, standard error of estimation, actual value, predicted value, average predicted value, and number of samples, respectively.

b. Landsat image processing

The first step of Landsat image processing was radiometric correction. The digital number (DN) of the Landsat ETM+ at different acquisition dates was converted to the corrected digital number (cDN) to eliminate the radiometric and atmospheric effects of the images so that they had comparable values. In this study, we used a simple radiometric correction model introduced by Pons and Solé-Sugrañes (1994). The variables used for the radiometric correction are shown in Tables 6.3 and 6.4. The form of the model is as follows:

$$cDN = 1000a(DN - K_l)d^2/[\mu_s S_0 e^{(-\tau_0/\mu_0)} e^{(-\tau_0/\mu_v)}] \quad (6.3)$$

(i) (if $250 < cDN \leq 318.3$; cDN = 254),

(ii) (if cDN > 318.3; cDN = 255),

(iii) (if $\mu_s \leq 0$; cDN = 255),

where cDN = corrected digital number

a = gain value of each Landsat band

DN = digital number

K_l = radiance value of zone completely under shade

d = actual Sun-Earth distance

μ_s = cosine of the incident angle

S_0 = exoatmospheric solar irradiance

τ_0 = optical depth of the atmosphere

μ_0 = cosine of the solar zenith angle

μ_v = cosine of the sensor view angle

Table 6.4 Values of τ_0(1), S_0(2), and a(3) for every spectral Landsat band for both healthy and water-deficient rice

Band	τ_0	S_0 ($Wm^{-2}\mu m^{-1}$)	a
ETM1	0.5	1997	0.7757
ETM2	0.3	1812	0.7957
ETM3	0.25	1533	0.6192
ETM4	0.20	1039	0.9655
ETM5	0.125	230.8	0.1257
ETM7	0.075	84.9	0.0437

Sources: (1) Dozier (1989); (2) Chander *et al.* (2009); (3) our image with calculations.

A Landsat spectral was obtained for the location of the rice grain sampling (Table 6.2). The Normalized Vegetation Index (NDVI) was then calculated according to the following expression:

$$NDVI = \frac{Infrared\ band - Red\ band}{Infrared\ band + Red\ band} \quad (6.4)$$

The red and infrared bands of the NDVI equation were band-3 and band-4 of Landsat respectively, which were radiometrically corrected. The next step is to determine the relationship between NDVI and rice yield with the equation below:

$$y = f(x) \quad (6.5)$$

where y and x are rice yield and NDVI, respectively. To develop the rice yield estimation model, we used the data of rice yield and Landsat images for 2009.

c. Accuracy assessment

An accuracy assessment was performed to determine the accuracy of the rice yield estimation obtained from the analysis of the Landsat images. The value resulting from the estimated equation (Equation 6.5) compared with the reference rice yield was obtained from a statistical agency (BPS, 2009). Both the rice yield from the estimated result and the reference data were plotted on the chart to determine the level of agreement between the estimated result and the reference data. Schematically, the research procedure is shown in following flowchart.

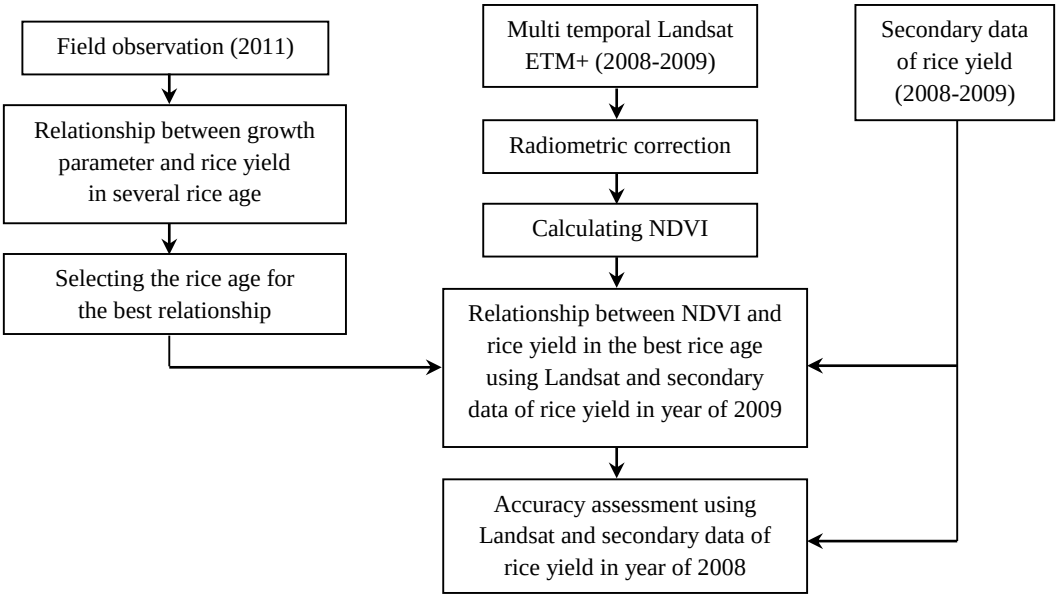

Figure 6.2 Research procedure used in this study

6.3 Result and Discussion

6.3.1 Relationship between rice growth parameters and rice yield based on field observations

There were three parameters of rice growth evaluated in this study: rice plant height, leaf greenness, and plant height times leaf greenness. Tables 6.5-6.7 show the field measurement of the third rice growth parameters starting from a rice age of 28 days due to the unmeasured leaf greenness in the early rice age. The trend of rice height increased from the transplanting date to the age of 77 days, and it decreased until harvest time. Similar to rice height, the greenness of the rice leaves also increased from 28 days to 56 days after transplanting and decreased until the harvesting period. For rice height times leaf greenness, the peak value mostly occurred at a rice age of 63 days.

Table 6.5 Plant height at several rice ages

	Rice height (cm)							
Age	I-1	I-2	II-1	II-2	III-1	IV-1	IV-2	V-1
28	40.91	42.22	43.51	40.18	58.72	53.65	49.74	80.46
35	60.77	62.08	54.89	54.64	63.81	71.53	70.77	85.45
42	77.55	78.79	65.63	67.55	68.76	86.67	88.28	90.01
49	91.24	92.34	75.74	78.90	73.55	99.04	102.26	94.14
56	101.85	102.73	85.21	88.70	78.20	108.67	112.71	97.84
63	109.36	109.97	94.05	96.93	82.70	115.54	119.64	101.10
70	113.79	114.06	102.25	103.61	90.01	119.66	123.04	103.94
77	115.14	114.99	109.81	108.72	91.26	121.02	122.90	106.34
84	113.39	112.76	116.73	112.28	95.32	119.63	119.24	108.32
91	108.56	107.38	123.02	114.28	99.23	115.48	112.06	109.86

Table 6.6 Greenness of rice leaves at several rice ages

	Rice greenness (SPAD unit)							
Age	I-1	I-2	II-1	II-2	III-1	IV-1	IV-2	V-1
28	35.70	35.66	34.93	35.09	38.66	45.11	36.48	28.96
35	38.22	36.62	36.83	36.69	38.00	43.13	37.81	32.86
42	39.78	37.00	37.92	37.82	37.38	41.34	38.58	35.48
49	40.38	36.79	38.22	38.47	36.83	39.75	38.77	36.82
56	40.01	35.99	37.71	38.63	36.34	38.36	38.40	36.87
63	38.69	34.60	36.39	38.32	34.00	37.16	37.46	35.64
70	36.41	32.63	34.27	37.53	35.53	36.16	35.95	33.12
77	33.16	30.06	31.35	36.25	35.21	35.35	33.87	29.32
84	28.96	26.91	27.63	34.50	34.96	34.74	31.22	24.24
91	23.79	23.17	23.10	32.26	34.76	34.33	28.01	17.87

Table 6.7 Height times greenness of rice leaves at several rice ages

Age	Rice height x Rice greenness							
	I-1	I-2	II-1	II-2	III-1	IV-1	IV-2	V-1
28	1460.53	1505.43	1519.59	1409.67	2270.52	2420.17	1814.41	2330.04
35	2322.82	2273.57	2021.44	2005.09	2424.57	3085.21	2676.10	2808.12
42	3084.89	2915.10	2489.13	2554.89	2570.38	3583.01	3405.56	3193.76
49	3684.00	3396.97	2894.66	3035.21	2709.07	3937.24	3964.84	3466.01
56	4075.16	3697.29	3213.09	3426.68	2841.73	4168.30	4328.04	3607.24
63	4231.18	3805.27	3422.57	3714.40	2811.77	4293.37	4481.29	3603.13
70	4142.67	3721.29	3504.32	3887.98	3198.15	4326.40	4422.74	3442.71
77	3818.01	3456.84	3442.61	3941.52	3213.68	4278.09	4162.58	3118.29
84	3283.38	3034.54	3224.80	3873.60	3332.10	4155.90	3723.03	2625.54
91	2582.74	2488.16	2841.33	3687.29	3449.16	3964.06	3138.35	1963.44

Based on the statistical analysis, the rice plants at 63 days after transplanting showed the best relationship between rice growth parameters and rice yield. From the three parameters evaluated in this study, the rice plant height times leaf greenness provided the highest coefficient of determination (R^2) and lowest standard error (SE). The R^2 and SE values were 0.9598 and 0.139, respectively, whereas the R^2 and SE for rice height and rice leaf greenness individually were 0.8897 and 0.225 and 0.7171 and 0.364, respectively (Figures 6.3-6.5).

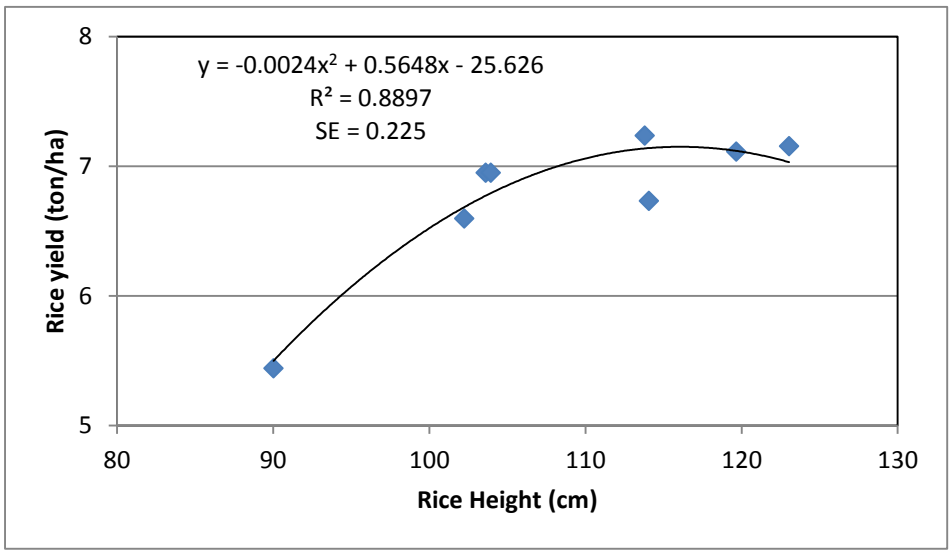

Figure 6.3 Relationship between rice height and rice yield at 63 days

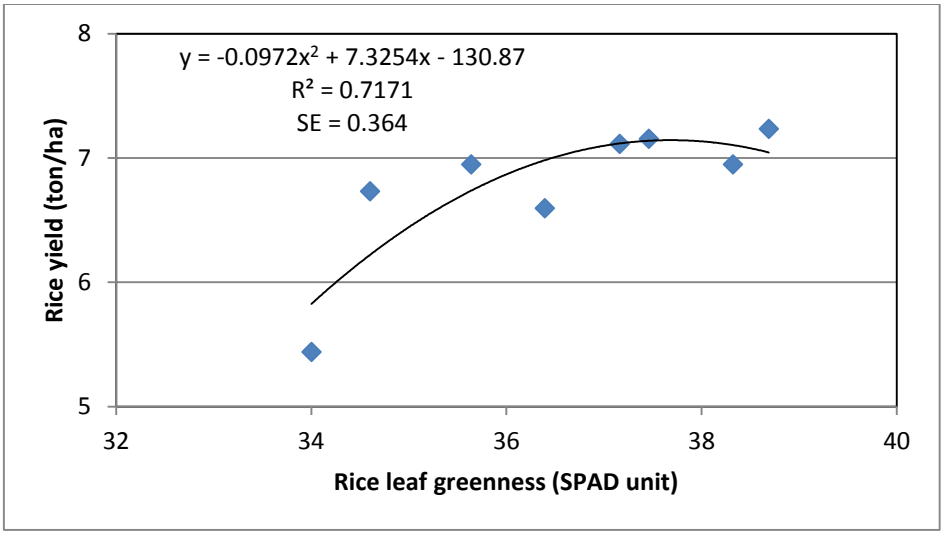

Figure 6.4 Relationship between rice leaf greenness and rice yield at 63 days

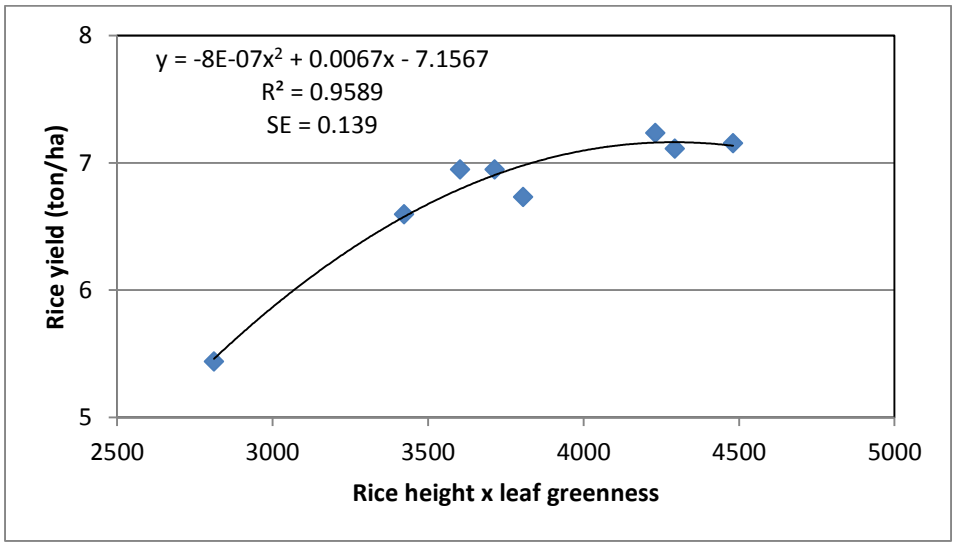

Figure 6.5 Relationship between rice height times rice leaf greenness and rice yield at 63 days

The height of rice plants indicates the volume of biomass, and rice leaf greenness expresses the chlorophyll content of the rice plant. The multiplication of rice height by leaf greenness illustrates the total chlorophyll content of the biomass of rice. Chlorophyll is the most important component of the rice plant for photosynthetic activity, which produces carbohydrates to form rice plant tissue and the rice grain, and it has a significant effect on the rice yield at harvesting time. Therefore, the chlorophyll content of the biomass has a close relationship with rice yield.

The highest relationship of all rice growth parameters evaluated in this study with rice yield was found at an age of 63 days. This stage of rice growth represents the peak of its vegetation index and the highest chlorophyll content in its life. This period is also a transition stage of vegetation and generation (Nuarsa and Nishio, 2007).

6.3.2 Relationship between vegetation index of Landsat images and rice yield

Based on the field observation results, the best rice age for estimating rice yield from rice growth parameters is two months after transplanting. Therefore, an estimation of rice yield using remote sensing data (Landsat ETM+) was performed at that rice age. Landsat ETM+ and location rice grain samples were selected for a rice age of two months. After radiometric correction to the Landsat ETM+ images, the digital values of the rice field in Landsat image were collected, and vegetation index (NDVI) was calculated using equation 6.4. From the 14 samples selected in the study (Table 6.8), there was an exponential relationship between NDVI and rice yield, with the equation $y = 0.3419e^{4.1587x}$ and an $R^2 = 0.852$ (Figure 6.6), where y and x are the rice yield and NDVI, respectively.

Table 6.8 Samples of Landsat image pixels of B3, B4, NDVI, and rice yield

Site no.	B3	B4	NDVI	Rice yield Ton/ha
1	27.21	137.21	0.67	5.70
2	27.11	138.01	0.71	6.51
3	24.41	130.02	0.68	5.14
4	28.17	136.81	0.69	6.37
5	32.80	125.43	0.59	3.58
6	26.54	142.90	0.73	6.91
7	23.09	153.69	0.63	5.15
8	27.83	154.11	0.69	5.50
9	29.69	148.40	0.67	6.13
10	34.33	168.07	0.73	7.65
11	29.48	155.59	0.68	5.92
12	30.25	158.85	0.74	7.49
13	26.31	153.87	0.64	5.15
14	27.88	162.98	0.71	6.16

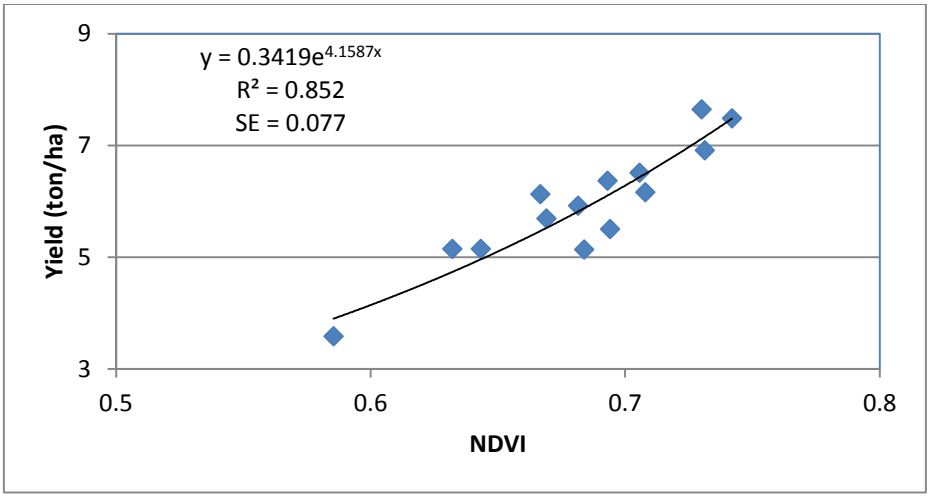

Figure 6.6 Relationship between NDVI and rice yield at 63 days

The exponential relationship between the NDVI and rice yield indicates that increasing NDVI values at approximately two months will increase the rice yield. Increasing NDVI significantly improves the rice yield at an NDVI value between 0.6 and 0.75. However, above 0.75, any increase in the NDVI value produces only a slight improvement in the rice yield.

The NDVI formula is formed by the red (B3) and near-infrared (B4) bands of Landsat ETM+. The NDVI value is directly proportional to the value of the near-infrared band and is inversely proportional to the value of the red band (Equation 6.4). An increase of the B3 value will decrease the NDVI value, and an increase of the B4 value will increase the NDVI value. Chlorophyll pigments present in the leaves absorb the red band. The near-infrared reflectance of rice is directly related to green biomass (Casanova *et al.*, 1998). In the near-infrared portion, the radiation is scattered by the internal spongy mesophyll leaf structure, which leads to higher values in the near infrared (NIR) channels (Baret and Guyot, 1991; Harrison and Jupp, 1989). Thus, high NDVI values are indicative of high chlorophyll content. Chlorophyll is the most important component of the rice plant for photosynthetic activity to produce rice plant tissues and the rice grain.

6.3.3 Accuracy assessment of rice yield estimation

To determine the accuracy of the rice yield estimation based on the spectral value of Landsat images (NDVI), an accuracy assessment was performed. The collection procedure of the Landsat images and the rice yield sample was the same as with the development of the rice yield estimation model. The Landsat images used in this method

were from 2008. The Landsat spectral values (B3, B4, and NDVI), rice yield from the reference, and rice yield resulting from the estimation equation are shown in Table 6.9. Based on the statistical analysis, there was a linear relationship between the referenced rice yields and the estimated rice yield with the equation $y = 0.7781x + 1.1441$. The R^2 and standard error of the estimation were 0.9262 and 0.21 ton/ha, respectively (Figure 6.7). The coefficient of determination greater than or equal to 0.8 demonstrates the strong agreement between the remotely sensed estimation and the reference data (Lillesand and Kiefer, 2000; Congalton *et al*., 1983).

Table 6.9. Comparison between rice yield resulting from the estimation and the reference data

Site no.	B3	B4	NDVI	Rice yield (ton/ha)	
				Reference	Estimation
1	25.97	148.55	0.70	7.23	6.35
2	29.20	168.82	0.71	6.90	6.42
3	26.84	159.11	0.71	7.03	6.59
4	30.40	157.29	0.68	5.97	5.69
5	31.16	146.86	0.65	5.34	5.10
6	31.16	157.24	0.67	5.46	5.53
7	28.96	163.27	0.70	6.70	6.25
8	32.11	177.31	0.69	6.06	6.11
9	28.12	165.23	0.71	6.74	6.53
10	29.28	185.47	0.73	7.33	7.04
11	30.11	188.69	0.72	7.18	6.96
12	31.34	223.90	0.75	8.66	7.88

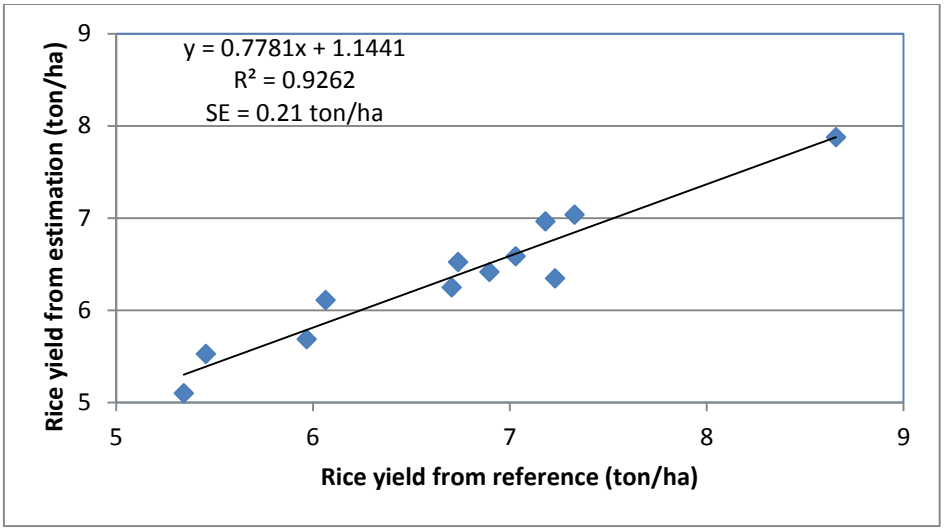

Figure 6.7. Relationship between rice yield resulting from the estimation and the reference data

6.3. Conclusions

The multiplication of rice height by rice leaf greenness at an age of 63 days showed the best relationship with rice yield based on the field observation. The form of this relationship was quadratic, with the equation of $y = -8E\text{-}07x^2 + 0.0067x - 7.1567$, and the R^2 and SE of the estimation were 0.9589 and 0.139, respectively. The estimation of rice yield using the vegetation index (NDVI) of Landsat ETM+ images produced an exponential relationship with the equation $y = 0.3419e^{4.1587x}$, where y and x are rice yield and NDVI, respectively. The R^2 and SE of the estimation were 0.852 and 0.077, respectively. An accuracy assessment of rice yield estimation using Landsat images was performed by comparing the rice yield resulting from the estimation result and the reference data. The result showed a linear relationship with the equation $y = 0.7781x + 1.1441$, where y and x were rice yield from the estimate result and reference data, respectively, with the R^2 and SE of the estimation at 0.9262 and 0.21, respectively. The R^2 greater than or equal to 0.8 demonstrates a strong agreement between the remotely sensed estimation and the reference data. Thus, Landsat ETM+ has a good potential for application to rice yield estimation.

CHAPTER 7

GENERAL CONCLUSIONS

Characteristics of rice plants with diversity of land cover are a challenge in mapping of rice fields using remote sensing data. By using analysis of variance, the challenge is actually an advantage because of differences in the high variant of rice plants can easily be separated by other land cover. Temporal variance analysis is a new algorithm developed in this study. The algorithm was suitable method to map the rice areas using Modis images with the overall accuracy and Kappa value were 87.91% and 0.8371 respectively. This accuracy is better than other previous method.

To estimate rice production continuously, we not only need the rice field distribution map, but also information about rice age. Rice growth vegetation index (RGVI) is a new vegetation index developed in this study to predict the rice age. The RGVI is a better vegetation index to describe difference of rice age than existing vegetation indexes. Landsat ETM+ has good capabilities to monitor and map rice plants using RGVI. Quantitative comparison of rice plants between analysis results and reference data showed coefficient of determination (R^2) is 0.975 with standard error of this estimation is 41.14 ha.

Because water for irrigation was a limiting factor for rice cultivation in Indonesia, especially in the study areas, the information about the differences of spectral characteristics between rice plants in healthy and water stress condition should be known. Thus, the accuracy rice production estimation would be more appropriate. Based on the result of this study, rice spectral under water deficiency had significant differences compared to those of healthy rice and could be detected by Landsat data. the Red band of Landsat images and ratio vegetation index (RVI) is the best Landsat spectral for both early detection of water deficiency and distinguish the two rice conditions.

Before we perform rice production estimation, is necessary to study the rice plant growth parameters that most influence on rice production, and what kind of remote sensing parameter can be used to detect. The result showed that Normalized difference vegetation index (NDVI) had a good relationship to the rice yield using Modis images. Total NDVI during the lifetime of the rice plant ($\sum$NDVI) showed the strongest

exponential relationship to the rice yield (R^2 = 0.9203) and the lowest standard error of estimation (SE = 0.076).

After we know that ∑NDVI is the most influential factor on rice production, field observation needs to be done to find out at what rice age NDVI showed the best relationship. It's important to do so that rice yield prediction can be performed at the age of rice. Thus, the research will become more efficient without the need to make observations on the entire lifetime of rice plant. Based on field observations, rice spectral at an age of 63 days after transplanting showed the best relationship with rice yield. The estimation of rice yield using the vegetation index (NDVI) of Landsat ETM+ images produced an exponential relationship with the equation $y = 0.3419e^{4.1587x}$, where y and x are rice yield and NDVI, respectively. An accuracy assessment of rice yield estimation was performed by comparing the rice yield resulting from the estimation result and the reference data. The R^2 and SE of the estimation were 0.9262 and 0.21, respectively.

Study of rice plant using remote sensing data especially in the tropical area has many challenges. Rice plants with a short lifespan of about three months on narrow area require high spatial and temporal resolution of satellite images. Modis images have good temporal resolution with daily revisit time. However it has a quite coarse spatial resolution. The finest resolution of Modis images is 250 m. On the other hand, Landsat TM/ETM+ have enough good spatial resolution of 30 m for rice mapping. However, their temporal resolution is only 16 days. At present, the use of Landsat and Modis together is the best solution to complement the disadvantages of each other. The challenges of cloudy image in the tropical area can be solved by creating a composite image and choose the time of research in the dry season.

For further research needs to be done a fusion image between Landsat, Modis and other image to maximize the use of satellite data for rice field mapping and production estimation.

ACKNOWLEDGEMENT

I wish to express my deepest and most sincere gratitude to Prof. Fumihiko Nishio, in Center for Environmental Remote Sensing, Chiba University, for inspiring guidance, encouragement, support and constructive criticism through course of this work. I am deeply grateful to Dr. Chiharu Hongo and Prof. Josaphat Tetuko Sri Sumantyo for providing me guidance, valuable suggestions, and supporting for obtain a JSPS Ronpaku scholarship. I am also very thanks to Prof. Nozomu Takeuchi for valuable command and suggestion during the seminar. My special thanks to late Prof. Yasuhiro Sugimori and Prof. Tasuku Tanaka, Director of Center for Remote Sensing and Ocean Sciences (CReSOS) Udayana University, Indonesia, late Prof. Nyoman Arya, Prof. Gede Mahardika, Dr. Takahiro Osawa. I also appreciate for their help and support to Prof. Fumihiko Nishio secretary, Mariko Shimaya san and CEReS student, I Wayan Gede Astawa Karang san, Shimada san, Onuma san and others. For my family, thanks a lot of the support. Finally, thank you very much to the Japanese government especially Japan Society for the Promotion of Science (JSPS) Ronpaku for scholarships granted to complete the Ph.D. program

REFERENCES

Ahlrichs. J. S. and Bauer, M.E, 1983, *Relation of agronomic and multispectral reflectance characteristics of spring wheat canopies*. Agronomy Journal, 75, pp. 987 - 993.

Asner, G.P., 1998, *Biophysical and biological sources of variability in canopy reflectance*. Remote Sensing of Environment, 64, pp. 234-253.

Atkinson, P.M. and Lewis, P., 2000, *Geostatistical classification for remote sensing: an introduction*. Computers and Geosciences, 26, pp. 361–371.

Bachelet, D., 1995, *Rice paddy inventory in a few provinces of China using AVHRR data*. Geocarto International, 10, pp. 23–38.

Bailey, J. S., Wang, K., Jordan, C. and Higgins, A., 2001, *Use of precision agriculture technology to investigate spatial variability in nitrogen yields in cut grassland*. Chemosphere, 42, pp. 131-140.

Bappenas, 2002, *Does Indonesia Face a Food Security Time Bomb*? Indonesian Food Policy Program. Available: http//:www.macrofoodpolicy.com (Accessed November 15, 2009).

Baret, F. and Guyot, G., 1991, *Potentials and limits of vegetation indices for LAI and APAR assessment*. Remote Sensing of Environment, 35, pp. 161-173.

Baret, F., Vanderbilt, V.C., Steven, M.D. and Jacquemoud ,S., 1994, *Use of spectral analogy to evaluate canopy reflectance sensitivity to leaf optical properties*. Remote Sensing of Environment, 48, pp. 253–260.

Barnett, T. L. and Thompson, D. R., 1982, *The use of large-area spectral data in wheat yield estimation.* Remote Sensing of Environment, 12, pp. 509-518.

Barrett, E.C. and Curtis, L.F., 1992, *Introduction to environmental remote sensing*. In: Introduction to Environmental Remote Sensing, 3, p. 426 (Barrett, E.C. and Curtis, L.F., Eds.), Chapman & Hall, London, U.K.

Barrs, H. D. and Prathapar, S. A., 1996, *Use of satellite remote sensing to estimate summer crop areas in the Coleambally Irrigation Area, NSW*. CSIRO, Division of Water Resources Consultancy Report 96/17, pp. 35.

Benedetti, R. and Rossini, S., 1993, *On the use of NDVI profiles as a tool for agricultural statistics: the case study of wheat yield estimate and forecast in Emilia Romagna*. Remote Sensing of Environment, 45, pp. 311-326.

Boehm, H.-D.V. and Siegert, F., 2001 Ecological impact of the one million hectare rice project in Central Kalimantan, Indonesia, Using Remote Sensing and GIS. Paper Presented at the 22nd Aian Conference on Remote Sensing. Asian Association on Remote Sensing.

Boschetti, M., Stroppiana, D., Brivio, P. A. and Bocchi, S., 2009, *Multi-year monitoring of rice crop phenology through time series analysis of MODIS images*. International Journal of Remote Sensing, 30, pp. 4643 - 4662.

Bouman, B.A.M., 1995, *Crop modeling and remote sensing for yield prediction*. Netherlands Journal of Agricultural Science, 43, pp. 143-161

Bouvet, A., Le Toan, T. and Lam-Dao, N., 2009, *Monitoring of the Rice Cropping System in the Mekong Delta Using ENVISAT/ASAR Dual Polarization Data*. IEEE Trans. Geoscience and Remote Sensing, 47, pp. 517 – 526.

BPS, 2003, *Tabanan in Number*. Annual Report, Statistic Center Agency of Tabanan Regency, pp 34 – 45.

BPS, 2005, *Report of Monthly Rainfall. Meteorological and Geophysical Agency*. Bali Province, Indonesia, pp. 45-50.

BPS, 2009, *Report of Monthly Rainfall of Bali Province, Indonesia*. Meteorological and Geophysical Agency, pp. 57-63.

BPS, 2010, *Report of Monthly Rainfall of Bali Province, Indonesia*. Meteorological and Geophysical Agency, pp. 51-56.

Carter, G.A. and Knapp, A.K., 2001, *Leaf optical properties in higher plants: Linking spectral characteristics to stress and chlorophyll concentration*. American Journal of Botany, 88, pp. 677–684.

Casanova, D., Epema, G.F. and Goudriaan, J., 1998, *Monitoring rice reflectance at field level for estimating biomass and LAI*. Field Crops Research, 55, pp. 83-92

Chakraborty, M. and Panigrahy, S., 2000, *A Processing and software system for rice crop inventory using multi-date RADARSAT ScanSAR data*. ISPRS Journal Photogrammetry and Remote Sensing, 55, pp. 119– 128.

Chander, G., Markham, B.L., Dennis L. Helder, D.L., 2009, *Summary of current radiometric calibration coefficients for Landsat MSS, TM, ETM+, and EO-1 ALI sensors*. Remote Sensing of Environment, 113, pp. 893-903.

Chen, E. X., Li, Z. Y. Li, Tan, B. X., Pang, Y., Tian, X., Li, B. B. Li, 2007, *Supervised wishart classifier for rice mapping using multi-temporal envisat asar aps data*. Proc. Envisat Symposium 2007, Montreux, Switzerland, pp 1-6.

Christopher Small, 2004, *The Landsat ETM+ spectral mixing space*. Journal of Remote Sensing of Environment, 93, pp. 1-17.

Congalton, R.G. and Green, K., 1999, *Assessing the Accuracy of Remotely Sensed Data*: Principles and Practices, pp. 43–70 (Florida: Lewis Publishers).

Congalton, R.G., Oderwald, R.G. and Mead, R.A., 1983, *Assessing Landsat Classification Accuracy Using Discrete Multivariate Analysis Statistical Techniques*. PERS, 49, pp. 1671–1678.

Currey, B., Fraser, A. S. and Bardsley, K. L., 1987, *How useful is Landsat monitoring*. Nature, 328, pp. 587-590.

David, D., Frolking, S., Li, C., 2003, *Trends in Rice-Wheat Area in China*. Field Crops Research, 87, pp. 89-95.

Dozier, J., 1989, *Spectral signature of Alpine snow cover from the Landsat Thematic Mapper*. Remote Sensing of Environment, 28, pp. 9-22.

Ehlers, M., Jadkowski, M. A., Howard, R. R. and Brostuen, D. E., 1990, *Application of SPOT data for regional growth analysis and local planning*. Photogrammetric Engineering and Remote Sensing, 56, pp. 175–180.

Fang, H. L., Wu, B. F., Liu, H. Y. and Huang, X., 1998, *Using NOAA AVHRR and Landsat TM to estimate rice area year-by-year*. International Journal of Remote Sensing, 19, pp. 521-525.

Fang, H., Wu, B., Liu, H. and Xuan, H., 1998, *Using NOAA AVHRR and Landsat TM to estimate rice area year-by-year*. International Journal of Remote Sensing, 3, pp. 521–525.

FAO, 2009. *World Rice Production Quantity*. Available online on http://faostat.fao.org/site/567/DesktopDefault.aspx?PageID=567, accessed on 26 October 2011.

Food Crops Agriculture Department, 2006, *Annual report of food crops*, pp. 125–135 (Department Agriculture of Local Governent).

Food Crops Agriculture Department, 2010, *Annual report of food crops*, 3 pp. 145-160 (Department Agriculture of Local Government, Bali Province Indonesia).

Gausman, H. W., 1974, *Leaf reflectance of near-infrared*. Photogrammetric Engineering and Remote Sensing, 40, pp. 183-191.

Gumma,M.K., Nelson, A. , Singh, A.N., Thenkabail , P.S. 2011. *Mapping rice areas of South Asia using MODIS multitemporal data*. Journal of Applied remote sensing, 5, pp: 1-26

Gupta, R.K., 1993, *Comparative study of AVHRR ratio vegetation index and normalized difference vegetation index in district level agriculture monitoring*. International Journal of Remote Sensing, 14, pp. 53–73.

Hall, A., Lamb D.W., Holzapfel, B. and Louis J., 2002, *Optical remote sensing applications for viticulture—a review*. Australian Journal of Grape and Wine Ressearch, 8, pp. 36–47.

Harris, P. M. and Ventura, S. J., 1995, *The integration of geographic data with remotely sensed imagery to improve classification in an urban area*. Photogrammetric Engineering and Remote Sensing, 61, pp. 993–998.

Harrison, B. A. and Jupp, D. L. B., 1989, *Introduction to remotely sensed data*, CSIRO Publications, pp 141-165.

Harrison, B. A., Jupp, D. L. B., Ibrahim, A. A. and Angus, J. F, 1984, *The use of Landsat data for monitoring growth of irrigated crops*. Third Australasian Remote Sensing Conference, Queensland, pp. 36-43.

Honghui, L., Xiaohuan, Y. and Naibin, W., 1999, *Remote sensing based estimation system for winter wheat yield in North China Plain*. Chinese Geographical Journal, 9, pp. 40-48.

Huang, J.F, Tang, S.C., Ousama A.I. and Wang R.C, 2002, *Rice yield estimation using remote sensing and simulation*. Journal of Zhejiang University Science, 3, pp. 461 – 466.

Huete, A. R. and Escadafal, R., 1991, *Assessment of biophysical soil properties through spectral decomposition techniques*. Remote Sensing of Environment, 35, pp. 149-159.

Huete, A. R. and Warrick, A. W., 1990, *Assessment of vegetation and soil water regimes in partial canopies with optical remotely sensed data*. Remote Sensing of Environment 32, pp. 115–167.

Huete, A., Didan, K., Miura, T., Rodriguez, E. P., Gao, X. and Ferreira, L. G., 2002, *Overview of the radiometric and biophysical performance of the MODIS vegetation indices*. Remote Sensing of Environment, 83, pp. 195–213.

Huete, A.R., 1988, A *soil-adjusted vegetation index (SAVI)*. Remote Sensing of Environment, 25, pp. 295–309

Hutchinson, C.F., 1982, *Techniques for combining Landsat and ancillary data for digital classification improvement*. Photogrammetric Engineering and Remote Sensing, 8, pp. 123–130.

Inoue, Y., Moran, M. S. and Horie, T., 1998, *Analysis of spectral measurements in paddy field for predicting rice growth and yield based on a simple crop simulation model*. Plant Production Science, 1, pp. 269-279.

IRRI, 1993, *1993–1995 IRRI Rice Almanac*. Manila: International Rice Research Institute, pp 178-185

Jacquemoud, S., 1993, *Inversion of the PROSPECT+SAIL canopy reflectance model from AVIRIS equivalent spectra: theorectical study*. Remote Sensing of Environment, 44, pp. 281-292.

Jacquemoud, S., Baret, F. and Hanocq, J.F., 1992, *Modeling spectral and bidirectional soil reflectance*. Remote Sensing of Environment, 41, pp. 123-132.

Jensen, J. R., 1986, *Introductory digital image processing: A remote sensing perspective*, pp. 205–220 (New Jersey: Prentice-Hall).

Khush, G.S, 2005, *What it will take to feed 5 billion rice consumers in 2030*. Plant Molecular Biology, 59, pp. 1-6.

Kirnak H, Kaya C, Tas I, Higgs D., 2001, *The influence of water deficit on vegetative growth, physiology, fruit yield and quality in eggplants*. Bulgarian J. Plant Physiol., 27, pp. 34–46.

Knipling, E. B., 1970, *Physical and physiological basis for the reflectance of visible and near-infrared radiation from vegetation*. Remote Sensing of Environment, 1, pp. 155-159.

Köksal, E.S., Kara, T., Apan, M., Üstün, H. and İlbeyi, A., 2008, *Estimation of green bean yield, water deficiency and productivity using spectral indexes during the growing season*. Irrigation and Drainage Systems, 22, pp. 209–223.

Khosa, M.K., Sidhu, B.S., and Benbi, D.K. ,2011, Methane emission from rice fields in relation to management of irrigation water. Journal of Environmental Biology, 32, pp: 169-192

Kupiec, J.A. and Curran, P.J., 1995, *Decoupling effects of the canopy and foliar biochemicals in AVIRIS spectra*. International Journal of Remote Sensing, 16, pp. 1731-1379.

Kuroso, T., Fujita, M. and Chiba, K., 1997, *Monitoring of rice fields using multi-temporal ERS-1 C-band SAR data*. International Journal of Remote Sensing, 18, pp. 2953-2965.

Lane, D., Lu J., Peres C., and Zitek E., 2008, *Online Statistics: An Interactive Multimedia Course of Study*. http://onlinestatbook.com/index.html (Visited June 23, 2010).

Le Toan, T., Ribbes, F., Wang, L.F., Floury, N., Ding, K.H., Kong, J.A., Fujita, M. and Kurosu, T., 1997, *Rice crop mapping and monitoring using ERS-1 data based on experiment and modeling results*. IEEE Trans. Geoscience and Remote Sensing, 35, pp. 41 – 56.

Lee, Y.-J., Yang, C.-M., Chang, K.-W. and Shen Y., 2008, *A simple spectral index using reflectance of 735 nm to assess nitrogen status of rice canopy*. Agronomy Journal, 100, pp. 205–212.

Liew, S.C., Kam, S.P., Tuong, T.P., Chen, P., Minh, V.Q., Balababa, L. and Lim, H., 1998, *Application of multitemporal ERS-2 synthetic aperture radar in delineating rice cropping systems in the Mekong River Delta, Vietnam*. IEEE Trans. Geoscience and Remote Sensing, 36, pp. 1412 – 1420.

Lillesand, T. M. and Kiefer, R. W., 2000, *Remote sensing and image interpretation*, pp 715–735 (New York: Wiley & Son).

Lillesand, T.M. and Kiefer, R.W., 1994. *Remote Sensing and Image Interpretation*, 3, pp. 427-517 (New York: John Wiley and Sons).

Liu, W. T. and Kogan,F., 2002, *Monitoring Brazilian Soybean Production Using NOAA/AVHRR Based Vegetation Condition Indices*. International Journal of Remote Sensing, 23, pp. 1161-1179.

Martin, R. D. J. and Heilman, J. L., 1986, *Spectral reflectance patterns of flooded rice*. Photogrammetric Engineering and Remote Sensing, 52, pp. 1885-1890.

Mas, J.F. and Ramı´rez, I., 1996, *Comparison of land use classifications obtained by visual interpretation and digital processing*. ITC Journal, 4, pp. 278-283.

Maas, S. J., 2000, *Linear mixture modeling approach for estimating cotton canopy ground cover using satellite multispectral imagery*. Remote Sensing of Environment, 72, pp. 304-308.

Maselli, F., Conese, C., Petkov, L. and Gilabert, M., 1992, *Use of NOAA-AVHRR NDVI data for environmental monitoring and crop forecasting in the Sahel. Preliminary Results*. International Journal of Remote Sensing, 13, pp. 2743-2749.

Matthews, R. B., Wassmann, R., Knox, J. W. and Buendia, L. V., 2000, *Using a crop/soil simulation model and GIS techniques to assess methane emissions from rice fields in Asia: Upscaling to national levels*. Nutrient Cycling in Agroecosystems, 58, pp. 201– 217.

McVicar, T. R., Jupp, D. L. B., Reece, P. H. and Williams, N. A., 1996a, *Relating LANDSAT TM vegetation indices to in situ leaf area index measurements*. CSIRO, Division of Water Resources Technical Memorandum 96.14, pp. 80.

Meaille, R. and Wald, L., 1990, *Using geographic information system and satellite imagery within a numerical simulation of regional urban growth*. International Journal of Geographic Information Systems, 4, pp. 445–456.

Mensha, J.K., Obadoni, B.O., Eroutor, P.G., Onome, I.F., 2006, *Simulated flooding and drought effects on germination, growth and yield parameters of Sesame* (*Sesamum indicum* L.), Afr. J. Biotech., 5, pp. 1249-1253.

Mohd, M.I.S., Ahmad, S. and Abdullah, A., 1994, *Agriculture Application of Remote Sensing: Paddy Yield Estimation from Landsat-5 Thematic Mapper Data*. Available on line at http://www.a-a-r-s.org/acrs/proceeding/ACRS1994/Papers/AGS94-3.htm, cccessed on 12 September 2011.

Myneni, R.B., Ross, J. and Asrar, G., 1989, *A review on the theory of photon transport in leaf canopies*. Agricultural and Forest Meteorology, 45, pp. 1-153.

National Land Agency, 2008, *Land Use Map of Bali Province*, pp 1–2 (Local Government of National Land Agency).

Naugle, B. I. and Lashlee, J. D., 1992, *Alleviating topographic influences on land-cover classifications for mobility and combat modeling*. Photogrammetric Engineering and Remote Sensing, 58, pp. 1217-1221.

Nemani, R. R. and Running, S. W., 1989a, *Estimation of regional surface resistance to evapotranspiration from NDVI and thermal-IR AVHRR data*. Journal of Applied Meteorology, 28, pp. 276-284.

Niel, V. T. G. and McVicar, T. R, 2000, *Assessing and improving positional accuracy and its effects on areal estimation at Coleambally Irrigation Area*. Cooperative Research Centre for Sustainable Rice Production Technical Report 101/00, pp. 101.

Niel, T.G.V. and McVicar, T.R, 2003, *A Simple method to improve field-level rice identification: toward operational monitoring with satellite remote sensing*. Australian Journal of Experimental Agriculture, 43, pp. 379–387.

Niel, T.G.V. and McVicar, T.R., 2001, *Remote Sensing of Rice-Based Irrigated Agriculture: A Review*. Rice CRC Technical Report P1105-01/01. Available online at: www.ricecrc.org (Accessed 5 October 2009).

Niel, T.G.V., McVicar, T.R., Fang, H. and Liang, S., 2003, *Calculating environmental moisture for per-field discrimination of rice crops*. International Journal of Remote Sensing, 24, pp. 885–890.

Notohadiprawira, T., 2006. Rationalizing the use of water resources in Indonesia. Paper presented on Gadjah Mada University Seminar, Indonesia, pp:1-6.

Nuarsa I.W., Kanno, S., Sugimori, Y. and Nishio, F, 2005, *Spectral Characterization of Rice Field Using Multi-Temporal Landsat ETM+ Data*. International Journal of Remote Sensing and Earth Sciences, 2, pp. 65-71.

Nuarsa, I.W. and Nishio, F, 2007, *Relationships between Rice Growth Parameters and Remote Sensing Data*. International Journal of Remote Sensing and Earth Sciences, 4, pp. 102-112

Nuarsa, I.W., Nishio, F. and Hongo, C., 2011, *Spectral Characteristics and Mapping of Rice Plants Using Multi-Temporal Landsat Data*. Journal of Agriculture Science, 3, pp. 54-67.

Oette, D. R., Warren B. C., Mercedes B., Maiersperger, T.K., and Kennedy, R.E, 2000, *Land Cover Mapping in Agricultural Setting Using Multiseasonal Thematic Mapper Data*. Remote Sensing of Environment, 76, pp. 139-155.

Okamoto, K. and Kawashima, H., 1999. *Estimation of rice -planted area in the tropical zone using a combination of optical and microwave satellite sensor data*. International Journal of Remote Sensing, 20, pp. 1045-1048.

Paine, D.P., 1981, *Aerial Photography and Image Interpretation for Resource Management*. New York: John Wiley and Sons, pp. 176-189.

Pan, X.Z., Uchida, S., Liang, Y., Hirano, A. and Sun, B., 2010, *Discriminating different landuse types by using multitemporal NDXI in a rice planting area*. International Journal of Remote Sensing, 31, pp. 585–596.

Panigrahy S, Parihar, J.S. and Patel, N.K., 1992, *Kharif rice acreage estimation in Orissa using NOAA-AVHRR data*. Journal of the Indian Society of Remote Sensing, 20, pp. 35-42.

Panigrahy, S. and Sharma., S.A., 1997, *Mapping of Crop Rotation Using Multidate Indian Remote Sensing Satellite Digital Data*. ISPRS Journal of Photogrammetry & Remote Sensing, 52, pp. 85-91.

Patel, N. K., Singh, T. P., Sahai, B. and Patel, M. S., 1985, *Spectral response of rice crop and its relation to yield and yield attributes*. International Journal of Remote Sensing, 6, pp. 657 - 664.

Pax-Lenney, M. and Woodcock, C. E, 1997, *The effect of spatial resolution on the ability to monitor the status of agricultural lands*. Remote Sensing of Environment, 61, pp. 210-220.

Pirzad, A , Shakiba, R.M., Salmasi, Z.S., Mohammadi, S.A., Darvishzadeh, R., and Samadi, A, 2010, *Effect of water stress on leaf relative water content, chlorophyll, proline and soluble carbohydrates in Matricaria chamomilla L.* Journal of Medicinal Plants Research, 5, pp. 2483-2488.

Pierce, F.J., Nowak, P. and Roberts, P.C., 1999, *Aspects of Precision Agriculture*, p.1-84. In D.L. Sparks (ed.) Advances in Agronomy, 67, Academic Press, San Diego, CA, USA.

Pons, X. and Solé-Sugrañes, L., 1994, *A simple radiometric correction model to improve automatic mapping of vegetation from multispectral satellite data*. Remote Sensing of Environment, 48, pp. 191-204.

Qin, Z. and Zhang, M., 2005, *Detection of rice sheath blight for inseason disease management using multispectral remote sensing*. International Journal of Applied Earth Observation and Geoinformation , 7, pp. 115–128.

Quarmby, N. A., Townshend, J. R. G., Settle, J. J., White, K. H., Milnes, M., Hindle, T. L. and Silleos, N., 1992, *Linear mixture modelling applied to AVHRR data for crop area estimation*. International Journal of Remote Sensing, 13, pp. 415-425.

Quarmby, N. A., Milnes, M., Hindle, T. L. and Silleos, N., 1993, *The use of multi-temporal NDVI measurements from AVHRR data for crop yield estimation and prediction*. International Journal of Remote Sensing, 14, pp. 199-210.

Rasmussen, M. S., 1992, *Assessment of millet yields and production in northern Burkina Faso using integrated NDVI from AVHRR*. International Journal of Remote Sensing, 13, pp. 3431-3442.

Rasmussen, M. S., 1997, *Operational yield forecast using AVHRR NDVI data: reduction of environmental and inter-annual variability*. International Journal of Remote Sensing, 18, pp. 1059-1077.

Rasmussen, M. S., 1998, *Developing simple, operational, consistent NDVI-vegetation models by applying environmental and climatic information: Part II: Crop yield assessment*. International Journal of Remote Sensing, 19, pp. 119-139.

Reynolds, C.A., Yitayew, M., Slack, D.C. Hutchison, C.F., Huete, A., and Petersen, M.S., 2000, *Estimating crop yields and production by integrating the FAo crop specific*

water balance model with real-time satellite data and ground based ancilliary data. International Journal of Remote Sensing, 21, pp. 3487-3508.

Ribbes, F. and Toan, L. T., 1999, *Rice field mapping and monitoring using RADARSAT data*. International Journal of Remote Sensing, 20, pp. 745– 765.

Richardson, A. J., Wiegand, C. L., Arkin, G. F., Nixon, P. R. and Gerbermann, A . H, 1982, *Remotely-sensed spectral indicators of sorghum development and their use in growth*. Agricultural Meteorology, 26, pp. 11-23.

Rosenthal, W. D., Hammer, G. L. and Butler, D.,1998, *Predicting regional grain sorghum production in Australia using spatial data and crop simulation modelling*. Agricultural and Forest Meteorology, 91, pp. 263-274.

Rugege, D., 2002, *Regional Analysis of Maize – Based on Land Use System for Early Warning Application*. Unpublished PhD Thesis, Wageningen University, Wageningen.

Sakamoto, T., Yokozawa, M., Toritani, H., Shibayama, M., Ishitsuka, N. and Ohno, H., 2006, *A crop phenology detection method using time-series MODIS data*. Remote Sensing of Environment, 96, pp. 366–374.

Sari, D.K., Ismullah1, I.H., Sulasdi, W.N., and Harto, H.B. 2010. *Detecting Rice Phenology in Paddy Fields with Complex Cropping Pattern Using Time Series MODIS Data A Case study of Northern Part of West Java – Indonesia*. ITB Journal Science, 42, pp:91-106Sawasawa, Haig L.S., 2003, *Crop Yield Estimation: Integrating RS, GIS, and Management Factor. A case study of Birkoor and Kortigiri Mandals, Nizamabad District India*. Available on http://www.itc.nl/library/papers_2003/msc/nrm/sawasawa.pdf, 1-9 (Accessed April 10, 2011)

Schuppler, U., He, John, P.C.L., and Munns, R, 1998, *Effect of Water Stress on Cell Division and Cell-Division-Cycle 2-Like Cell-Cycle Kinase Activity in Wheat Leaves*. Plant Physiol.,117: 667–678.

Senanayake, N., Naylor, R. E. L., De Datta, S. K. and Thomson, W. J., 1994, *Variation in development of contrasting rice cultivars*. Journal of Agricultural Science, Cambridge, 123, pp. 35-39.

Shao, Y., Fan, X., Liu, H., Xiao, J., Ross, S., Brisco, B., Brown, R. and Staples, G., 2001, *Rice monitoring and production estimation using multitemporal RADARSAT*. Remote Sensing of Environment, 76, pp. 310–325.

Shao, Y., Wang, C., Fan, X., and Liu, H., 1997, *Evaluation of SAR image for Rice Monitoring and Land Cover Mapping*. In Presented at Geomatics in Era of RADARSAT, Ottawa, Canada, pp. 15.

Sidik M., 2004, *Indonesia Rice Policy In View Of Trade Liberalization*. FAO Rice Conference, Rome, Italy.

Smith, R. C. G., Adams, J., Stephens, D. J. and Hick, P. T., 1995, *Forecasting Wheat Yield in a Mediterranean-type environment from the NOAA Satellite*. Australian Journal of Agricultural Research, 46, pp. 113-125.

Steininger, M. K., 1996, Tropical secondary forest regrowth in the Amazon: age, area and change estimation with Thematic Mapper data. International Journal of Remote Sensing, 17, 9–27.

Strahler, A. H., Boschetti, L., Foody, G.M., Friedl, M.A., Hansen, M.C., Herold, M., Mayaux, P., Morisette, J.T., Stehman, S.V. and Woodcock, C.E, 2006, *Global Land Cover Validation: Recommendations for Evaluation and Accuracy Assessment of Global Land Cover Maps. Office for Official Publications of the European Communities*. Available: http://wgcv.ceos.org/docs/plenary/ wgcv26/GlobalLandCover Validation_JeffMorisette.pdf (Accessed July 25, 2009.)

Thenkabail, P. S., Smith, R. B. and Pauw, D. E., 2000, *Hyperspectral vegetation indices and their relationships with agricultural crop characteristics*. Remote Sensing of Environment, 71, pp. 158-182.

Thenkabail, P. S., Ward, A. D., Lyon, J. G. and Merry, C. J., 1994b, *Thematic Mapper vegetation indices for determining soybean and corn growth parameters*. Photogrammetric Engineering and Remote Sensing, 60, pp. 437-442.

Tingting, L. and Chuang, L., 2010, *Study on extraction of crop information using time-series MODIS data in the Chao Phraya Basin of Thailand*. Advances in Space Research, 45, pp. 775-784.

Tong, Q.T.Q., Pu, R., Guo, X., and Zhao, C., 2001, *Spectroscopic determination of wheat water status using 1650–1850 nm spectral absorption features*. International Journal of Remote Sensing, 22, pp. 2329-2338.

Treitz, P. M., Howard, P. J. and Gong, P., 1992, *Application of satellite and GIS technologies for land-cover and land-use mapping at the rural-urban fringe: a case study*. Photogrammetric Engineering and Remote Sensing, 58, pp. 439–448.

Tucker, C. J., Holben, B. N., Elgin, J. H. Jr., Mc- Murtrey, 1980, *Remote sensing of dry matter accumulation in winter wheat*. Remote Sensing of Environment, 11, pp. 171-189.

Uchida, S. 2010. *Monitoring of planting paddy rice with complex cropping pattern in the tropical humid climate region using Landsat and Modis data, a case of West Java, Indonesia*. International Archives of the Photogrammetry, Remote Sensing and Spatial Information Science, Volume XXXVIII, Part 8, Kyoto Japan.

Vermote, E. F., Vermeulen, A., 1999, *Atmospheric correction algorithm: Spectral reflectance (MOD09), MODIS algorithm technical background document, version 4.0*. University of Maryland, Department of Geography, pp 234.

Wataru, T, Taikan, O., and Yoshifumi, Y., 2006, *Investigating an integrated approach on rice paddy monitoring over Asia with MODIS and AMSR-E*. Proceedings of the Conference of the Remote Sensing Society of Japan, 40, pp. 173-174.

Westmoreland, S. and Stow, D. A., 1992, *Category identification of changed land-use polygons in an integrated image processing/geographic information system*. Photogrammetric Engineering and Remote Sensing, 58, pp. 1593–1599.

Xiao, X., Boles, S., Liu, J., Zhuang, D., Frolking, S., Li, C., Salas, W. and Moore, B. (2005). *Mapping paddy rice agriculture in southern China using multi-temporal MODIS images*. Remote Sensing of Environment, 95, pp. 480–492.

Xiao, X., Braswell, B., Zhang, Q., Boles, S., Frolking, S. and Moore, B., 2003, *Sensitivity of vegetation indices to atmospheric aerosols: Continental-scale observations in Northern Asia*. Remote Sensing of Environment, 84, pp. 385–392.

Xiao, X., He, L., Salas, W., Li, C., Moore, B. and Zhao, R., 2002, *Quantitative relationships between field-measured leaf area index and vegetation index derived from VEGETATION images for paddy rice fields*. International Journal of Remote Sensing, 23, pp. 3595–3604.

Yang, C.-M. and Su, M. R., 2000, *Analysis of spectral characteristics of r ice canopy under water deficiency: Monitoring changes of spectral characteristics of dehydrating rice canopy*. Asian Conference on Remote Sensing, 21, pp. 13-18.

Yang, C.-M., and Chen, R.-K., 2004, *Modeling rice growth using hyperspectral reflectance data. Crop Science*, 44, pp. 1283–1290.

Yang, C.-M., and Cheng, C.-H., 2001, *Spectral characteristics of rice plants infested by brown planthopper*. Proceedings of the National Science Council, 25, pp. 180–186.

Yang, C.-M., Cheng, C.-H. and Chen, R.-K., 2007, *Changes in spectral characteristics of rice canopy infested by leaf folder and brown planthopper*. Crop Science, 47, pp. 329-335.

Yang, C.-M., Liu, C.C., and Wang, Y.W., 2008, *Using Formosat-2 Satellite Data to Estimate Leaf Area Index of Rice Crop*. Journal of Photogrammetry and Remote Sensing, 13, pp. 253-260.